ISSN 2518-3125

Volume 2 Number 1 June 2017

Sonargaon University (SU) Journal

UGC & Govt. Approved
Sonargaon University (SU)
সোনারগাঁও ইউনিভার্সিটি (এসইউ)
147/I, Green Road, Dhaka-1215.

WE WILL RISE UP
WE WILL SHINE

Sonargaon University Journal

Volume 2, Number 1, June 2017

ISSN 2518-3125

Sonargaon University (SU)

Published by:

Registrar
Sonargaon University (SU)

Published in: June 2017

© Copyright: Reserved by the Publisher

Printed by:

Sonargaon University (SU)

147/I, Green Road, Dhaka-1215, Bangladesh

Cover page designed by:
Md. Hafizur Rahman
Md. Abu Hanif

Editorial and Business Office:

Editor, Sonargaon University Journal
147/I, Green Road, Dhaka-1215, Bangladesh
Tel:
E-mail: journal@su.edu.bd

Price: Tk 200, $6

ISSN 2518 3125

Disclaimer: *Sonargaon University Journal is peer reviewed journal. The editorial board is not responsible for views expressed by the writers.*

Chief Patron:
Engineer Md. Abdul Alim
General Secretary, Board of Trustees
Sonargaon University (SU)

Chief Advisor:
Professor M.A. Razzaque
Vice-Chancellor, Sonargaon University (SU)

Editor in Chief:
Prof. Dr. Md. Abdur Razzaq Akhanda
Pro-VC &
Dean, Faculty of Science & Engineering
Sonargaon University (SU)

Editorial Board:
Prof. Dr. Mohammad Ali
Dept. of Mechanical Engineering
Bangladesh University of Engineering & Technology (BUET)

Prof. Dr. Md. ShahjadaTarafder
Dept. of Naval Architecture & Marine Engineering
Bangladesh University of Engineering & Technology (BUET)

Prof. Dr. Mahmuda Akter
Department of Accounting & Information Systems
University of Dhaka

Ms. Shamim Ara Hassan
Associate Professor
Dept. of Architecture
Bangladesh University of Engineering & Technology (BUET)

Mr. Abul Kalam
Associate Professor & Dean, Faculty of Business
Sonargaon University (SU)

Senior Assistant Editor
Md. Ferdous Wahid
Lecturer
Department of Civil Engineering, Sonargaon University (SU)
Email: mdfwahid@gmail.com
Cell: + 08801955529810

Editorial

We are happy to publish the third Issue (Volume-2, No.-01) of the Sonargaon University (SU) Journal. It is a peer-reviewed journal which is published twice in a year. As mentioned in earlier issues this University has three faculties-faculty of Science and Engineering, faculty of Arts and Humanities and faculty of Business. Authors from this university and also from different Public and Private Universities contribute to this Journal. The present Issue will focus some ideas on Science, Engineering & Business. We are grateful to the founder members of the Trustee Board of the University Engr. Mr. Abdul Aziz and Engr. Mr. Md. Abdul Alim whose supports and guidance have materialized ideas of this Journal. Our sincere thanks to the Vice-Chancellor Professor M. A. Razzaque for his guidance and supports. We also extend our sincere thanks to the reviewer for assessing different papers of the Journal. Thanks, are also to Mr. Md. Abu Hanif, Assistant Registrar & PS to the Vice-Chancellor for cover design and secretarial work and Mr. Md. Rahomat Ali, PS to the Vice-Chancellor for secretarial work.

Finally, but not the least to the editorial board for their kind suggestions and valuable advice.

Professor Dr. Md. Abdur Razzaq Akhanda
Editor in Chief
Sonargaon University Journal (SUJ)
Email: journal@su.edu.bd
Cell: + 08801955544903

and

Md.Ferdous Wahid
Senior Assistant Editor
Sonargaon University Journal (SUJ)
Email: mdfwahid@gmail.com
Cell: + 08801955529810

Sonargaon University Journal (SUJ)

Volume-2, Number-1, June-2017

Contents

Sl. No.	Title of Paper	Author(s)	Page No
1.	Energy Storage in a Technical Grade Phase Change Material in a Horizontal Double Pipe Heat Exchanger: Part-I	Tonny Tabassum[1] Mainul Hasan[2] Latifa Begum[3 *]	01-36
2.	Reasons of Labor Dispute and Role of BGMEA, Industrial Police & Labor Union in disputes settlement procedure – a study from Bangladesh RMG industry units of Dhaka & Gazipur	Md. Al Amin Molla[1*], Md. Baney Amin Mollah[2]	37-52
3.	Study of Natural Convection Heat Transfer in a Rectangular Enclosure from One Cooled Side Wall	*Mostofa M.M[1] Sarkar, M.A.R[2], Huq A.M.A[3] and Islam, M.A[4]	53-60
4.	Comparison of Physical and Micro-Structural Characteristics of Various Fine Aggregates in Bangladesh	Tafsirojjaman[1*], Md. Sabbrojjaman[2], Md. N Islam[3], Md. R Alam[4], Md. K Hasan[5], Md. N Islam[6], Md. M R Majumder[7], Sheikh Mohammed[8], Enamul Haque[9]	61-70
5.	Mechanical Properties of Jute hybrid Epoxy Composites and Its Applications in Car Panels	Shekh Md. Mamun Kabir[1*], Rezaul Karim[2] and Md. Khayrul Islam[3]	71-82
6.	Numerical Simulation Of Non-Newtonian Spiral Flow Through Stenosed Artery With 75% And 96% Area Reductions	Md Ferdous Alam[1*]; Muhammad Rubayat Bin Shahadat[2]; Md. Alamgir Kabir[3]; Md. Mostofa Hossain[4]	83-98

7.	Product Diversification and The Enhancement of Export Volume From Bangladesh To EU & Non-Traditional Markets	Md. Ahshan Habib[1]*, Md. Jahangir Karim[2]	99-118
8.	A Study on The Performance of Hybrid Power Generation System	Md. Mahe Alam*[1] and Md. Sirajul Islam[2]	119-134
9.	Study of Performance of an Air Conditioning System and Cooling Load Calculation By Using Developed Software For A Building	Khandakar Mozammel Hossan[1*], Dr. S M Nazrul Islam[2], Dr. Md.Quamrul Islam[3]	135-151
10.	An Evaluative Study of Development and Impact on Maritime and Coastal Tourism	S M Nurul Huda[1], Mohammed Mojahid Hossain Chowdhury[2*]	152-159
11.	A Suggested Proposal for The Bangladeshi Universities to Implement ISO-9001 Quality Management System for External Peer Review of Institutional Quality Assurance Cell as Required by The University Grants Commission	Prof. Dr. Chowdhury Mrinal Ahmed [1*], Dr. Md. Al Amin Mollah[2], Monira Ahmed [3]	160-175
12.	The Latest ISO 14001:2015 EMS and the Present Scenario in Construction Sector of Bangladesh for Sustainable Construction.	Chowdhury Mrinal Ahmed[1*] Md. Al Amin Molla[2], Monira Ahmed[3], Md. Baney Amin Mollah[4]	176-186

Energy Storage in a Technical Grade Phase Change Material in a Horizontal Double Pipe Heat Exchanger: Part-I

Tonny Tabassum[1], Mainul Hasan[2] and Latifa Begum[3] *

***Corresponding Author:** [3]Department of Mining & Materials Engineering McGill University, Canada.
[1,2]Department of Mining & Materials Engineering McGill University, Canada.

Email: Latifa.begum@mail.mcgill.ca

Abstract

A transient two-dimensional numerical model was developed to investigate the melting characteristics of an impure phase-change material (PCM) embedded between two concentric circular horizontal cylinders. The modeled transport equations were suitably non-dimensionalized and were solved numerically in its primitive variables form on a staggered grid arrangement employing a control-volume finite difference method. The selected PCM melts over a temperature range. To easily account the latter aspect in the model, an enthalpy-porosity based fixed grid scheme was used to solve the convection-diffusion mushy region phase change problem. The inner cylindrical tube was heated to a constant temperature by a heat transfer fluid while the outer tube was insulated. Time-wise evolutions of the temperature distributions are presented. Various quantities such as, the average Nusselt number over the inner tube surface, the total melt fraction, and the total cumulative stored energy, all as a function of the melting time are reported for three inner wall temperatures and for an initially saturated solid PCM and also for a sub-cooled condition of 10°C of the PCM. The predicted results show that the melting rate increases rapidly up to the melting time of about 41.18 min. After this time the melting rate increases but at a considerably slower rate. The storage of thermal energy increases with the increase of the inner wall temperature and initial temperature of the solid PCM. The energy charged is greatly influenced by the change of the inner tube wall temperature compared to the change of the initial solid PCM temperature.

Keywords: Impure PCM, 2-D numerical modeling, transient melting, double pipe heat exchanger, mushy region, thermal energy storage.

Nomenclature

A	Darcy coefficient
g	gravitational acceleration [m. s^{-2}]
h	sensible heat
Nu_L	local Nusselt number

$\overline{Nu}_{avg}$	circumferential average Nusselt number based on cylinder radius
P	pressure, Pa
Pr	Prandtl number = $\frac{\nu_f}{\alpha_f}$
r_i	radius of inner cylinder [m]
r_o	radius of outer cylinder [m]
R_i	dimensionless radius of inner cylinder
R_o	dimensionless radius of outer cylinder
Ra	Rayleigh number = $\frac{g\beta_{PCM}(T_{WALL}-T_{SOLIDUS})D_i^3\rho}{\mu_{PCM}\alpha_{PCM}}$
Ra^*	modified Rayleigh number = $\frac{Ra}{Ste}$
Ste	Stefan number = $\frac{C_P(T_{WALL}-T_{SOLIDUS})}{\lambda}$
T	temperature [^{0}C]
T_{WALL}	inner cylinder wall temperature [^{0}C]
T_i	initial temperature of the working materials [^{0}C]
ΔT	temperature difference between the inner cylinder surface and solidus temperature of PCM [^{0}C]
T_{ref}	reference temperature [^{0}C]
t	time
h^*	dimensionless enthalpy = $\frac{C_P(T-T_{SOLIDUS})}{\lambda}$
h^*_{WALL}	dimensionless enthalpy at the inner wall
h^*_i	initial dimensionless enthalpy in the domain
u, v	interstitial velocity components along θ and r directions respectively [ms^{-1}]
U, V	dimensionless interstitial velocity components along θ and r directions respectively
θ , r	polar coordinates, degree and m

Greek symbols

α	thermal diffusivity [m^2s^{-1}]
β_f	coefficient of thermal expansion, $-\left(\frac{1}{\rho}\right)\left(\frac{\partial\rho}{\partial T}\right)_P$, K^{-1}
ν_f	kinematic viscosity [m^2s^{-1}]
ρ	density [$kg.m^{-3}$]
μ	dynamic viscosity [$kg.m^{-1}.s^{-1}$]
λ	latent heat of fusion [$kJ.kg^{-1}$]
ΔH	nodal latent heat
τ	Fourier number, $\frac{t\alpha_{PCM}}{D_i^2}$
f_l	fluid fraction

Subscripts

L	liquid
S	solid
i	inner cylinder
o	outer cylinder
ref	reference value

Superscripts

* non-dimensional variable

1.0. Introduction

Latent Heat Thermal Energy Storage (LHTES) devices have attracted considerable worldwide attention because of their large potential for energy savings and their ability to provide or absorb/relatively large amount of thermal energy particularly when there is a mismatch in the supply and demand of the energy sources [1]. Any LHTES system mainly consists of three basic components: (a) a phase change material (PCM), (b) a suitable container to hold the PCM, and (c) a conductive heat transfer surface or surfaces for exchanging heat from the heat source to the PCM and from the latter to the heat sink [2,3]. One of the most popular heat exchanging devices for LHTES is a double-pipe heat exchanger. The latter stores/discharges thermal energy through the phase change process by melting (charge)/solidification (discharge) of a PCM embedded in the annular gap [4-7]. Over the last

two decades, the thermal storage technology based on the usage of PCMs has attracted a significant interest because of its capacity to store/release the relatively large amount of thermal energy through the solid-liquid phase-change process [8]. Intermittent energy sources, such as solar and waste heat from industrial processes can be stored and later conveniently used through the LHTES devices. Because of their high storage capacity, these devices are advantageous in reducing thermal energy storage volume, heat loss, and insulation cost.

Fig.1. presents a proposed integrated latent heat storage arrangement for solar energy utilization which can be used for domestic hot water supply source. The system consists of the following main components: (a) a flat plate collector, (b) a double-pipe LHTES heat exchanger, and (c) an insulated storage tank. The flat plate collector can be placed on the top of a building or any other suitable structure which absorbs directly both the solar beam and the diffuse radiation. Such a device can absorb solar energy, convert it into heat and then transfer that heat to the circulating cold water. The heated water (heat transfer fluid, HTF) passes through the inner pipe of the double-pipe heat exchanger and delivers the heat by melting a PCM placed in the annular gap. During the charging phase, pump-1 and control valves 1, 3, 5 and 7 are open while pump-2 is inactive and valves 2, 4, 6 and 8 are closed. This flow control loop, named as an inner loop, should only work when the solar energy is available. When the solar energy is not available pump-2 is active and will circulate cold water from the insulated storage tank through the outer loop connecting the heat exchanger and the insulated storage tank. In this discharge period, while passing through the LHTES device, the circulating cold water in the outer loop will gain heat from the melted PCM by solidifying it. During this time, pump-1 is idle and control valves 1, 3, 5 and 7 are closed while pump-2 is active and valves 2, 4, 6 and 8 are opened.

Here all the connecting pipes used between (a) the collector and the heat exchanger and (b) the heat exchanger and the insulated storage tank are all insulated and there is a minimum heat loss from the connecting pipes. Thus, there will be a minimum temperature drop for hot water flowing through the system. The inner loop and outer loop do not work simultaneously which should be controlled by an automatic control unit. In the insulated storage tank, an electric heater can be placed as back up for low solar radiation or for overcast/rainy days or for night time. There could be a number of possible variations of the proposed solar energy storage and utilization facility.

As one can see, one of the important units in the proposed system is the heat exchanger. Thus, designing an optimum double pipe heat exchanger is important for dynamic thermal performances. The mathematical modeling is a justifiable first option for designing an optimum LHTES device without performing a number of trial experimental runs. Such a modeling exercise

can save both energy and cost. After getting an optimal design of the heat exchanger through the numerical simulations then a prototype/model experimental heat exchanger can be built to arrive at a final design for operational purposes.

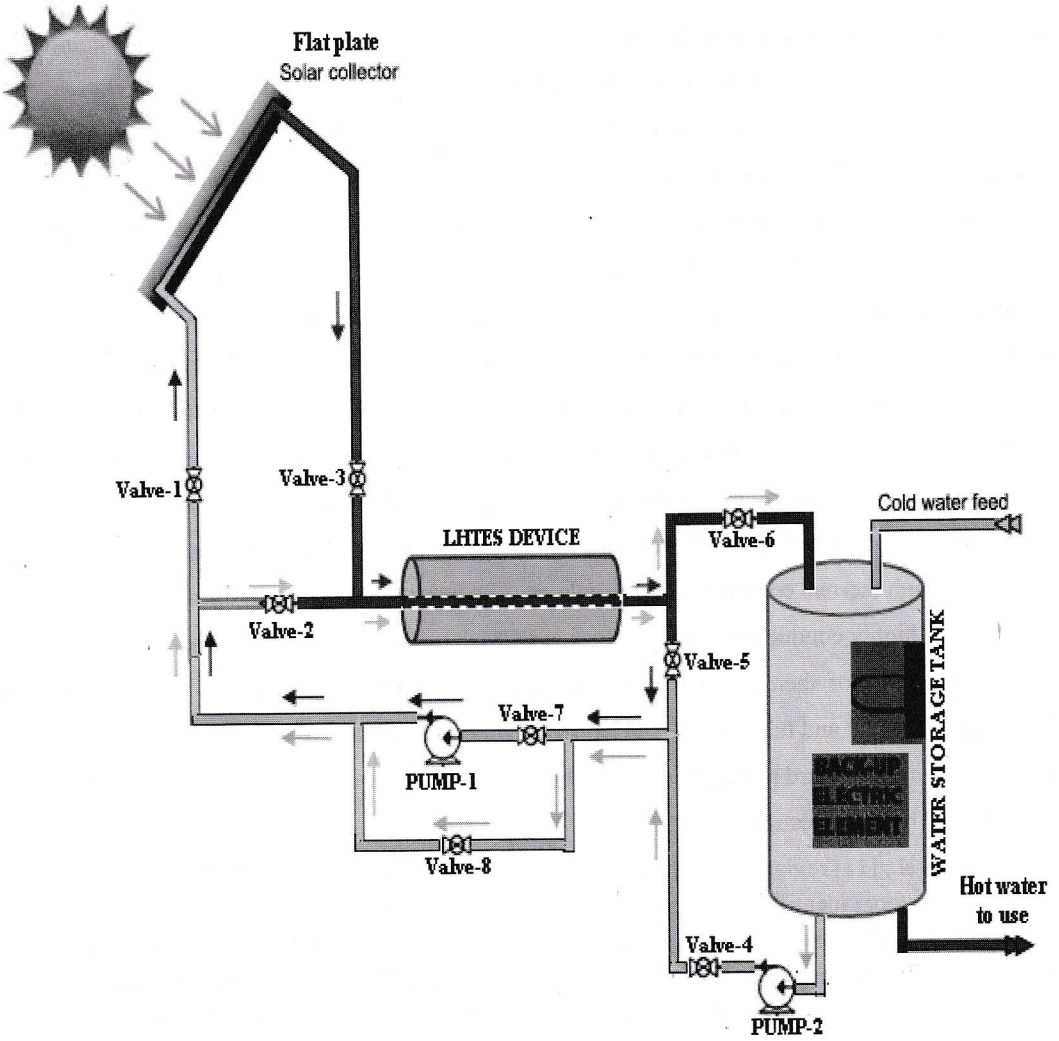

Fig. 1. Schematic view of solar energy storage system for domestic hot water.

Over the years a large number of review papers concerning energy storage/discharge in PCM have appeared in the literature. In the following, only the relevant and the latest review papers are discussed.

Verma et al., [9] reviewed various mathematical modeling techniques which have been used for studying the latent heat thermal energy storage (LHTES) systems using PCM. Unfortunately, the authors concentrated only on the transient conduction type of models while completely ignoring the convective aspect of the phase change process which dominates the melting process as stated earlier in such systems. The authors divided their review between the first and the second law of thermodynamics and pointed out the deficiencies of the first law analysis for LHTES systems. The above paper does not provide any information on the design aspect of the heat exchangers.

Agyenim et al., [10] reviewed 135 articles related to solid-liquid phase change heat transfer concerning the LHTES and recovery in various PCM. The survey covered different aspects of the LHTES systems which appeared for three decades prior to the year 2010. The authors provided critical assessments of the PCM employed, the heat exchanging units investigated, and the various enhancement techniques adopted to increase the low thermal conductivities of the PCM by different researchers. The authors noted that for the low-temperature applications of PCM the investigators mostly concentrated on paraffin, Glauber's salts, wax, stearic acid, and n-octadecane. Regarding the modeling efforts, most of the researchers in recent years have used enthalpy approach to model the phase-change phenomena by incorporating the effect of natural convection. The authors mentioned that for the enhancement of the low thermal conductivity of the used PCM, the researchers used fins, insertion of high thermal conductivity materials, multi tubes, micro- or macro-encapsulation, and the dispersion of highly conductive nano-particles in PCM. They classified the commonly used LHTES units on the basis of their geometries as (a) pipe model, (b) cylinder model (double-pipe heat exchanger), (c) shell and tube model, and (d) rectangular or slab unit. Depending on the geometrical configurations with regard to the gravity field, both horizontal and vertical systems were seen to have been adopted by the investigators.

Dutil et al., [11] reviewed the modeling of melting and solidification of PCMs for the LHTES systems. The authors identified various geometries which investigators considered concerning LHTES systems. They include rectangular, cylindrical and spherical geometries along with the studies on annular geometries with the PCM embedded therein. The authors noted that although an exhaustive amount of literature has appeared on the modeling of such systems, unfortunately, the models were verified with other's modeling results and a very few of such models have compared with the experimental data. Even the numerical modelers who compared their predictions with experimental measurements have done so by taking the results from the reported graphs and hence such comparisons can be at best qualitative in nature since numerical values of the various quantities were approximated from the charts.

The authors indicated that the mathematical modelers in this area after the 1990s are 'blindly' using the commercial CFD codes because of their easy availability. This trend on the dependency of the commercial CFD codes is intensifying day-by-day. Furthermore, most of the reported results using CFD codes are found to be incomplete since velocity field in the melt, heat flux on the heat transfer surfaces, and the local and average Nusselt number values are seen to be missing in many such studies. In the review, the authors mentioned that the investigators in some published papers used various types of thermal conductivity enhancement techniques to increase the low conductivity of the PCM. Among these methods include the addition of metallic fins on the surfaces of the tubes, high conductivity porous metallic matrix within the PCM, dispersion of nanoparticles, nanofibers and nanotubes in the PCM, multi-tubes in the shell-and-tube heat exchangers, etc. The researchers in the latter cases only focused on the enhancement of the melting or solidification rate but did not analyze the issue of energy storage considering the technical-economical criteria.

Khan et al., [12] provided a comprehensive review of the various heat transfer aspects of the LHTES systems of the most studied PCM namely organic paraffin and inorganic salt hydrates. These authors also discussed different melting and solidification rate enhancement techniques which include container configurations, the inclusion of extended surfaces and fins, additives for enhancing thermal conductivity, employment of multi-PCM and encapsulation of PCM. One important aspect of this review is that the authors have discussed the long-term thermo-physical stability of the above classes of PCMs and their compatibility with various container materials. This study provides some useful guidelines in selecting a reliable PCM and the corresponding material for the container along with the efficient geometrical configurations to achieve the maximum thermal utilization of the PCM. The authors suggested that before using industrial grade PCM, the repeated thermal cycling tests are required for checking their long-term stability concerning the thermophysical properties of the PCM.

Zhang et al., [13] provided a review of thermal energy storage regarding sensible, latent and thermochemical studies which appeared in the literature until 2016. Regarding the latent heat storage, the authors only examined the inorganic substances and the materials for their containment vessels. This review also discussed various configurations of the containment vessels as well as the different techniques for improving the heat transfer rate between the circulating heat transfer fluid and the PCM in the containers. The author also discussed some thermal conductivity enhancement techniques of the PCM. This review on the LHTES system is not very comprehensive, although the authors have spent a lot of journal's space in discussing the sensible energy and thermochemical storage systems.

Khyad et al., [14] mainly reviewed various PCM and provided their systematic classifications, which are critical for selecting an appropriate PCM for LHTES and discharge during solid-liquid

phase change. This paper is particularly useful for its thorough review of low-temperature thermal energy storage applications, particularly, for organic PCMs like paraffin waxes. The authors have recommended the use of technical grade PCM for their low costs and easy availability.

From the above literature review, it is apparent that the preferred configurations of the LHTES units which have been studied by various investigators are horizontal and vertical double-pipe heat exchangers. Multiple PCMs have been studied for the storage/retrieval of energy in the above devices particularly for low-temperature thermal energy applications, and they include paraffin wax, fatty acids and their mixtures, salt hydrates and their mixtures, etc. [15]. Unfortunately, all such modeling studies have dealt with mostly regular geometries and pure PCM.

In general, a pure PCM has a relatively high latent heat of fusion compared to the impure PCM. A pure PCM melts or solidifies at a fixed temperature, and it is capable of storing/releasing a significant amount of energy during melting/solidification. Unfortunately, pure paraffin waxes are quite expensive, about ten to 100 times costlier than its technical grade (commercial grade). As a result, the technical grade paraffin is more economical compared to the pure paraffin wax for LHTES [16]. Commercially available technical grade paraffin is a mixture of many saturated hydrocarbons and, therefore, has a melting or freezing temperature range rather than a sharp melting point. Thus, if technical grade paraffin is used as a PCM then during the transient phase-change process, there will be solid, liquid and mushy regions (a mixture of solid and liquid) in the LHTES systems. The main criterion of selection of a PCM for a particular application is the melting temperature or the phase change temperature range of the PCM. Some other important parameters must also be taken into consideration for an appropriate usage of LHTES systems. These are latent heat, stability to thermal cycling, thermal conductivity and cost.

To numerically model the mushy region accurately of the impure PCM particularly during the melting phase is a difficult exercise because of the convection of the melt in the mushy region. The present authors have failed to find a single modeling study in the literature where the used PCM melts and solidifies over a temperature range of more than 2^0C or higher. In this study, the melting process of an impure PCM which melts over a temperature range of 8.7^0 C is placed in the annular space between concentric horizontal circular-shaped tubes for the constant temperature boundary condition of the inner tube. The authors have noted that there is no comparable work in the literature of the studied problem.

2.0. Mathematical model

2.1. Problem description

As depicted in **Fig.2.** , the physical domain is selected to be two horizontal concentric cylinders in which the volume located between them is filled with a PCM. Here, Do, and D_i is

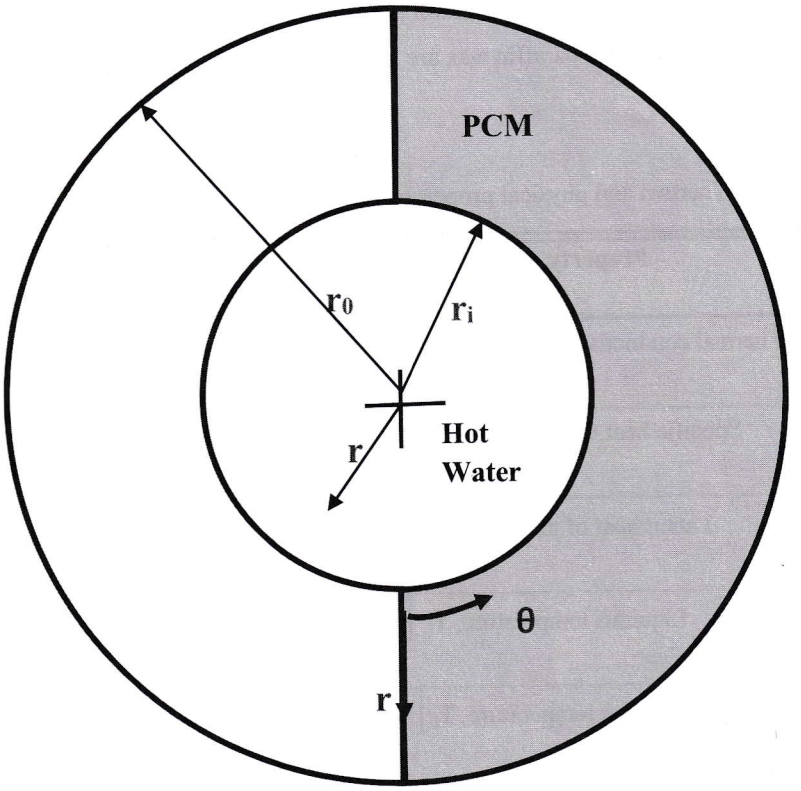

Fig. 2. Schematic view of the cross-section of the double-pipe heat exchanger with the blue part representing the computational domain.

the diameter of the outer and inner cylinders, respectively. The values of the diameter of the inner and outer cylinder are arbitrarily set to 0.04 m and 0.104 m, respectively. Therefore, the calculated cross-sectional area of the annulus gap is 72.38 cm^2, which can hold 5.718 kg of PCM when the length of the cylinder is 1.0 m. Due to symmetry in the θ -direction, the computation has been conducted on the right-half of the domain. The coordinate system is adopted in a way such that the gravity is acted in both r-θ directions and the origin is placed at the center of the cylinders.

Initially, the solid PCM embedded in the cylindrical annulus is at a uniform temperature (T_i) that is either equal or below the solidus temperature (T_S) of the PCM. When the initial temperature is below the solidification temperature of the PCM, this thermal condition is designated as a sub-cooled condition. For time t > 0, a constant temperature (T_W) is imposed on the surface of the inner cylinder, which is greater than the liquidus temperature (T_L) of the PCM, i.e., $T_W > T_L$. The outer wall of the annulus is maintained at the adiabatic condition throughout the whole melting process. The relevant thermophysical properties of the paraffin wax are taken from the literature [17] and are listed in **Table 1.**

Table 1. Thermal and physical properties of paraffin wax (PCM).

Property, symbol [unit]	**Values**
Thermal conductivity, K_S and K_L $[kW/(m \times K)]$	0.22×10^{-3}
Specific heat, C_{PS} and C_{PL} $[kJ/(kg \times K)]$	2.15
Latent heat of melting, λ $[kJ/kg]$	190
Liquidus temperature, T_L $[^oC]$	59.9
Solidus temperature, T_S $[^oC]$	51.2
Kinematic viscosity, ν $[m^2/s]$	5.2×10^{-6}
Thermal diffusivity, α $[m^2/s]$	1.2953×10^{-7}
Density, ρ_S and ρ_l $[kg/m^3]$	790
Liquid thermal expansion coefficient, β $[1/^oC]$	1.0×10^{-3}

- Density, specific heat and thermal conductivity used in the numerical model is considered at 59.9°C

2.2. Assumptions

The following idealizations are made in developing the current mathematical model of the physical problem for the phase-change process with the mushy region in the presence of the buoyancy-driven convective flows:

[1]. The melt behaves as an incompressible Newtonian fluid.

[2]. The convective motion in the melt is laminar and two-dimensional.compared to the radii of the two cylinders, the length of the cylinders is long such that there are no end effects on the selected cross-section along the longitudinal direction.

[3]. No-slip conditions are applicable for the velocity components at the boundaries.

[4]. Thermophysical properties of the PCM are assumed to be constant in both solid and liquid phases except for the density variations in the melt are considered in so far as they contribute to the buoyancy forces.

[5]. Buoyancy forces are incorporated in the momentum equations based on the Boussinesq approximations.

[6]. The physical properties of the PCM are temperature independent within each phase and are evaluated at the liquidus temperature.

[7]. No viscous dissipation occurred in the calculation domain.

[8]. Variation of liquid fraction in the mushy region is assumed to be a linear function of temperature.

[9]. The effects of volume change associated with the solid-liquid phase change are neglected.

[10]. There is no heat loss or gain from the surroundings.

2.3. Numerical formulation

2.3.1. Governing equations for laminar melt velocity and enthalpy

A general conservative form of dimensional governing equations such as mass, momentum and energy equations for r-θ coordinates are given as follows:

Continuity equation: $$\frac{\partial \rho_r}{\partial t} + \frac{1}{r}\frac{\partial(\rho_r r v)}{\partial r} + \frac{1}{r}\frac{\partial(\rho_r u)}{\partial \theta} = 0 \quad \text{.....} \quad (1)$$

U-momentum equation:

$$\frac{\partial(\rho_r u)}{\partial t}+\frac{1}{r}\frac{\partial}{\partial r}(\rho_r ruu)+\frac{1}{r}\frac{\partial}{\partial\theta}(\rho_r uv)=\frac{1}{r}\frac{\partial}{\partial r}\left(\mu r\frac{\partial u}{\partial r}\right)+\frac{1}{r}\frac{\partial}{\partial\theta}\left(\frac{\mu}{r}\frac{\partial u}{\partial\theta}\right)-\frac{1}{r}\frac{\partial p}{\partial\theta}+2\frac{\mu}{r^2}\frac{\partial v}{\partial\theta}-\mu\frac{u}{r^2}-$$

$$\rho_r\frac{uv}{r}-\rho g\sin\theta-\mathrm{Au} \qquad \text{.....} \quad (2)$$

V-momentum equation:

$$\frac{\partial(\rho_r v)}{\partial t}+\frac{1}{r}\frac{\partial}{\partial r}(\rho_r ruv)+\frac{1}{r}\frac{\partial}{\partial\theta}(\rho_r vv)=\frac{1}{r}\frac{\partial}{\partial r}\left(\mu r\frac{\partial v}{\partial r}\right)+\frac{1}{r}\frac{\partial}{\partial\theta}\left(\frac{\mu}{r}\frac{\partial v}{\partial\theta}\right)-\frac{\partial p}{\partial r}-2\frac{\mu}{r^2}\frac{\partial u}{\partial\theta}-\mu\frac{v}{r^2}-\rho_r\frac{u^2}{r}$$

$$+\rho g\cos\theta-\mathrm{Av} \qquad \text{.....} \quad (3)$$

Energy equation:

$$\frac{\partial(\rho_r C_P\mathrm{T})}{\partial t}+\frac{1}{r}\frac{\partial}{\partial r}(\rho_r rvC_P\mathrm{T})+\frac{1}{r}\frac{\partial}{\partial\theta}(\rho_r uC_P\mathrm{T})=\frac{1}{r}\frac{\partial}{\partial r}\left(\frac{K}{C_P}r\frac{\partial(C_P\mathrm{T})}{\partial r}\right)+\frac{1}{r}\frac{\partial}{\partial\theta}\left(\frac{K}{C_P}\frac{1}{r}\frac{\partial(C_P\mathrm{T})}{\partial\theta}\right)$$

.....(4)

The following dimensionless variables are employed to non-dimensionalize the transport equations and the associated initial and boundary conditions:

$$R=\frac{r}{D_i}\ ;\ U=\frac{u}{\alpha/r_i}\ ;\ V=\frac{v}{\alpha/\mathrm{D}_i}\ ;\ \mathrm{h}^*=\frac{C_P(\mathrm{T}-\mathrm{T}_{SOLIDUS})}{\lambda}\ ;\ Ra=\frac{D_i^3\beta_T g(\mathrm{T}_{WALL}-\mathrm{T}_{SOLIDUS})}{\nu\alpha}$$

$$p^*=\frac{PD_i^2}{\rho\alpha^2}\ ;\ \tau=\frac{\alpha t}{D_i^2}\ ;\ \nabla H^*=\frac{\nabla\mathrm{H}}{\lambda} \qquad \text{.....}(5)$$

The non-dimensionalized conservative form of the governing equations, applicable in the computational domain, can be written as follows:

Continuity equation: $$\frac{\partial\rho_r}{\partial\tau}+\frac{1}{R}\frac{\partial(\rho_r RV)}{\partial R}+\frac{1}{R}\frac{\partial(\rho_r U)}{\partial\theta}=0$$

.....(6)

U-momentum equation:

$$\frac{\partial U}{\partial \tau}+\frac{1}{R}\frac{\partial}{\partial R}(RUU)+\frac{1}{R}\frac{\partial}{\partial \theta}(UV)=\Pr\frac{1}{R}\frac{\partial}{\partial R}\left(R\frac{\partial U}{\partial R}\right)+\Pr\frac{1}{R}\frac{\partial}{\partial \theta}\left(\frac{1}{R}\frac{\partial U}{\partial \theta}\right)$$
$$-\frac{1}{R}\frac{\partial P^*}{\partial \theta}+2\frac{\Pr}{R^2}\frac{\partial V}{\partial \theta}-\Pr\frac{U}{R^2}-\frac{UV}{R}+Ra^*\Pr\left(h^*-h^*_{REF}\right)\sin\theta-A^*U \quad \text{.....(7)}$$

V-momentum equation:

$$\frac{\partial V}{\partial \tau}+\frac{1}{R}\frac{\partial}{\partial R}(RUV)+\frac{1}{R}\frac{\partial}{\partial \theta}(VV)=\Pr\frac{1}{R}\frac{\partial}{\partial R}\left(R\frac{\partial V}{\partial R}\right)+\Pr\frac{1}{R}\frac{\partial}{\partial \theta}\left(\frac{1}{R}\frac{\partial V}{\partial \theta}\right)-\frac{\partial P^*}{\partial R}-2\frac{\Pr}{R^2}\frac{\partial U}{\partial \theta}$$
$$-\Pr\frac{V}{R^2}+\frac{U^2}{R}-Ra^*\Pr\left(h^*-h^*_{REF}\right)\cos\theta-A^*V \quad \text{.....(8)}$$

Energy equation:

$$\frac{\partial h^*}{\partial \tau}+\frac{1}{R^2}\frac{\partial}{\partial R}\left(RVh^*\right)+\frac{1}{R}\frac{\partial}{\partial \theta}\left(Uh^*\right)=\frac{1}{R}\frac{\partial}{\partial R}\left(R\frac{\partial h^*}{\partial R}\right)+\frac{1}{R}\frac{\partial}{\partial \theta}\left(\frac{1}{R}\frac{\partial h^*}{\partial \theta}\right)$$
$$-\frac{1}{R}\frac{\partial\left(RV\nabla H^*\right)}{\partial R}-\frac{1}{R}\frac{\partial\left(U\nabla H^*\right)}{\partial \theta}-\frac{\partial \nabla H^*}{\partial \tau} \quad \text{.....(9)}$$

2.3.2. Modeling of the various aspects involved

2.3.2.1. Solidification modeling

Here, the single domain approach is followed in the present simulation since it does not require the tracking of the unknown interface (melting front). In the current work, the enthalpy based method is implemented [18-21]. The technique is characterized by decomposing the enthalpy into sensible and nodal latent heat in the energy equation:

$$H = h + \Delta H \quad (10)$$

Where h is the sensible heat defined as:

$$\int_{h_{ref}}^{h} dh = \int_{T_{ref}}^{T} c_p dT \qquad \text{.....} (11)$$

For constant c_p, and taking $h_{ref} = 0$ at T_{ref}, the above equation can be integrated to obtain the sensible heat as:.

$$H = c_p (T - T_{ref}) \qquad \text{.....} (12)$$

In order to establish the region of phase change, the latent heat contribution is specified as a function of temperature, i.e. $\Delta H = f(T)$.

Since the energy equation is valid in the entire calculation domain including solid, liquid, and mushy regions, the nodal latent heat can be related to the liquid fraction. It becomes zero in the solid phase and equals the latent heat of fusion (λ) in the liquid phase. In the mushy region, the latent heat can be any function of liquid fraction. In the current model, it is assumed to be linear.

$$\Delta H = \lambda f_l \qquad \text{.....} (13)$$

Where f_l is the liquid fraction, which is related to temperature as:

$$f_l = \begin{cases} 1 & when \quad T \geq T_L, \\ \dfrac{T - T_s}{T_L - T_s} & when \quad T_L \geq T \geq T_s, \\ 0 & when \quad T \leq T_s. \end{cases} \qquad \text{.....} (14)$$

Where T_L and T_S are the liquidus and solidus temperatures, respectively.

2.3.2.2. Modeling of fluid flow in the mushy region

In the current model, the Darcy law for porous media is adopted to model the flow of PCM in the mushy region. The law is based on the empirical measurement of the permeability. Darcy's law for a porous media can be written as:

$$u_i = -\frac{K}{\mu}\left(\frac{\partial P}{\partial x_i} - \rho g_{xi}\right) \qquad \text{.....(15)}$$

Where K is the permeability, which is a function of porosity, or in the case of a mushy region of a commercial material, a function of liquid fraction. In the model, the permeability decreases with decreasing liquid fraction and ultimately it forces all the velocities to become zero in the case of a stationary solid. The coefficient $\frac{\mu}{K}$ decreases from a large value in the solid phase to zero in the liquid phase. Consequently, the Darcy source term vanishes as the liquid fraction becomes one. The Carman-Koseny equation is adopted for the relation between the permeability and the liquid fraction [22].

$$\frac{\mu}{K} = \frac{C(1-f_l)^2}{f_l^3 + q} \qquad \text{..... (16)}$$

where q is a small positive number introduced to avoid division by zero in the numerical calculations. C is a constant that depends on the morphology of the porous media. The value of C has been estimated from the expression given by Minakawa et al., [23] as:

$$C = 180/d^2 \qquad \text{..... (17)}$$

where d is assumed to be constant and is equal to the secondary dendrite arm spacing. In this study, the value of 'd' has been arbitrarily taken as 1×10^{-4} m.

2.3.3. Boundary conditions

Because of symmetry, the right-half of the annulus is chosen as the solution domain and the non-dimensional form of the boundary conditions are listed here:

[1]. At time, $\tau = 0$: $\quad h_i^* = \frac{C_P(T_i - T_S)}{\lambda}$

At time, $\tau > 0$:

[2]. On the inner cylinder surface, i.e., $R_i = 0.5$; U=V=0 ; $\quad h_W^* = \frac{C_P(T_W - T_S)}{\lambda}$

[3]. On the outer cylinder surface, i.e., $R_o = 1.3$; U=V=0 ; $\frac{\partial h^*}{\partial R} = 0$

[4]. Lower plane of symmetry; i.e., $\theta = 0$; U=0 ; $\frac{\partial V}{\partial \theta} = \frac{\partial h^*}{\partial \theta} = 0$

[5]. Upper plane of symmetry; i.e., $\theta = \pi$; U=0 ; $\frac{\partial V}{\partial \theta} = \frac{\partial h^*}{\partial \theta} = 0$

2.3.2. Governing parameters

Numerical simulations have been conducted by varying the various parameters associated with the model under consideration. The basic governing parameters of the system include Rayleigh number (*Ra*), wall Stefan number (Ste_w), radius ratio of the annulus (R_0/R_i), initial sub-cooling parameter (initial Stefan number, Ste_i), and Prandtl number (*Pr*). The parameters, such as Ra, Ste_w, and Pr appear in the non-dimensional governing equations. The radius ratio of the annulus and Ste_w appear in the boundary conditions. For the initial condition, the initial sub-cooling parameter, Ste_i, appears in the modeled equations. For all the production runs reported here, the Pr is assigned a value of 40.15, which corresponds to commercial paraffin wax used in this study. The ratio of the outer radius to the inner radius of the tubes is assigned a value of 2.6. The parameters, namely, Rayleigh number, wall Stefan number and initial Stefan number are varied.

2.3.3. Numerical solution procedure

In order to achieve the numerical solution, all of the partial differential equations have to be set in an algebraic form, this is called discretization. The discretized equations are derived by integration of differential equations over each control volume of the calculation domain by using an implicit time-step method [24]. The whole domain is described by a displaced or staggered grid system. Power-law difference scheme of Patankar [24] is used to discretize the convection-diffusion terms. Here, the SIMPLE algorithm, which stands for Semi-Implicit Method for Pressure-Linked Equations, has been employed for resolving the pressure-velocity coupling in the momentum equations [24]. A block correction procedure has been used to enhance the convergence of the solution procedure [25].

The discretized equations were solved iteratively using an implicit relaxation technique and by employing the well-known line-by-line Tri-Diagonal Matrix Algorithm (TDMA) solver until a converged solution was obtained for each time step. The termination of an iteration loop depended on the value of residuals for U, V, ∇ P and T at any instant of time. At every time step, the iterations were terminated when the relative change to maximum values of the absolute residuals at every grid points

for each calculated variable (R_Φ) was less than 10^{-5}. Mathematically, the convergence criterion described above can be defined as follows:

$$R_\Phi = \left| \frac{\Phi^{k+1} - \Phi^{k}}{\Phi^{k}_{Max}} \right| \qquad (18)$$

where, k in the number of iterations. In the present study, much effort has been paid to find the relevant under-relaxation factors. Various combinations of under-relaxation factors were examined and after numerous runs for energy, and other variables under-relaxation factors were selected as 0.3.

2.0. Code validation

Before embarking on a detail parametric study, the developed code was validated with the experimental study of melting of pure gallium in a rectangular cavity with two thermally active vertical walls carried out by Gau and Viskanta [26]. The latter authors graphically provided among other quantities the liquid-solid interface positions for some specific instants of the melting time. The thermophysical properties of pure gallium metal were taken from Brent et al., [27]. Figure 3 shows the present predictions of the interface positions for three-time instants, namely 5 min, 10 min and 19 min and the experimental results of Gau and Viskanta. Also, in Fig. 3, the numerical predictions of the interface positions of the same melting problem by three other group of investigators [28-30] are shown. The comparison of the various numerical methods used by other listed authors in the figure shows that for 5 min and 10 min the predictions compare favorably with the experimental results but for 19 min the numerical predictions differ significantly among other authors compared to the present authors. The present results show a very good agreement with the experimentally measured data for 5 and 10 min. There is alittle discrepancy at the bottom and the top part of the cavity for the melting time of 19 min. At the middle of the domain for the aforementioned melting time the present predictions show very favorable results with respect to the experiments results. The above discrepancy at the lower and upper regions for 19 min could be due to the heat losses during the experiments in those regions and for the accompanied experimental uncertainty. Also, numerical uncertainty, numerical grid generation method, application of the enthalpy-porosity scheme which is an indirect scheme for tracking the solid/liquid interface, the employment of artificial mushy region for the pure metal in the enthalpy-porosity method, value of the mushy region morphology constant C, etc. could be the other factors responsible for the discrepancies. In Fig. 4, the predicted temporal progression of the liquid-

solid interface during melting of pure gallium in the cavity is presented for the sake of better visualization of the present results.

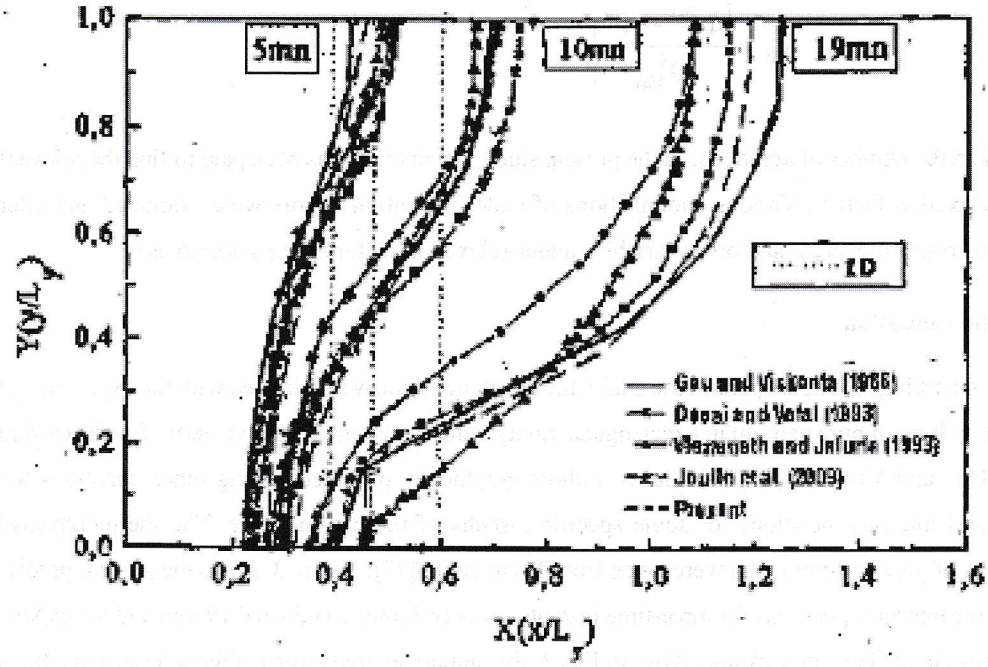

Fig. 3. Comparison of liquid-solid interface movement of pure gallium inside a rectangular cavity.

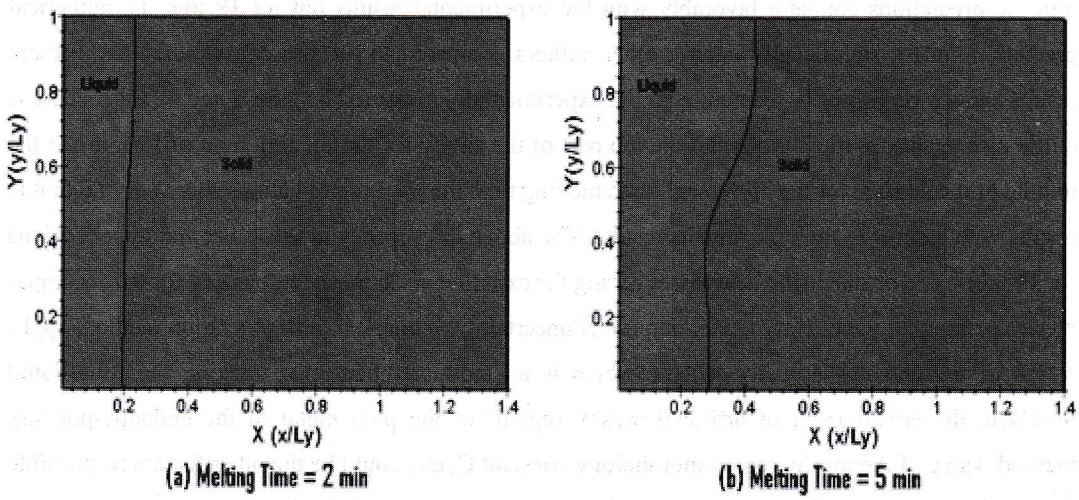

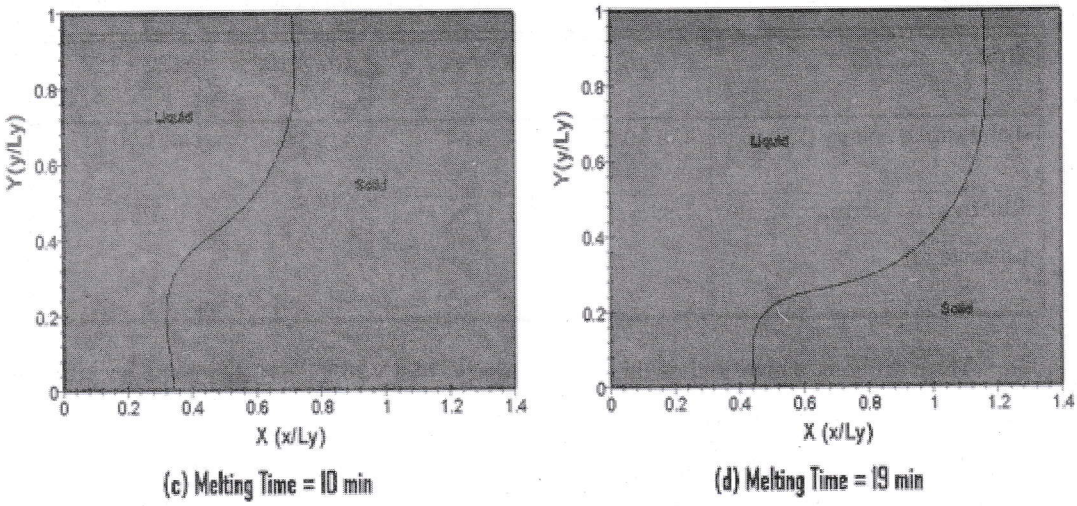

Fig. 4. Predicted liquid-solid interface movements of pure gallium inside a rectangular cavity for melting time of: (a) 2 min, (b) 5 min, (c) 10 min and (d) 19 min.

2.0. Grid and time independent tests

The grid and time independent tests were carried out for the transient melting problem for the impure PCM and the studied geometry as shown in Fig. 2. The total cumulative energy stored during the melting process in the domain for a total time of 41.18 min was used as a verification criterion. Four grid distributions were selected for the tests. The grid points were 62×62, 82×82, 102×102, 122×122, where the first number represents the number of grid points in the r -direction and the second number represents the number of grid points in the θ-direction. The grid independent tests were carried out for the constant inner cylinder wall temperature of 69.9^0C and the corresponding Rayleigh number, and Stefan number were 1.09×10^6, and 0.2116, respectively. The non-dimensional time step was taken as 5.0×10^{-4}, which corresponds to the dimensional time of 6.2 seconds. The initial temperature of the solid PCM was taken as 41.2^0C which translated to a sub-cooling parameter (initial Stefan number, Ste_i = -0.113). As can be seen from Table 2 that less than 2% differences in the total stored energy were found with respect to the highest number of grid points during the melting process. To lend credibility in the results and for the sake of numerical accuracy, the grid system having 122×122 grid points was chosen for all production runs.

Table 2. Grid independent tests on the cumulative total stored energy for time, t = 41.18 min

Grid	62×62	82×82	102×102	122×122
Total stored energy (kJ/m)	430.10	426.64	425.36	421.70
Relative error (in percentage)	1.99%	1.17%	0.87%	0.0%

Three different dimensionless time steps, namely, 1.25×10^{-4}, 2.5×10^{-4}, and 5.0×10^{-4} were tested for the time step independent test. A B-type staggered grid mesh having 122×122 grid points were used to discretize the governing equations. Other parameters were kept identical as used in the grid independent tests. The total cumulative stored energy in the annulus for an elapsed dimensional time of 41.18 minutes was selected as a basis for the time-step independent tests. The tests results are shown in Table 3. Only about 3 % variations in results were obtained for a nondimensional time step of 2.5×10^{-4} compared to the higher dimensionless time step of 5.0×10^{-4}. For the sake of the computational economy and costs, all simulation runs were carried out using the time step of 5.0×10^{-4}. Detailed grid and time independent tests were reported in Tabassum [31].

Table 3. Time-step independent tests on the cumulative total stored energy for time, t = 41.18 min

Time step non-dimensional ($\Delta\tau$) / dimensional (Δt)	1.25×10^{-4} / (1.55 sec)	2.5×10^{-4}/ (3.1 sec)	5.0×10^{-4}/ (6.2 sec)
Total stored energy (kJ/m)	425.33	409.50	421.70
Relative error (in percentage)	0.86%	2.89%	0.0%

2.0. Definitions of various quantities

In the present study, since phase change of a commercial PCM is the main concern, the volume of melted liquid is evaluated by summing the volume fraction of the melt in every cell in the liquid phase and in the partially melted mushy zone at each time step. For the above calculations, correct identification of the mushy region is important to accurately account for the liquid fraction in that region. Because of the existence of the mushy region, the total liquid fraction can be derived as follows:

$$\text{Total liquid fraction} = \frac{\text{Total volume of liquid}}{\text{Volume of the annulus}}$$

$$\text{Total volume of liquid} = \sum_{i=1}^{n} f_i CV_i$$

$$f_i = \frac{\text{Volume of liquid in the i}^{\text{th}}\text{ cell}}{(\text{Volume of liquid} + \text{Volume of solid})\text{in the i}^{\text{th}}\text{ cell}}$$

Here, 'n' represents the total number of control volumes in the computational domain.

The maximum stored energy within the annulus can be evaluated from the following expression:

$$Q_{\max} = \int_{T_{Initial}}^{T_{Solidis}} m_{PCM} C_P(T)dT + \int_{T_{Solidus}}^{T_{Liquidus}} m_{PCM} C_P(T)dT + m_{PCM}\lambda$$

$$+ \int_{T_{Liquidus}}^{T_{Wall}} m_{PCM} C_P(T)dT \quad \text{.....(19)}$$

It is to be noted that the PCM used here has a Prandtl number of 40.15 and the mass of this PCM (M_{PCM}) for the half of the annulus is 2.859 kg when the length of the tube is assumed to be one meter.

The local Nusselt number at the surface of the inner tube is calculated from the following equation.

$$Nu_{L\ at\ r=r_i} = \frac{h(\theta)r_i}{k}; \qquad \text{where,} \qquad h(\theta) = \frac{q_w}{T_w - T_{ref}};$$

$$q_{w\ \text{at}\ r=r_i} = -k\frac{\partial T(r_i, \theta)}{\partial r} \quad \text{.....(20)}$$

The circumferential average Nusselt number on the inner tube is calculated from:

$$\overline{\mathrm{Nu}}_{avg}\ \text{at r=r}_i = \frac{\int_0^L\int_0^\pi (Nu_L)_{r=r_i} r_i d\theta dZ}{\int_0^L\int_0^\pi r_i d\theta dZ} \quad \text{.....(21)}$$

It is to be noted here that in all the above expressions, the solidus temperature of the PCM is considered as a reference temperature. The details derivations of the above quantities can be found in Ref. [31]. The definition of the initial sub-cooling parameter is as follows:

$$St_i = \frac{C_P(T_{initial} - T_S)}{\lambda_{PCM}} \quad \text{.....(22)}$$

2.0. Results and discussion

For easy reference, Table 4 lists the pertaining process parameters for the studied cases. In this study, three governing parameters are varied which are the Rayleigh number, wall Stefan number and the initial Stefan number. Three inner cylinder wall temperatures and two initial thermal conditions of the solid PCM are selected. For the modeled PCM, three Rayleigh numbers (Ra), namely, 1.09×10^6, 1.38×10^6 and 1.67×10^6 are obtained for three inner cylinder wall temperatures of 69.9°C, 74.9°C, and 79.9°C, respectively. The corresponding three wall Stefan numbers are 0.2116, 0.2682, and 0.3248. The two initial Stefan numbers are $Ste_i = 0$, (for $T_i = 51.2$°C) and $Ste_i = -0.113$ (for $T_i = 41.2$°C) and they represent the saturated and sub-cooled conditions of the initial solid PCM, respectively. In this section, the effect of the above process parameters will be presented and discussed in detail. Because of the vertical symmetry along the $\theta - axis$, a right-half of the domain is simulated. By mirror imaging the results of the simulated half, the results for the entire cross-section could be easily obtained.

Table 4. Computational cases studied (Pr = 40.15, diameter of the inner cylinder, $D_i = 0.04$ m).

Case	Initial temperature of PCM (T_i) (^oC)	Inner tube wall temperature (T_W) (^oC)	$\Delta T = (T_W - T_{Solidus})$ (^oC)	Rayleigh number (Ra)	Stefan number (Ste_w)	Melting time (t) (min)
1	51.2	69.9	18.7	1.09×10^6	0.2116	t = 20.59, t = 41.18, t = 61.78, t = 82.37
2	51.2	74.9	23.7	1.38×10^6	0.2682	
3	51.2	79.9	28.7	1.67×10^6	0.3248	
4	41.2	79.9	28.7	1.67×10^6	0.3248	

6.1. Temperature field

For case-1 the temperature contours in a flooded format within the right half of the cross-section of the annulus are shown in Figs. 5(a-d) for four different time instants. The blue color region corresponds to the mixed zone of liquid-solid which is located between the two isotherms of 59.9^{0}C (liquidus temperature) and 51.2^{0}C (solidus temperature). Above the liquidus isotherm, the regions show the melted PCM. During the early stage of the melting process heat conduction dominates the heat transfer and a circular shape of the temperature contour is formed at the outer surface of the inner cylinder wall (Figs. not shown here). As melting time progresses, more solid PCM turns into liquid as a result, the natural convection starts to intensify. As the isotherms begin to follow the inner cylinder wall boundary, it starts to separate from the inner cylinder surface and deviate from the concentric ring patterns to form a pear-shaped melted region, indicating that convection begins to affect the melting process. The small plume originating from the top of the inner tube has frequently been observed during the melting experiments for a pure PCM around the horizontal cylinders by others [32]. It is to be noted here that a similar type of temperature profiles in the melt of a pure PCM in a concentric horizontal annulus around a circular inner cylinder was experimentally observed by Bathelt et al., [33] for the natural convection melting problem.

The separation of the isotherms from the inner cylinder wall indicates that the heat transfer between the melt and the inner wall decreases smoothly. Since the melting temperature is lower than the inner cylinder wall temperature and the isothermal boundary condition is imposed on the inner cylinder surface, the larger temperature difference between the melt and the heated surface results in a larger heat transfer rate near the lower portion of the inner cylinder wall. The concentrated temperature contours on the lower part of the inner cylinder wall indicate that the maximum heat transfer rate occurs in this part. As the melt moves upward along the inner cylinder wall, the melt is being heated up. The temperature difference between the wall and the melt is reduced gradually during upward movement of the melt and as a consequence the heat transfer rate decreases. Convective current leads to the movements of the isotherms outward from the inner cylinder wall and thereby distorting the isotherms in the upper part of the annulus. While going down from the top of the annulus to bottom, the pear-shaped isotherms start to turn to become horizontal in shape suggesting that the convection has been replaced by the conduction mode of heat transfer. At the lower part of the annulus, the heat transfer is controlled predominantly by conduction for all the four-time instants as shown in Figs. 5(a-d), and this conduction mode of heat transfer is further aggravated by the low thermal conductivity of the PCM. Looking at the point of onset of melting inside the annulus [Figs. 5(a-d)], it can be seen that as time progresses from 41.18 min to 82.37 min, the mushy layer remains practically stagnant at the lower portion of the annulus ($\theta \sim 450$).

As a result, the melting rate in the bottom region (θ~45^0) is significantly slower than any other regions within the annulus.

The reason behind this is that the most of the charged energy is transferred to the top of the annulus by the convective flow which gradually thermally stratifies the top part of the annulus. A similar phenomenon has been reported by other researchers in the literature during melting of a pure PCM within horizontal concentric cylinders [34]. This state of affair is not beneficial for energy storage since only sensible energy, which is much less compared to the latent energy, is stored after the threshold time of 41.18 min. It is well known that the melting rate is augmented with the increase of the Rayleigh number. In the present study, the effect of two other higher values of Rayleigh numbers has been studied which is listed as case 2 and case 3 in **Table. 4.**

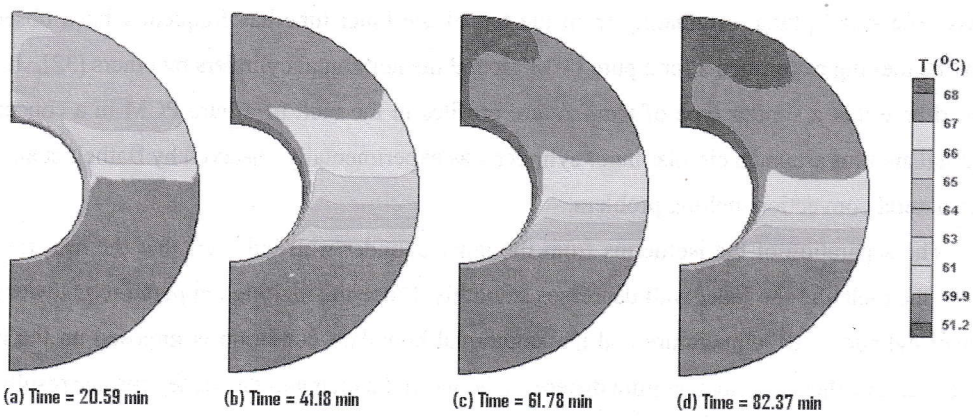

Fig. 5. 2-D temperature contours during melting for the wall temperature of 69.9°C and initial temperature of 51.2°C for four different time instants for case 1.

Figures 6(a-d) display the transient progression of the temperature distributions in the half of the annulus for case-2. As the inner tube wall temperature is enhanced by 5 ^oC compared to case-1, the progress of the melt front in the top region is greatly enhanced. For example, at 41.18 min, the 67^oC isotherm for case 1 is at the top of the annulus at ~1700 (refer to Fig. 5(b)) whereas for case 2 the same isotherm for the same time instant has appeared as a horizontal line at the lower part of the annulus at θ~700 which is seen in Fig. 6(b). It is evident from these figures that melting rate enhances with the increase of Rayleigh number. Next, the attention is turned to the lower part of the annulus. From Figs 6(b-d) it is observed that after the time of 41.18 min, due to conduction dominated heat transfer in the bottom region, the mushy region, represented by the blue color, is practically stagnant. At this stage, the qualitative features of the locations of the mushy zone appear to be the same as in

case 1. Thus, it shows that the conduction dominated bottom regime of the annulus remains unaffected after the threshold time of 41.18 min even for a higher Rayleigh number of 1.38×10^6.

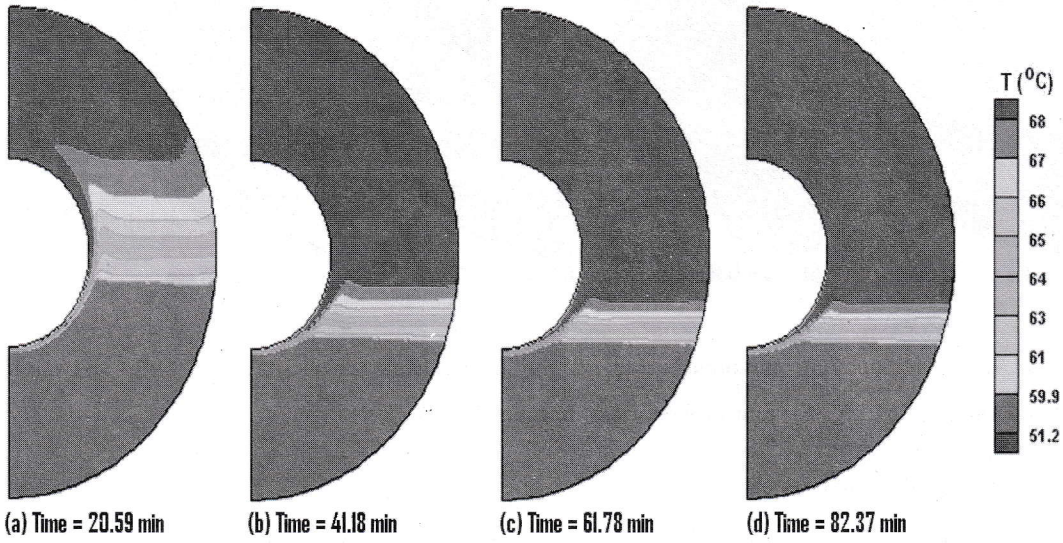

Fig. 6. 2-D temperature contours during melting for the wall temperature of 74.9°C and initial temperature of 51.2°C for four different time instants for case 2.

The temperature fields for case 3 are given in Figs. 7(a-d) for four-time instants. Compared to case 1 when the inner cylinder wall temperature is enhanced by 10^0C, an accelerated melting occurs in the very top region and the melting rate is the greatest compared to the cases 1 and 2. This is due to the fact that for the higher wall temperature there exists a high-temperature gradient in the melt for the same time instant compared to the other two cases. It thus follows that the intensed convection current in the liquid region for this case. Although the Rayleigh number for this case is the greatest among the three cases studied, the mushy region, which is bounded by the liquidus (59.9^0C) and solidus (51.2^0C) isotherms, seem to remain practically at the same locations due to conduction-controlled zone prevailing in that region which can be seen from Figs. 7(a-d). The latter region is very similar to cases 1 and 2. The increasing inner cylinder wall temperature has not altered the extent of the mushy region at the bottom part after the threshold time of 41.18 min.

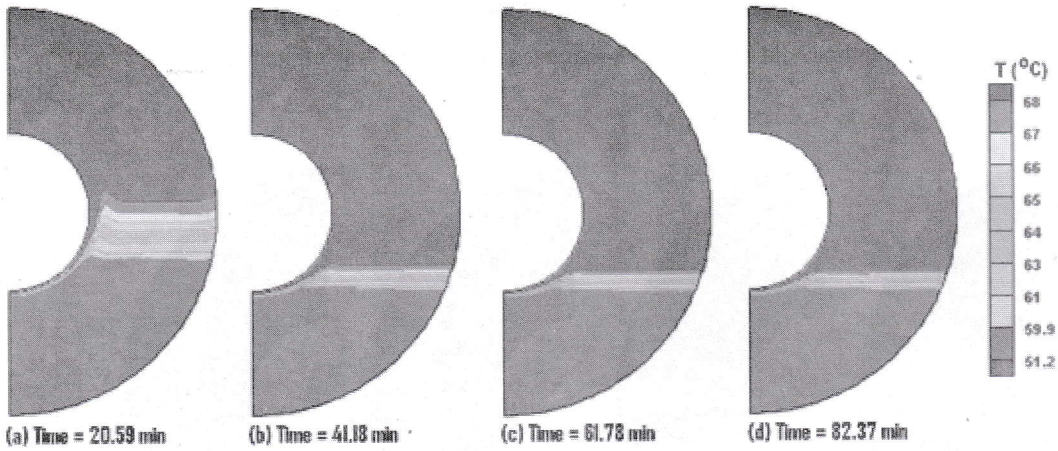

Fig. 7. 2-D temperature contours during melting for the wall temperature of 79.9°C and initial temperature of 51.2°C for four different time instants for case 3.

6.2. Quantitative analysis

6.2.1. Average Nusselt number ($\overline{Nu}_{avg}$) for cases (1-3) of Table 4 for $Ste_i = 0$

Figure 8 shows the variations of surface-averaged Nusselt number ($\overline{Nu}_{avg}$) for cases (1-3) of **Table.4** as a function of melting time for the initial temperature of 51.2 ^{O}C of the solid PCM. The $\overline{Nu}_{avg}$ is calculated by using Eq. (21) given in Section 5. This figure shows that the average Nusselt number decreases linearly with a sharp negative slope upto the melting time of 41.18 min for all the three cases (1-3) due to the increased thermal convection therein. Later, the average Nusselt number decreases rather slowly as the melt progresses towards the stratified condition. The reason for this trend of $\overline{Nu}_{avg}$ with time corroborates the temperature profiles discussed in the previous paragraph.

The average Nusselt number increases with the increase in Rayleigh number. The higher wall temperature introduces more heat that accelerates more convective flow in the annulus (at the top half part of the annulus), as well as it enhances the mixing of the hot and cold melt therein which resulted in the increase of heat transfer rate and thermal gradient.

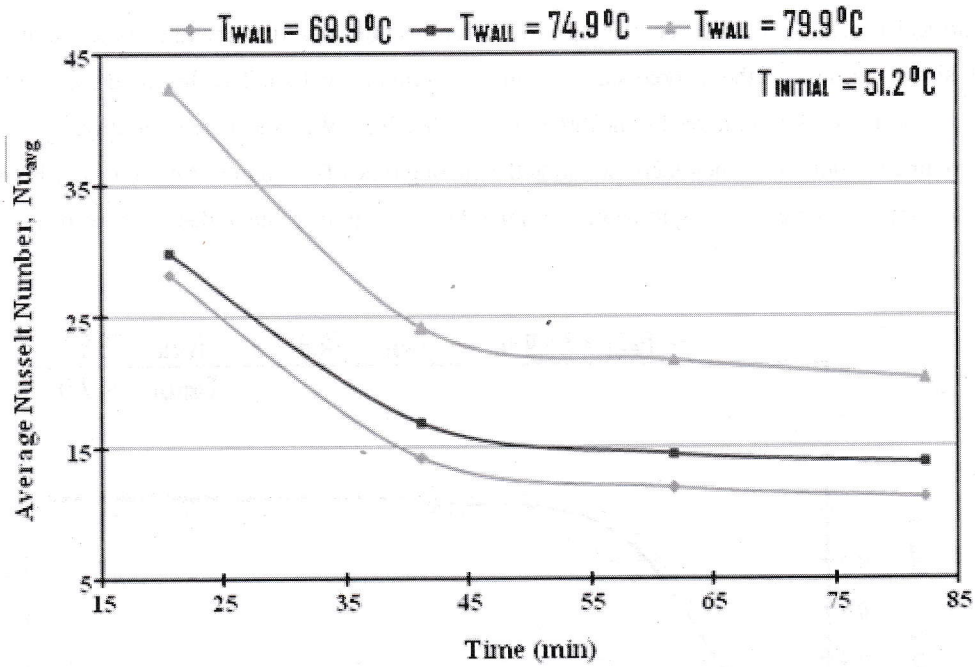

Fig. 8. Comparison of the variation with time of the average Nusselt number on the inner circular tube surface for cases (1-3) at Ti = 51.2oC for three wall temperatures of 69.9°C, 74.9°C, and 79.9°C.

6.2.2. Transient evolution of melt fraction (f_L) and the total stored energy for cases (1-3) of Table 4 for Stei = 0

In order to assess the overall role of convection in the melting process, the total liquid volume fraction and the total stored energy for three cases (1-3) are plotted in Figs. 9 and 10, respectively. The numerical calculation procedure for the total melt volume fraction and the total stored energy are all given in Section 5. From Fig. 9, it can be seen that the cumulative total melt fraction increases as the melting time increases for all the three cases as expected. At any instant of time, the slope of a graph indicates the melting rate. The sharp increase in the slope of the graph at the beginning of the melting is observed for all the three cases. After a certain time, the sharpness of the graph decreases. This happens due to conduction and convection induced melting process. With time, as the melt gets heated the temperature difference between the inner cylinder wall and the melt reduces. As a result, the heat transfer rate from the inner cylinder to the melt also decreases. At this stage of the melting process, the natural convection is suppressed remarkably. With the further progression of time the melting rate of the PCM is greatly reduced, which can be seen from the flattening nature of the curves in the figures for all the three cases. Because in this stage the heat exchange process is getting close to the thermal

equilibrium state. It can be concluded that the melting proceeds efficiently in a concentric cylindrical annulus up to a certain melting time. After this threshold time the rate of melting increases very slowly because of the marked suppression of natural convection. The threshold melting time is found to be about 41.18 minutes for the three cases studied here. With the increase in Rayleigh number, the volume fraction of the melt increases up to the melting time of 41.18 min. After this transition time, the melt fraction increases insignificantly with the Rayleigh number due to thermal stratification.

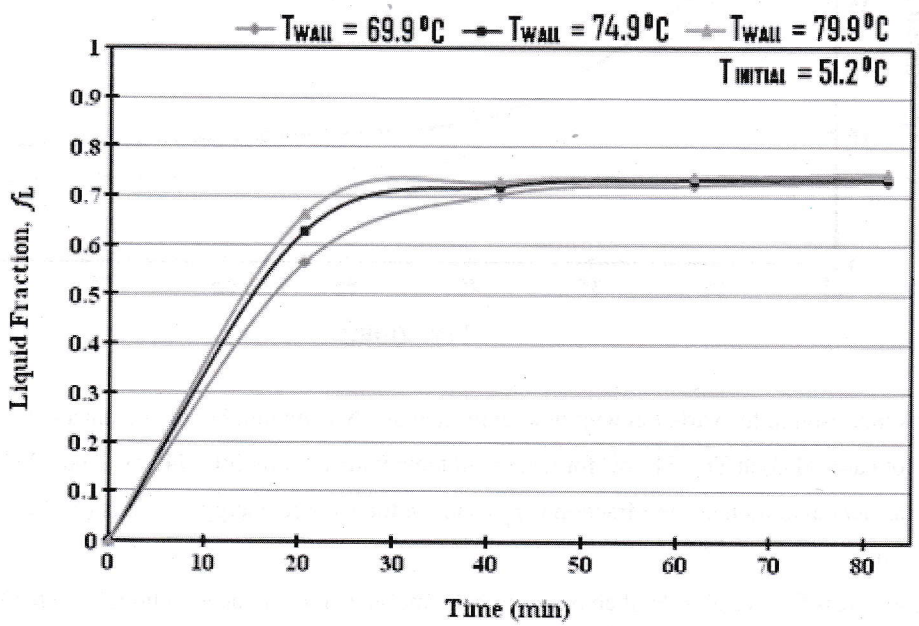

Fig. 9. Comparison of the variation with time of the cumulative total liquid fraction in the annulus for cases (1-3) at Ti = 51.2°C for three wall temperatures of 69.9°C, 74.9°C, and 79.9°C.

An inspection of Fig. 10 reveals that during the first half of the melting process as the melting time progresses the total stored energy all increases rapidly. After that elapsed time, the rate of increase of the charged total stored energy begins to slow down. The reason behind this phenomenon is explained in the previous paragraph. To understand the above statement, a quantitative comparison of the stored energy in percentage is given below against the charging time. From Fig. 10, it is seen that for case 1, at the melting time of 61.78 min, the total stored energy is 458.45 kJ/m, which in comparison to the melting time of 82.37 min, is only 1.05 % less. Whereas at the threshold time of 41.18 min, the total stored energy is 444.71 kJ/m, which in comparison to the lower melting time of 20.59 min, is

about 21.85 % higher and in comparison to the higher melting time of 61.78 min, it is only 3.09 % lower.

For cases 2 and 3, at the melting time of 61.78 min, the total stored energies are 481.87 kJ/m and 503.08 kJ/m (refer to Fig. 10), respectively which in comparison to the melting time of 82.37 min, is only 0.79 % and 1.03 % less, respectively. Whereas, at the threshold time of 41.18 min, the total stored energies are 471.45 kJ/m and 494.41 kJ/m, which in comparison to the lower melting time of 20.59 min, are about 15.08 % and 12.23 % higher and in comparison to the higher melting time of 61.78 min, they are only 2.21 % and 1.75 % lower, respectively for case 2 and for case 3.

It has been found that for $1.09 \times 10^6 \leq Ra \leq 1.67 \times 10^6$, the influence of the Rayleigh number on the amount of energy storage after this threshold melting time (t = 41.18 min) is insignificant for all the three cases because at the later time period the heat transfer process is predominantly dominated by the conduction mode of heat transfer and mostly sensible energy is stored. With the increase of Ra, the rate of enhancement of the total amount of stored energy has decreased because at higher wall temperature the melt goes to thermally stratified condition earlier compared to the lower wall temperature. Thus, less amount of sensible energy is stored for the higher Ra compared to the lower Ra.

From the above quantitative analysis, it can be concluded that for the studied LHTES unit it is not beneficial to store energy beyond the threshold melting time of about 41.18 minutes since after this time mainly sensible heat storage takes place.

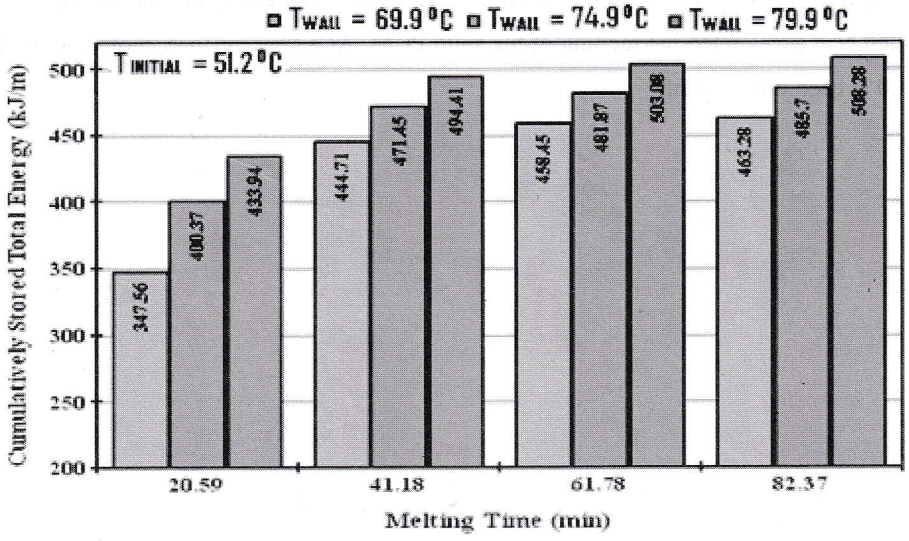

Fig. 10. Comparison of the variation with time of the cumulatively stored total energy in the annulus for cases (1-3) at T_i = 51.2°C for three wall temperatures of 69.9°C, 74.9°C, and 79.9°C.

6.2.3. A Comparison of the temperature contour and on the total cumulative stored energy between $Ste_i = 0$ (Case 3) and $Ste_i = -0.113$ (Case 4)

From a more practical point of view, it is also interesting to determine the influence of the degree of initial sub-cooling of the PCM during the melting process. For this purpose, the Ste_i is only changed assigned a value of -0.133 (10^0C sub-cooling) which is denoted as case 4 where all other parameters are kept fixed as case 3. The initial Stefan numbers are calculated by using Eq. (22) given in Section 5. Figures 11(a-d) illustrate the temperature distributions in the right half of the annulus for $Ste_i = -0.133$, for four-dimensional times and for $Ra = 1.67 \times 10^6$. Upon examination of the results for this case and that of the corresponding case presented in Figs.7(a-d) for case 3, it can be concluded that the thermal fields are very similar for both of these two cases. The only differences are in the local positions of the temperature contours and the length of the mushy region for the two cases. For $Ste_i = 0$, a thicker mushy region formed, which is located near the lower part of the geometry, compared to the case for $Ste_i = -0.113$. A substantial amount of solid PCM is seen at the lower part of the annulus for $Ste_i = -0.113$ at the melting time of 82.37 min.

A comparison of the two initial Stefan numbers on the total cumulative stored energy (kJ/m) is given in Table 5. The quantitative results indicate that for the identical operating conditions and process parameters, with the increase in the initial temperature of the solid PCM, the total stored energy increases, this is true for each time instant. Compared to the case for Stei = - 0.113, in the case for Stei = 0, about 61.47 kJ/m sensible energy is saved which is required for the former case to achieve the solidus temperature for the calculation domain (half of the LHTES unit). For this reason, for Stei = 0, the supplied heat accelerated the melting of the solid PCM. As a consequence, more energy is stored for $Ste_i = 0$ at each time instant.

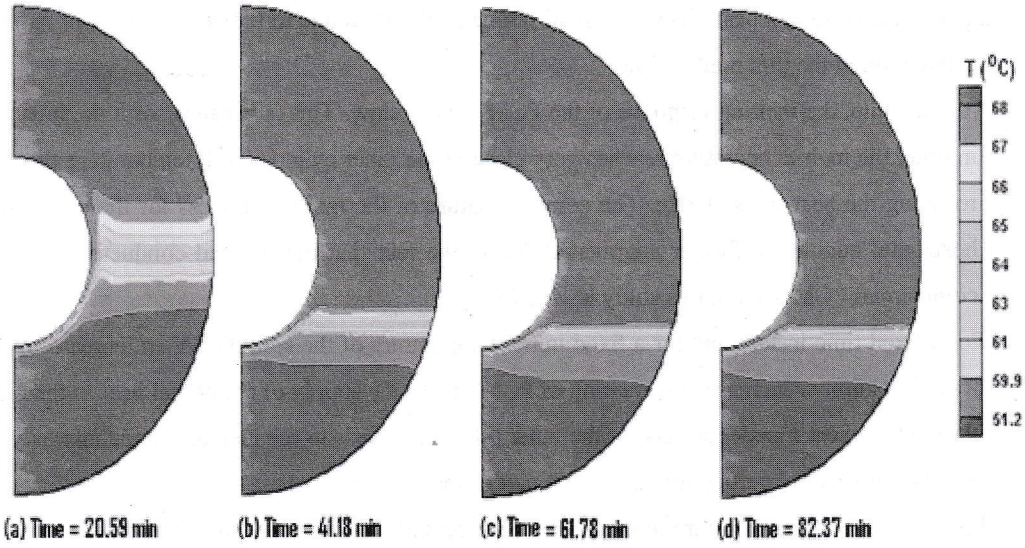

Fig. 11. 2-D temperature contours during melting for the wall temperature of 79.9°C and initial temperature of 41.2°C for four different time instants for case 4.

Table 5. The total cumulative stored energy (kJ/m) for case 3 ($Ste_i = 0$) and for case 4 ($Ste_i = -0.113$) for four different time instants

Total stored energy (kJ/m)	Melting time (min)			
	20.59	41.18	61.78	82.37
$Ste_i = 0$ (case 3)	433.94	494.41	503.08	508.28
$Ste_i = -0.113$ (case 4)	372.82	468.32	487.75	494.13

7.0. Concluding remarks

Based on the findings of the present numerical study of the combined conduction and buoyancy-driven melting of a commercial PCM within the annulus, the following conclusions can be made:

[1]. Initially, with the increase in melting time melting rate is enhanced in all the cases

[2]. As the buoyancy-driven convection is strengthened due to the growth of the melt zone, it is observed that melting in the top region of the annulus is much faster than other regions. Similar

to a single-phase system, a pear-shaped thermal plume is observed due to the development of natural convection in the thin melt region.

[3]. After a while, the melting response of the PCM is very slow. This is because, with the increase in time, the melt temperature reaches very close to the inner cylinder wall temperature thereby reducing the heat transfer rate. The complex nature of the melting process for the concentric horizontal annulus is further aggravated due to the fact that the thermal conductivity of the commercial PCM used in this study is very low.

[4]. For a fixed time instant and for a fixed initial temperature of the solid PCM, an increase in the Rayleigh number increases the melting of PCM due to the supply of additional heat to the melt through the heat transfer surface of the inner tube. This leads to the increase in the intensity of natural convection, particularly at the top part of the annulus.

[5]. For a fixed initial temperature of the solid PCM, the surface-averaged Nusselt number increases with the increase in the Rayleigh number. With the increase in the melting time, the average Nusselt number decreases with a sharp negative slope at the early stage of melting and then it decreases rather at a slower rate for all the three Rayleigh numbers. The sharp slope of the graph is due to the gradual attainment of the intensified natural convection and the slower decrease of the slope is the consequence of the thermal stratification in the melt.

[6]. For all the three Rayleigh numbers after a threshold time of about 41.18 min, the melting rate decreases significantly due to the progression towards the thermal equilibrium condition by the melt.

[7]. For a fixed elapsed time and for a fixed Rayleigh number, the cumulatively stored total energy is greater for the initial Stefan number, $Ste_i = 0$, compared to the case when the initial Stefan number is lower ($Ste_i = -0.113$). This is because, for $Ste_i = 0$, the melting starts right from the beginning and thereby more energy is stored in the form of latent heat without losing some sensible heat which is required to heat-up the subcooled solid to reach the solidus temperature.

From this study, it is observed that neither the increase in the melting time nor the enhanced Rayleigh number can increase the melting of the PCM especially at the bottom part of the annulus particularly after the melting time of about 41.18 min. To enhance the heat transfer performance in the above thermal storage system and to promote the practical utilization of solar energy, more work is needed to optimize a complex LHTES system. In Part-II, the predictions regarding the dynamic thermal performance of a LHTES unit is presented for the same geometrical configuration as Part-I by employing three longitudinal divergent fins at the bottom part of the inner cylinder.

Acknowledgments

This work is partially supported by the National Sciences and Engineering Research Council (NSERC) of Canada Discovery Grant RGPIN48158 awarded to M. Hasan of McGill University, Montreal, for which authors are grateful.

References

[1]. Dincer, I., and Rosen, M.(Editors), 2003, "Thermal Energy Storage Systems and Applications," Chap-7: Modeling of Latent Heat Storage Systems, New York, Wiley.

[2]. Lacoris, M., 1993a, "Study of the Heat Transfer Behavior of a Latent Heat Thermal Energy Storage Unit with Finned Tube," Int. J. Heat Mass Transfer, 36(8), pp. 2083-2092.

[3]. Lacroix, M., 1993b, "Numerical Simulation of a Shell and Tube Latent Heat Thermal Energy Storage Unit," Solar Energy, 50(4), pp. 357-367.

[4]. Padmanabban, P. V., 1986, "Outward Phase Change in a Cylindrical Annulus with Axial Fins on the Inner Tube," Int. J. Heat Mass Transfer, 29(12), pp. 1855-1866.

[5]. Zhang, Y., and Faghri, A., 1996, "Heat Transfer Enhancement in Latent Heat Thermal Energy Storage System by Using Longitudinally Finned Tube," Int. J. Heat Mass Transfer, 39(5), pp. 3165-3173.

[6]. Sari, A., and Kaygusuz, K., 2001, "Thermal Performance of Myristic Acid as a Phase Change Material for Energy Storage Application," Renewable Energy, 24, pp.303–317.

[7]. Sari, A., Kaygusuz, K., 2002, "Thermal and Heat Transfer Characteristics in a Latent Storage System Using Lauric Acid," Energy Conversion Manage, 43, pp.2493–2507.

[8]. Regin, A. F., Solanki, S. C., and Saini, J. S., 2008, "Heat Transfer Characteristics of Thermal Energy Storage System Using PCM Sapsules: A Review," Renewable and Sustainable Energy Reviews, 12, pp. 2438-2458.

[9]. Verma, P., Varun, and Singal, S. K., 2008, "Review of Mathematical Modelling on Latent Heat Thermal Energy Storage Systems using Phase-Change Material," Renewable and Sustainable Energy Reviews, 12(1), pp. 999–1031.

[10]. Agyenim, F., Hewitt, N., Eames, P., and Smyth, M., 2010, "A Review of Materials, Heat Transfer and Phase Change Problem Formulation for Latent Heat Thermal Energy Storage Systems (LHTESS)," Renewable and Sustainable Energy Reviews, 14, pp. 615–628.

[11]. Dutil, Y., Rousse, D. R., Salah, N. B., Lassue, S., and Zalewski, L., 2011, "A Review on Phase-Change Materials: Mathematical Modelling and Simulations," Renewable and Sustainable Energy Reviews, 15, pp.112–130.

[12]. Khan, Z., Khan, Z. A., and Ghafoor, A., 2016, "A Review of Performance Enhancement of PCM Based Latent Heat Storage System within the Context of Materials, Thermal Stability and Compatibility," Energy Conversion and Management, 115, pp.132–158.

[13]. Zhang, H., Baeyens, J., Caceres, G., Degreve, J., and Lv, Y., 2016, "Thermal Energy Storage: Recent Developments and Practical Aspects," Progress in Energy and Combustion Science, 53, pp. 1–40.

[14]. Khyad, A., Samrani, H., and Bargach, M. N., 2016, "State of the Art Review of Thermal Energy Storage Systems using PCM Operating with Small Temperature Differences: Focus on Paraffin," Journal of Materials and Environmental Science, 7(4), pp.1184-1192.

[15]. Hasnain, S. M., 1998, "Review on Sustainable Thermal Energy Storage Technologies, Part 1: Heat Storage Materials and Techniques," Energy Conversion and Management, 39(11), pp. 1127-1138.

[16]. Sohns, J., Seifert, B., and Hahne, E., 1981, "The Effect of Impurities on the Melting Temperature and the Heat of Fusion of Latent Heat Storage Materials," International Journal of Thermophysics, 2(1), pp.1-7.

[17]. Farid, M. M., Khudhair, A. M., Razack, S. A. K., and Al-Halliaj, S. A., 2004, "A Review on Phase Change Energy Storage Materials and Applications," Energy Convers. Manage., 45, pp. 1593-1615.

[18]. Voller, V. R., 1990, "Fast Implicit Finite Difference Method for the Analysis of Phase Change Problems," Numerical Heat Transfer, Part. B, 17, pp. 155-169.

[19]. Voller, V. R.; Swaminathan, C. R., and Thomas, B. G., 1990, "Fixed Grid Techniques for Phase Change Problems: A Review," Int. J. Num. Methods in Eng., 30(4), pp. 875-898.

[20]. Date, A. W., 1991, "A Strong Enthalpy Formulation for the Stefan Problem," Int. J. Heat Mass Transfer," 34(9), pp. 2231-2235.

[21]. Savnarskil, A. A., Vabishcherich, P. N., Iliev, O. P., and Ghurbanov, A. G., 1993, "Numerical Simulation of Convection/Diffusion Phase Change Problems: A Review," Int. J. Heat Mass Transfer, 36(17), pp. 4095-4106.

[22]. Voller, V. R., and Prakash, C., 1987, "A Fixed Grid Numerical Modelling Methodology for Convection-Diffusion Mushy Region Phase-Change Problems," Int. J. Heat Mass Transfer, 30, pp. 1709-1719.

[23]. Minakawa, S., Samarasekera, I. V., and Weinberg, F., 1987, "Centerline Porosity in Plate Castings," Metall. Trans., 16B, pp. 245-255.

[24]. Patankar, S. V., 1980, "Numerical Heat Transfer and Fluid Flow," Hemisphere/Mc-Graw-Hill, Washington.

[25]. Patankar, S. V., 1991, "Computation of Conduction and Duct Flow Heat Transfer," Innovative Research, Inc., Minneapolis, Minn.

[26]. Gau, C., and Viskanta, R., 1986, "Melting and Solidification of a Pure Metal in a Vertical Wall," Transaction of the ASME Journal of Heat Transfer, 108, pp.174-181.

[27]. Brent, A. D., Voller, V. R. and Reid, K. J., 1988, "Enthalpy-Porosity Technique for Melting Convection-Diffusion Phase Change: Application to the Melting of a Pure Metal," Numerical Heat Transfer, Part B; Fundamentals, 13, pp. 297-318.

[28]. Viswanath, R., and Jaluria, Y., 1993, "A Comparison of Different Solution Methodologies for Melting and Solidification Problems in Enclosures," Numerical Heat Transfer, Part B; Fundamentals, 14, pp. 77-105.

[29]. Desai, C. P., and Vafai, K., 1993, "A Unified Examination of the Melting Process within a Two-Dimensional Rectangular Cavity," Transaction of the ASME Journal of Heat Transfer, 115, pp.1072-1075.

[30]. Joulin, A., Younsi, Z., Zalewski, L., Rousse, D. R., and Lassue, S., 2009, "A Numerical Study of the Melting of Phase Change Material Heated from a Vertical Wall of a Rectangular Enclosure," International Journal of Computational Fluid Dynamics, 23, pp. 553-566.

[31]. Tabassum, T., 2010, "A Numerical Study of a Double Pipe Latent Heat Thermal Energy Storage System," M.Eng. Thesis, Department of Mining and Materials Engineering, McGill University, Canada.

[32]. Viskanta, R., 1988, "Heat-transfer During Melting and Solidification of Metals," Journal of Heat Transfer, 110(48), pp. 1205-1219.

[33]. Bathelt, A. G., Viskanta, R., and Leidenfrost, W., 1979, "Latent Heat-of-Fusion Energy Storage: Experiments on Heat Transfer from Cylinders During Melting," Journal of Heat transfer, 101(3), pp. 453-458.

[34]. Li Z. and Wu, Z., 2015, "Analysis of HTFs, PCMs and Fins Effects on the Thermal Performance of Shell–Tube Thermal Energy Storage Units," Solar Energy, 122, pp. 382–395.

Reasons of Labor Dispute and Role of BGMEA, Industrial Police & Labor Union in disputes settlement procedure – a study from Bangladesh RMG industry units of Dhaka & Gazipur

Md. Al Amin Molla*[1], Md. Bany Amin Mollah [2]

[1,2] Department of Business Administration, Sonargaon University (SU)

*Corresponding Author: [1]Associate Professor & Treasurer, Sonargaon University (SU)

Email: alaminsu2013@gmail.com

Abstract

The export oriented ready-made garments (RMG) industry of Bangladesh occupied a large portion of Bangladesh economy. It is the second largest foreign currency earnings sector of Bangladesh. However, labor disputes become a common phenomenon now days in this sector. Researchers have tried to identify the reasons behind the labor disputes in RMG sector and the role BGMEA, Industrial Police & Labor Union in dispute settlement procedure. There are many reasons behind the labor disputes, but dissatisfaction from existing salary & bonus, delayed in salary payment, mandatory overtime, long working hours, leave without pay, unsafe working environment, physical abuse of female workers, mainly causes the labor disputes in RMG in Bangladesh. The standard for dispute settlement procedure should be as per the "Labor Law Act – 2006". Researchers also tried to focus on what role BGMEA, Industrial Police & Labor Union play to dissolve the disputes in RMG sector in Bangladesh.

Keywords: Labor disputes, RMG sector, dispute settlement, Labor union, industrial police.

1.0 Introduction

Bangladesh is going to be middle-income country with a few large and some moderate size industries of different kind. Among these, the past growing ready-made garments (RMG) industries are the prospective one. Although the least developed countries (LDCs) policymakers have approached at various times to make the agriculture as the primary field of economic progress and employment creation, this attempt has not worked due to the rapid growth of globalization. Because of the globalized agrarian economy is dramatically shifting to industrial economy, Bangladesh could be the more honest model of it. Though Bangladesh was the member of LDCs now it is a Next 11 developing nation with a US$209 billion economy and a per capita income of US$1, 190 [1] its development is traced in recent time by shifting from agro based economy to an industrial economy. The export-oriented RMG sector has made vital role in this above-mentioned revolution of the Bangladesh

economy. The RMG sector has seen an exponential growth science the 1980s. Embarking on its journey in the late 1970s a very little investment, the industry flourished between 1980s and 1990s and become the biggest manufacture in Bangladesh. This sector contributes significantly to the Gross Domestic Product (GDP) of the land. 1980s, there were only 50 factories employed few thousand people currently there are 4296 manufacturing units employing 4 million people and 81.71% the export earnings come from this sector [2]. The contribution of RMG entrepreneurs, workers, experts, policymakers and time-to-time incentives from the government make this sector most significant for the economic growth of the country that is shown in several stories issued by the previous researchers. In spite of studying in an impressive public presentation, the RMG industry has several problems, especially in conditions of repeated conflict & unrest between workers and management. These unrests lead to believe that there exist industrial dispute between owners and proletarians. These could be for the several reasons like – minimum payment of wages, unjust payment of wages, asymmetrical and ill-timed payment of wages, unfair dismissal, and retrenchment, physical and verbal harassment, and discrimination on the grounds of sexual, gender, racial and spiritual aspects [3]. This causes the serious obstacles to the productivity and shipments of garments. It this state, the relationship between owners and workers turns into turmoil and trepidation and overall economic and social status of the country remain jeopardized. This is a serious threat to the topmost foreign currency-earning sector of Bangladesh.

2.0 Literature Review

Academic literature suggests that Industrial dispute may be defined as a disagreement between the employer and employees or between groups of workers. Industrial disputes are divided into two categories are i) due to economic causes and ii) due to political Causes. Siddiqua & Chowdhury [4] Studied on industrial relation and dispute settlement procedure in RMG sector of Bangladesh and identified two major reasons of industrial disputes- economic reason and non-economic reason. In addition, suggested three major steps to settle the disputes these are: negotiation, conciliation, and arbitration. Working condition in the RMG sector is very much volatile to international labor standards and Codes of Conduct [5]. In the RMG sector, female workers are considered low-skill, low workers such as helpers, machinists, finishing helpers and sewing controllers. It is rare to find that women working as cutting masters, production managers, supervisors, finishing and machine operators [6]. The government of Bangladesh must undertake and effective initiative to eliminate discrimination based on gender, particularly in the RMG sector where 90% of

the workers are women [7]. Recruitment policies in Bangladesh ready-made garments are highly informal compared to the western standards and mostly there are no written formal contracts and appointment letters. Therefore, employees are vulnerable to losing their jobs at any time. However, fear of losing their jobs and unsatisfactory employment compel to disputes and rises different labor unrest [8]. Ensuring social compliance is very important in the garment industries to both maintain quality of product as well as meeting the expectation of the export market. Ensuring social complacence is very important in the garment industries to both maintain quality of products as well as meeting the expectations of the export market. Mr. Ferrous [9] has investigated working conditions in the Bangladesh ready-made garments sector. It found the working conditions are poor and facing the challenges Social compliance, despite Bangladesh labor laws and the country's membership of the World Trade Organization (WTO) and the International Labor Organization (ILO). These include an inadequate application of labor standards and labor rights, law and enforcement, collective bargaining activities, fair labor practices as well as the government of Bangladesh and entrepreneur's role in implementing the decent work in the RMG sector. That raises the most of the labor unrest in Bangladesh ready-made garments; it suggested monitoring is needed to ensure compliance with these laws. Lastly, it suggested improved human resource management in RMG factories could ensure social compliance. To avoid unrest in the RMG sector, Khan [10] argued for strengthening social compliance issues and labor standards to improve wages, working hours, overtime, job security, the right to form trade unions, social security and also occupational health and safety of the workers. Several authors have analyzed various aspects of the garment industry in Bangladesh. Of the various aspects of the industry, the problems and the working conditions of workers have received the greatest attention, but dispute settlement procedure received a very few attention. That is, a few number researchers have studied on dispute settlement procedure. That is the reason I feel further need to study on reasons of deputes and its settlement procedure.

3.0 Objectives of the study

The primary objective of this study is to identify the reasons behind the disputes in ready-made garments industry unit of Bangladesh and find the way or procedure that helps to settable these disputes. Therefore, the objectives of the study are as follows:

a) To identify the reasons of disputes in RMG industry units of Bangladesh
b) To identify the role of BGMEA, Labor Union, Labor Administration & Industrial Police in dispute settlement in RMG industry units of Bangladesh.

4.0 Methodology

Possible sources of industrial disputes could be (a) wages, bonus & overtime, (b) working hours, (c) leave, (d) working environment, (e) victimization of women, (f) discrimination on different issues like; gender, age, gender, wage, bonus, leave, overtime etc. in this study it is assumed that overall dissatisfaction created from these factors causes labor disputes. Therefore, a questionnaire survey haven conducted on 96 garments workers from 10 different garment factories in Dhaka and Savar. Among the respondents, 85 were female and 15 were male. Questionnaire consists of 16 questions. A questionnaire has been prepared by considering the above mention factors (a-f). Five Points Likert type scales has been used to measure workers' opinions. The judgmental sampling procedure was used to select the sample units from different garments. A descriptive analysis like frequency distribution, percentage, bar chart, pie char have been used to present the analysis of the data. SPSS version 22 has been used to analyze the survey data.

Table 01: Type of Respondents

Type of Respondent	**Number of Respondents**
Cutter Man	9
Cutting Helper	11
Finishing Helper	7
Line In charge	7
Loader	9
Operator	15
Supervisor	5
Sewing Helper	33
Total	96

BGMEA, Labor Union & Industrial police also play a vital role in dispute settlement so the roles of these bodies were studied. Both the formal & informal interview methods have been used for conducting the interview.

4.1 Sources of Data

The study was conducted based on both secondary and primary data. Secondary data were collected from different websites like BGMEA, BKMEA as well as from the authentic reports and research; those have already been published from different journals. Secondary information was collected from online journal, article, and newspaper report published on the issue. After that, Primary data have been collected by conducting a survey and taking expert opinion. Data from Bangladesh Bureau of Statistics (BBS), Labor Force Survey (LFS), Bangladesh Institute of Labor Studies (BILS), Department of Labor extensively used for the purpose of this study.

5.0 Findings and Analysis

5.1 Contribution of RMG industry to the export earnings & GDP

Garments Industry occupies a unique position in the Bangladesh economy. It is the largest exporting industry in Bangladesh, which experienced phenomenal growth during last two decades. The industry plays a key role in employment generation and in the provision of income to the poor. Nearly four million workers are directly and more than ten million inhabitants are indirectly associated with the industry. The sector has also played a significant role in the socioeconomic development of the country. In such a context, the trend and growth of garments export and its contribution to total exports has been examined the following table shows the position.

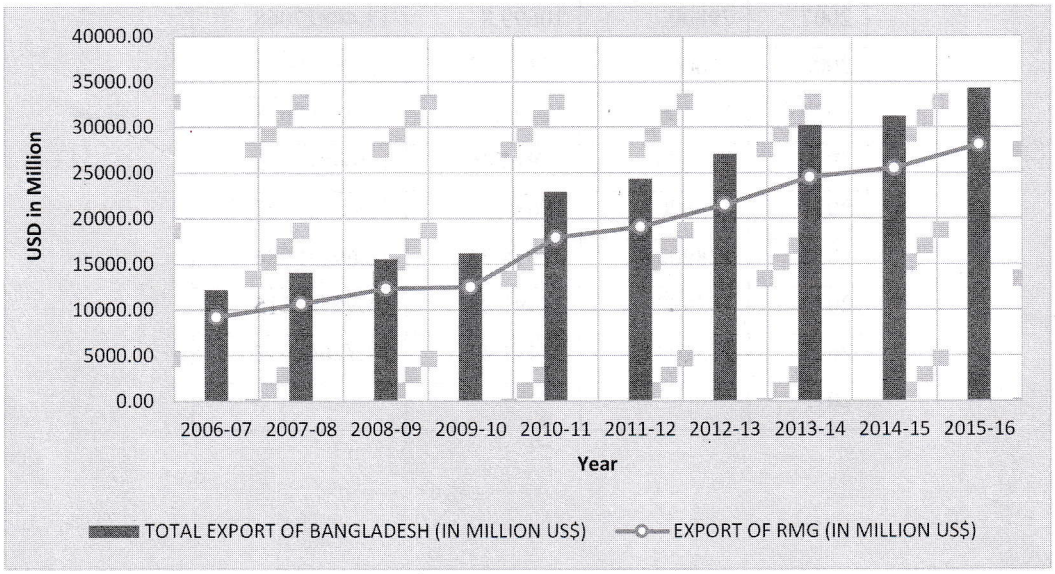

Fig. 01: Comparative Statement on Export of RMG and Total Export of Bangladesh [11]

Figure shows the continuous increase in the export earnings from RMG sector. In year 2001, it was 4859.83 million US Dollar where total export of Bangladesh was 6467.30 million US Dollar. That was 75.14% of total export earnings. It continues to increase and it reaches to 28094.16 million US Dollar in the year of 2015-16 that is 82% of total export earnings. In spite of various labor unrest, unexpected political instability, fire incident etc. our exponential RMG sector contributes to our export earning in a significant manner.

5.2 Contribution of RMG to GDP

Table 02: Contribution of RMG to GDP from the year 2000 to 2014

Year	Total GDP (in millions)	RGM Export (in millions)	RMG export of GDP (in %)
2000	45500	4859.83	10.68094505
2001	45400	4583.75	10.09636564
2002	47200	4912.09	10.40697034
2003	51700	5686.09	10.99823985
2004	55900	6417.67	11.48062612
2005	57600	7900.8	13.71666667
2006	70000	9211.23	13.1589
2007	79800	10699.8	13.40827068
2008	91600	12347.77	13.48009825
2009	102100	12496.72	12.23968658
2010	114500	17914.46	15.64581659
2011	123500	19089.69	15.45723887
2012	128900	21515.73	16.69179984
2013	153500	24491.88	15.95562215
2014	173100	25491.4	14.72640092
2015			

The **Table.2.** shows that in the year 2010 contribution of RMG sector was 10.68% and it continues almost in a same pattern up to 2003. An in the year 2004 it is increased to 11% and continues to increase still 2008. But in the year 2009 and 2013-2014 it fall down and decreases by 1.25% in 2009 and by 1.04% in 2013 as well as 1.13% decreases in 2014. One of the reasons for this decreasing growth rate could be that, there was huge political turmoil in 2009. Hortal in 2014 to 2015 and stopped the operation of 1654 factories in the year 2014. Reasons of labor disputes, In this part, the reasons of labor disputes have been identified. Therefore, I have analyzed the survey data collected from the primary sources and showed the finding by analyzing the collected data.

5.3 Descriptive Analysis of the study

Workers express their opinion in the Likert scale on whether they receive take as salary and bonus is satisfactory. Out of 96 respondents, 13% workers strongly agreed, 30% simply agreed, 3% demonstrated disagree and 54% workers state that they strongly disagree with the statement. That indicates that most the workers are not satisfied with existing salary & bonuses. Figure 02-12, Field Survey 2015, December [12]

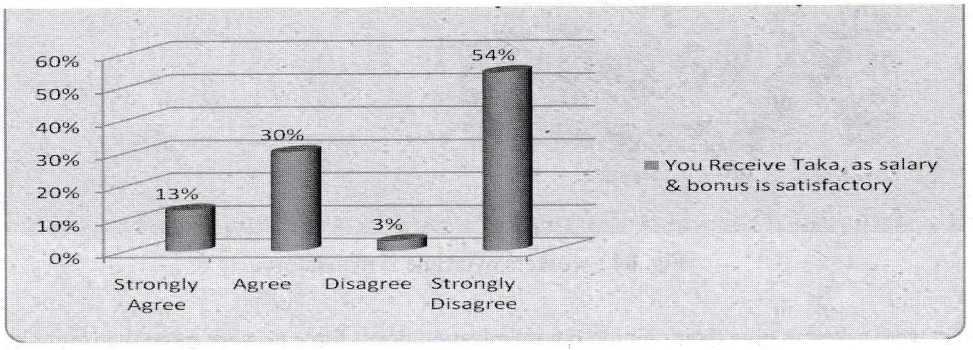

Fig. 02 : Worker receive, take, as salary is satisfactory

Garment workers were asked to give their opinion on whether salary is paid on time. About 3% of the respondent showed strongly agree, 16% were simply agree, 4% disagree rest of 77% of the respondents demonstrated that, they are strongly disagree with this statement. Therefore, it indicates that most of the cases, organizations do not pay salary on time.

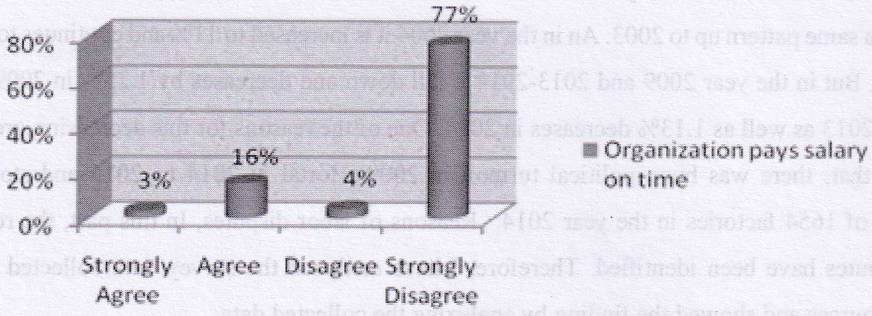

Fig. 03: Organization pays salary on time

Out of 96 respondents, 84% strongly with the statement that workers' overtime is mandatory and only 16% were agreed with the statement. Therefore, it is clear that most of the organization force worker to overtime and they do not take into consideration of the employees' mental satisfaction.

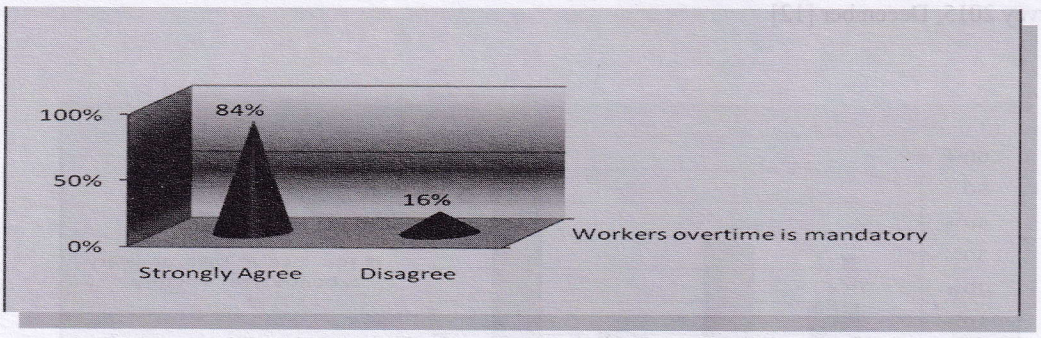

Fig. 04 : workers overtime is mandatory

Workers were asked to give their opinion on organization never force to work more than eight hours a day without overtime. Among them 55% of the respondents showed they are strongly disagree with this statement. 22% were disagreed & only 10 % of the respondents were strongly agreed with this statement. About 5% were neutral. Therefore, it is clear from a statement they have to work more than eight hours without overtime. Therefore, it is the violation of the labor law Act 2006 and it can be stated that work without overtime may also causes for labor disputes.

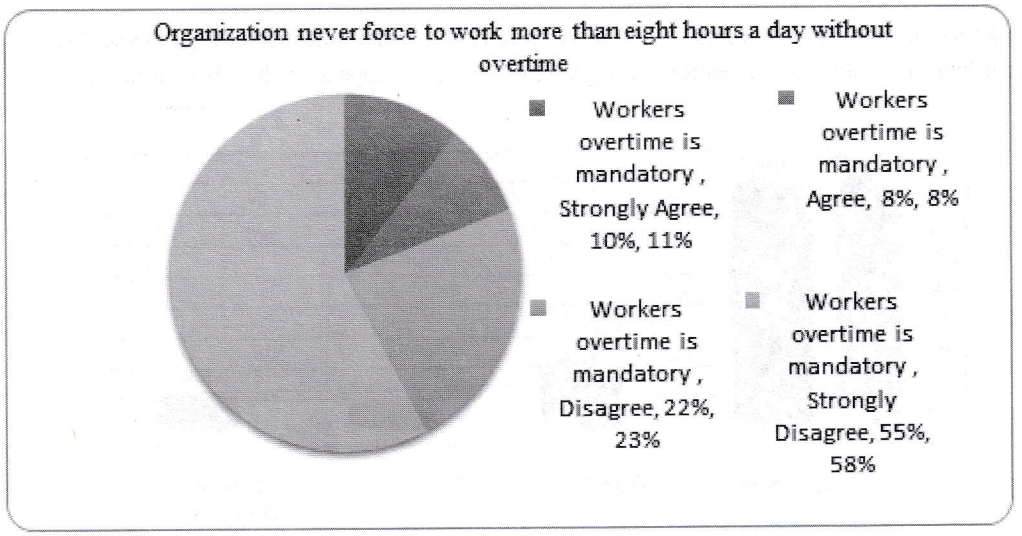

Fig. 05: organization never force to work more than eight hours a day without overtime

One of the statements in my questionnaire was working hour create no problem in family life among the 96 respondents 54% strongly opposed with this statements. About 38 % were simply disagree and rests of 4% were reluctant to show their opinion regarding this statement.

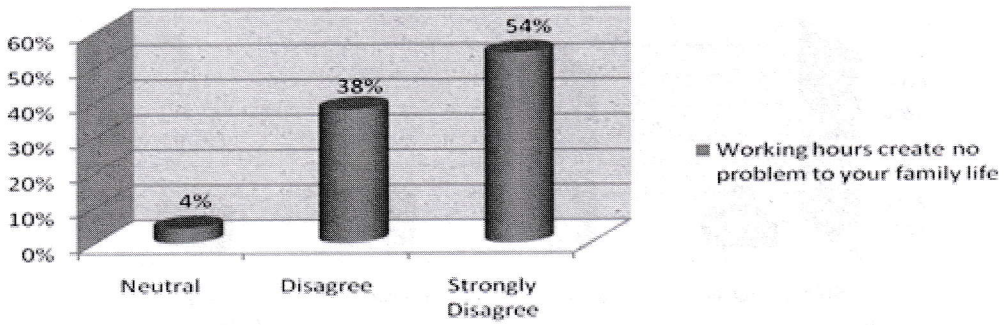

Fig. 06: Working hours create no problem to your family life

Respondents were asked to give their opinion on leave issue; therefore, in case of leave first statement was company gives 14 days sick leave with pay 74% of them were agreed with this statement and 14% were strongly agree. About 4% were disagree and rest of the 8% was strongly disagree. Therefore,

workers mostly workers were positive toward leave reveal. That indicates they get medical leave according to the standard. Therefore, it might have very little impact on the labor disputes.

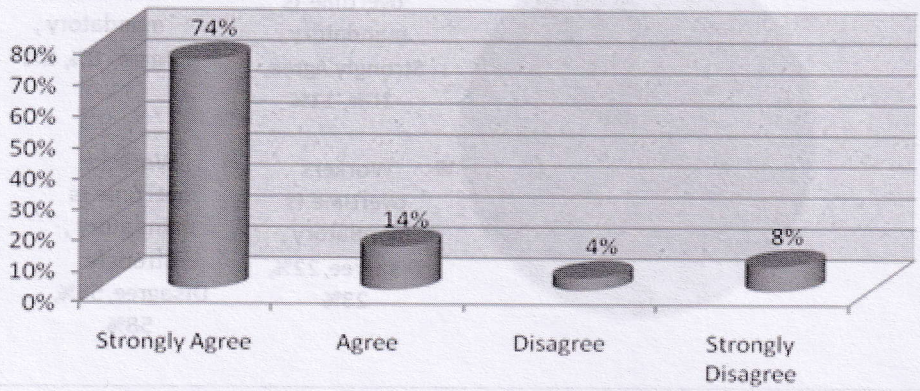

Fig. 07: Company gives 14 days sick leave with pay

About 60% of the respondents were agreed that female workers get maternity leave with pay. Very few were disagreed with this statement. Therefore; it can be said that female workers get maternity leave when they need as well as they get salary when they are in leave. Therefore, it might have very little impact on labor disputes in RMG sector.

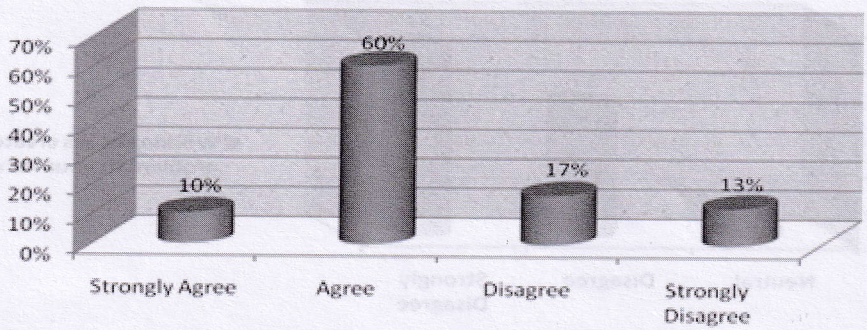

Fig. 08: Female workers get maternity leave with pay

Statement regarding working environment was that, working environment of the company is safe and is not overcrowded. About 10% of the respondents strongly oppose the statement and 39% strongly

agreed with the statement. In addition, 25% were simply agreed and rest of the 26% was disagreed with working environment.

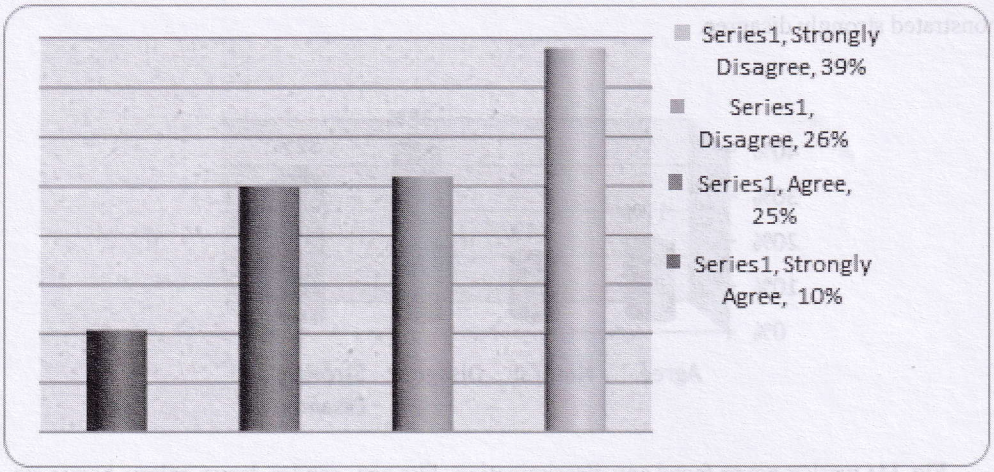

Fig. 09: Working environment of the company is safe & not overcrowded

Regarding victimization of women, I asked to give their opinion on female worker face no physical abuse by their supervisor. In this case 38% of the respondents were neutral and 28% were disagree with this statement and 17% were strongly disagree and 5% were strongly agree and rest of 12% were agree.

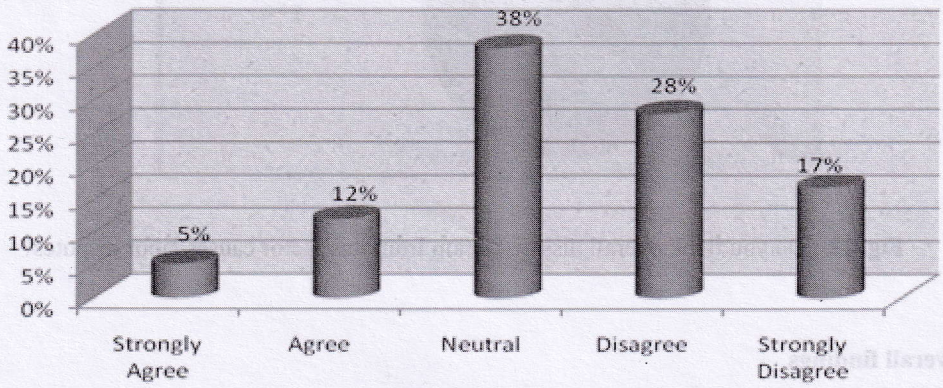

Fig. 10. Female worker face no physical abuse by their supervisor

The workers of the garments factory expressed their opinion on discrimination issue. The statement was you never face any discrimination- like age, gender, leave, salary; bonus etc. 17% respondents were agree with the statement and 14% of them were neutral 38% strongly disagree where as 32% demonstrated strongly disagree.

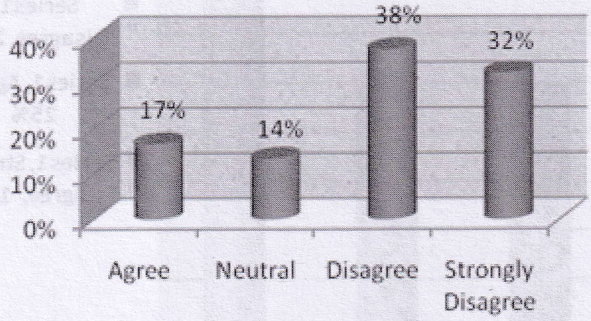

Fig. 11: worker never faced any discrimination- like age, gender, leave, salary, bonus etc

They respondents were asked do you think overall dissatisfaction from these factor causes labor disputes. About 68.75% respondents said that yea overall dissatisfaction causes labor disputes, 27.08% said no, and 4.17% give no comments on it.

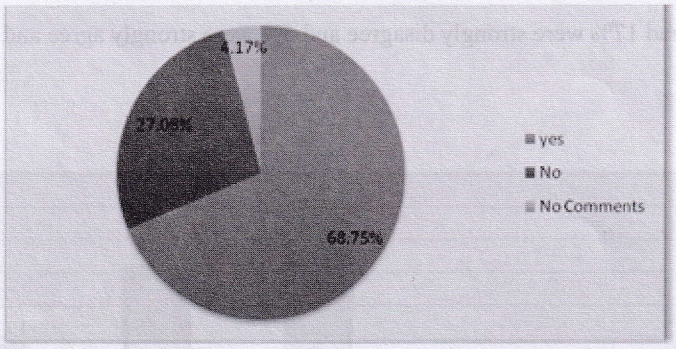

Fig. 12 : Do you think overall dissatisfaction from this factor causes labor disputes?

5.4 Overall findings

Most of the cases, RMG workers are not satisfied with existing salary & bonuses as well as they do not get their salary on time. They have to work for mandatory overtime that is the violation of

labor law act 2006. Mandatory overtime create problems in their family life. In addition to that working environment of the organization is not safe & is overcrowded that is very dangerous to their health. Overcrowding causes hearing problem. About 80% of the RMG workers are female, but according to the survey report in 45% cases, they become abused physically by their supervisor and face discrimination problem like- age, gender, leave, wages, bonus, overtime, others benefit etc. That is an alarming report for this sector. Overall study found that RMG workers are dissatisfied with their job and 68.75% of the respondent agreed with that, overall dissatisfaction created from this sector causes labor disputes. Therefore, it can be stated that, wages, bonus & overtime, working hours, leave, working environment, discriminations are the main reasons of labor disputes in RMG sector but these are not all the elements causes labor disputes. There might have many other reasons like Inter/Intra Union Rivalry, Work Load, unjust layoff & retrenchment without notice, political factors, indiscipline etc.

5.5 Role of BGMEA in Disputes Settlement

According to the statement of Present Secretary General of BGMEA, Named Ehsan UL Fattah, that BGMEA play active role in negotiation labor dispute in the ready-made garments sector in Bangladesh. They considered the Labor Law 2006 and ILO convention as the standard for any dispute settlement. He also mentioned that BGMEA was formed with the objective of settling the disputes between the workers and employers. Secretary General of BGMEA said that BGMEA give the service of the following to their members.

Legal Advice: BGMEA Labor Cell provides legal advice to its member-units in various labor and compliance related issues.

Bilateral Committee: BGMEA has formed a bilateral committee on 30 June 1997 with Registered Trade Union Federation to solve labor issues such as maternity leave, overtime, payment of wages, minimum wages.

Conciliation-cum-Arbitration Committee (CAC): Since 26 April 1998 CAC in accordance to Industrial Relations Ordinance (IRO) -1969 performs the following activities:

(a) The committee solves the grievances of the owners and the workers, rapidly to keep production uninterrupted;

(a) The committee tries to solve the disputes without any charge that arise between the owner and the employees of the factory before referring the matter to court.

5.6 Role of Labor Union in Disputes Settlement

Recognition of trade union in RMG sector is the outcome of a long struggle of the workers to organize them to realize their demands. The RMG workers' movement to organize trade unions was suppressed through administrative and political intervention and vehement opposition from the owners. In 1994, the workers called a strike for establishing minimum wages and implementing labor laws in the RMG sector. As a result, a tripartite committee, headed by the Labor Minister, was formed. It consisted of three workers' representatives and three representatives from employers and governments. The functions of the Committee were to review the demands of garment workers, and monitor violation of labor laws. In 1997, a bipartite committee, consisting of representatives from Grand Alliances of Workers and BGMEA, was formed to resolve individual (at factory level) disputes over wages and other matters between unions and industry managements. Its proposal to resolve disputes through arbitration was put into practice subsequently and was found to be successful. Until 1997, there were only three trade unions in the RMG sector.

Now there are as many as 168 registered trade unions for the whole RMG sector in Bangladesh except those in the EPZs. Out of 4,500 garment industry only 120 are affiliated with the unions, less than 5 percent of the garment workers. Knitwear garment workers are outside of the operations of the trade unions. Two national garments federation is registered with the Department of Labor. From 1994 to 2006 RMG workers' union signed seven agreements/MOUs with the BGMEA on matters of declaring and implementing minimum wages for garment workers, recognizing trade union activities, providing appointment letters and identity cards to the workers, fixing working hours and ensuring maternity leave and other holidays. The national tripartite agreement was concluded between the government, BGMEA and the organizations representing garment workers in 2006.

Popularly known as the national tripartite memorandum of understanding, it is seen as a landmark achievement towards resolving the above mentioned issues. Most of the demands were subsequently incorporated in the Bangladesh Labor Act 2006. Though the government has officially allowed trade unions in the RMG factories, the factory authorities are creating a critical situation for the workers who are engaged in trade union formation, labor leaders alleged said a trade union leader while intervening with new age. Labor rights activists said that under special circumstances (amid Bangladesh's efforts to regain GSP facility in the US market) the government was compelled to give

registration of trade unions in the sector, but the unions could not play its role in the factories due to barriers put by the factory authorities and lack of proper initiative from the government.

5.7 Role of Industrial Police in Disputes Settlement:

In a meeting between the Bangladeshi National Human Rights Commission (NHRC) and the Dhaka Metropolitan Police, the NHRC chair sharply rebuked the police for human rights violations by law-enforcement personnel and corruption within the force. The Daily Star reported: "cops try in vain to justify HR violation." The newspaper referred to police officials lamenting that "policemen themselves do not have human rights" so "how could they ensure the human rights of others?" Police reportedly said they are poorly paid and forced to work overtime without compensation and that is why they take bribes. They also "admitted that police at times torture arrestees to extract information from them as they (police) do not have the proper logistics for quizzing. However, industrial police play a vital role in smoothing the riots and in handling prevention of strikes occurring time to time for demanding several issues. They also provide the factory protection for the vandalizing if the authority informed them.

6.0 Conclusions

In respect of production, export, earning foreign exchange, contribution to GDP, employment, investment and business mobilization, RMG sector of Bangladesh has been a flourishing industry. Its importance has crossed geographical boundaries of the country. It involves stakeholders from various corners, covering public, private and international organizations. Given the fabulous volume of trade of the industry, the increasing trends of labor unrest in the RMG sector have been a matter of serious concern. Solving labor unrest in this sector is nearly impossible by a single agency like the government or BGMEA or a civil society organization. Findings from the data analysis show that public-private cooperation is the most chosen ways of addressing labor unrest in the RMG sector of Bangladesh. The objectives of this present study are to find out the causes of labor unrest and to know role of BGMEA, industrial police & labor union in disputes settlement procedure in RMG sector in Bangladesh. The responses of the respondents unfold that irregularities in payment, low wage, wages, bonus & overtime, working hours, leave, working environment, victimization of women, & discrimination are the major causes of labor unrest in the RMG sector of Bangladesh. Moreover, BGMEA can play active role in dispute settlement procedure, labor union take part in dispute settlement procedure but sometimes can't raise their voice or do not want to raise due to the pressure from the owners. Industrial police play a role to smoothing the instant riots; sometimes they also work for owner's interest by ignoring the workers demand.

References:

[1] http://newagebd.net/152988/rmg-sector-trade-unions-number-rising-but-most-remain-ineffective

[2] BGMEA Annual Report 2016, http://www.bgmea.com.bd/chart test/factory

[3] Ismail M Bhuiyan, "*Reasonable wages for workers to eliminate unrest in Bangladesh's ready-made garments sector*" Bangladesh development research working paper series, May 2013.

[4] Siddiqua, Chowdhury M.A.M & Islam, *"Industrial Relation and Dispute Settlement Procedure in RMG Sector of Bangladesh: A Critical Review*" international journal of innovation and applied studies, vol. 09, No. 03, Nov-2014.

[5] Dusgupta (2002), "Attributes Towards Trade Union in Bangladesh, Brazil, Hungary and Tanzania" , Journal Article on International Labor Review, Vol 14(1).

[6] Absar SS (2001). "Problems Surrounding Wages; The Ready-made Garments Sectors in Bangladesh,"
J. LMD Labour. Manag. Dev. Vol 2, P. 7.

[7] EBP (2008). EBP Report on Bangladesh Garments Statistics and Future Challenge.

[8] Bansari, N., "*Textile and Clothing Sector in Post MFA Regime: A case from Bangladesh gender and trade*", Commonwealth Secretariat, 2010

[9] Ferdous, Ph.D., "Improving Social Compliance in Bangladesh's Ready-made Garment Industry," labor and Management in Development, Vol 13, 2012.

[10] Khan, F.R (2006), Compliance: Need of the hour in the apparel industry; Law and our rights, Issue No.
249, report published in the Daily star on August 05, 2006.

[11] BGMEA Annual Report 2016, http://www.bgmea.com.bd/chart test/factory

[12] Analysis from Field Survey Data, December 2015.

Study of Natural Convection Heat Transfer In a Rectangular Enclosure from One Cooled Side Wall

***Mostofa M.M.[1], Sarkar, M.A.R[2], Huq A.M.A[3] and Islam, M.A[4]**

***Corresponding Author:** [1]Workshop Superintendent, Dhaka Polytechnic Institute, Bangladesh
[2]Professor, Dept. of Mech. Engg. BUET, Dhaka-1000, Bangladesh
[3]Former Professor, Dept. of Mech. Engg. BUET, Dhaka-1000. Bangladesh
[4]Associate Professor, Dept. of Mech. Engg. BUET, Dhaka-1000, Bangladesh

Email: mosto1956@gmail.com

ABSTRACT

An experimental investigation of natural convection heat transfer in rectangular enclosure from one cooled vertical side wall was carried out. In the experiment the side wall was cooled by a thermoelectric module (TEM). The measurements covered the temperatures of the cold plate and air in the enclosure at different interval of time at 14 different locations. From the temperature distribution data, stratification within the enclosure was observed. The stratification indicator γ was estimated at three different horizontal distances from the cold plate for the time interval of 15, 25, 50, 60 and 80 minutes and found to decrease with time in the enclosure. Heat transfer rate, heat transfer coefficient, Nusselt number and Rayleigh number were calculated from the measured experimental data during transient and steady state regime.

Keywords: Natural Convection, Rectangular, Enclosure, Cooled, side wall.

Nomenclature

T, Temperature °c
Nu_H, Nusselt number
Ra_H, Rayleigh number
γ Stratification factor
X, *Y*, Coordinate

1.0. Introduction

1.1. Natural convection in an enclosure

In many engineering applications natural convection u. Sys important role as a dominating mechanism of heat transfer [1]. Heat transfer by free convection in enclosed spaces has numerous engineering applications. For example. double glazing, nuclear insulation, ventilation room, solar energy collector, crystal growth in liquid the periodic energizing of electronic devices by the on and off heating and cooling mode, effective cooling of microelectronic equipment, refrigeration air conditioning

system with chilled ceiling etc [2].There are two elementary classes of nature convocation flows in enclosure, namely, those in vertical enclosures with two differentially heated vertical walls and those in horizontal enclosures with two differentially heated horizontal walls. With the ultimate aim to simulate realistic flows found in engineering applications. The surfaces may be plane horizontal or vertical or inclined. The determination of the on set free convection and the heat transfer coefficient in an enclosure associated with free convection has been the' subject of numerous investigations. Despite the vast number of experimental and analytical studies of free convection in enclosed spaces, the heat transfer correlation covering all ranges of parameters are not available. Numerous studies on natural convection in enclosure related to either side heating or bottom heating, have been reported [3-4]. But the natural convection in enclosure with one side cold and other sides adiabatic is relatively unknown. The main features of these types of natural convection transfer problem is that the boundary layer thickness. Hence the development of the flow is often strongly influenced by the shape of the boundaries [5-8].

Therefore, the heat transfer rate and heat transfer coefficient, are also dependent on the boundary conditions, of enclosure. For the discussion of basics. of natural convection along a vertical cold wall what it considered so, for the simplest model possible, that is the heat transfer interaction between a vertical wall and an isothermal fluid reservoir proceeding now, on the road from the simple to the complex. We take a closer look at the problems of modeling a heat transfer situation involving natural convection. Vertical walls are rarely in communication, with in finite isothermal pools of fluid. More often their height is finite and the cold boundary layer eventually hits the bottom. At that point the cold stream, has no choice but to discharge horizontally into the fluid reservoir. The direction of this discharge, is horizontal because the discharge contains fluid colder than the rest of the reservoir. The long-time effect of the discharge process is the thermal stratification characterized by warm fluid layers floating on top of colder layers. At this point it is sufficient to recognize that the air in any room with the door closed is thermally stratified in such a way that the lower layers assume the temperature of, the coldest wall and the highest layer near the ceiling approach the temperature of the warmest wall.

1.2 The present study

An experimental investigation on the natural convection heat transfer in a rectangular enclosure from one cooled side wall will be conducted which consists of the following objectives:

a) To measure temperatures of the cold vertical wall and air at different locations within the enclosure during transient period,

a) To measure temperatures of the cold vertical wall and of air at different locations within the enclosure during steady state condition,

b) To study the variation of average natural convection heat transfer coefficient h at different thermal potentials, ΔT,

c) To understand thermal stratification phenomenon for this enclosure and

d) To determine the Rayleigh numbers at different locations within the enclosure for both transient and steady state conditions.

e) To develop a correlation which will be recommended for estimation of heat transfer coefficient for the natural convection in the rectangular enclosure cooled from one of its vertical walls.

2.0. Experimental setup

2.1. General Description of the Experimental Facility

This section describes the experimental aspects of the investigation and includes a detailed description of the experimental facility. Fig.1. present schematically the experimental-set up and test section respectively. Major components of test apparatus are, rectangular enclosure, thermoelectric module, fan, rectifier converter heat sink, cold plate and data acquisition System. Details of the experimental set up given below.

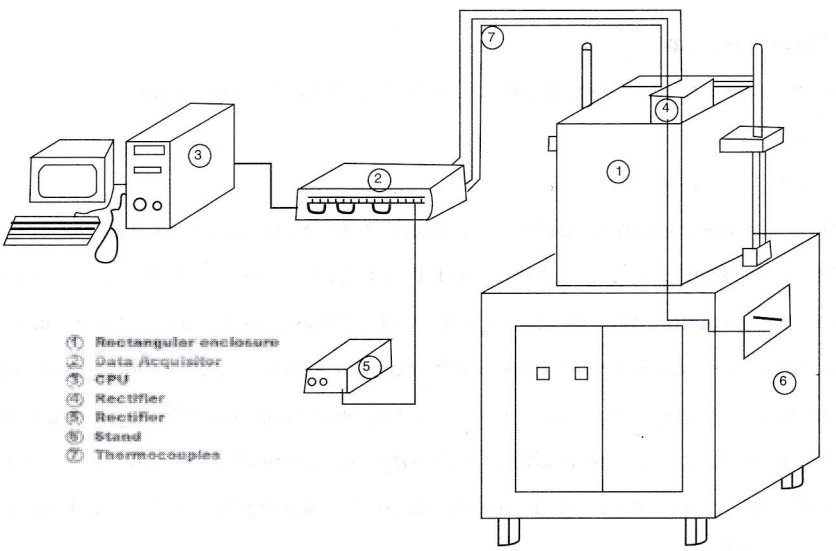

Fig-1: schematic diagram of the experimental set up

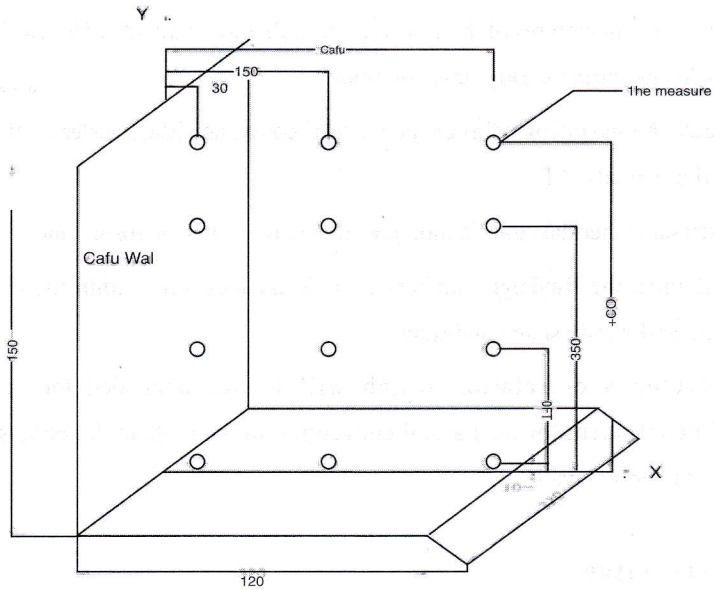

Fig-2: Positions of thermocouples in the enclosure

and the position of rows were 20mm, 150 mm 300 mm and 400 mm apart respectively from the bottom surface of the enclosure. Another two thermocouples were used to measure cold plate temperature and room temperature shown in **Fig.2.**

3.0 Data acquisition system

The system consists of (1) data acquisitor, (2) UPS, (3) CPU & (4) Monitor

3.1 Data acquisitor

The data acquisitor used to measure temperature at different locations was the component number 2 as shown in **Fig.3**. The acquisitor model is COLE-PARMER PCA-14. From the certifications of construction, the resolution and accuracy were found to be 16 bits and ±0.02% respectively. The dimension was of height 35cm width 10cm and depth 22.5 cm. The software supplied was menu driven and very easy to use with BASIC interpreter supplied with any computer. The menu appeared on the monitor and enabled to identify each-channel. Set up the name of data file, varied the time between storing sets of data on disk, display disk directories etc. No knowledge of programming was needed.

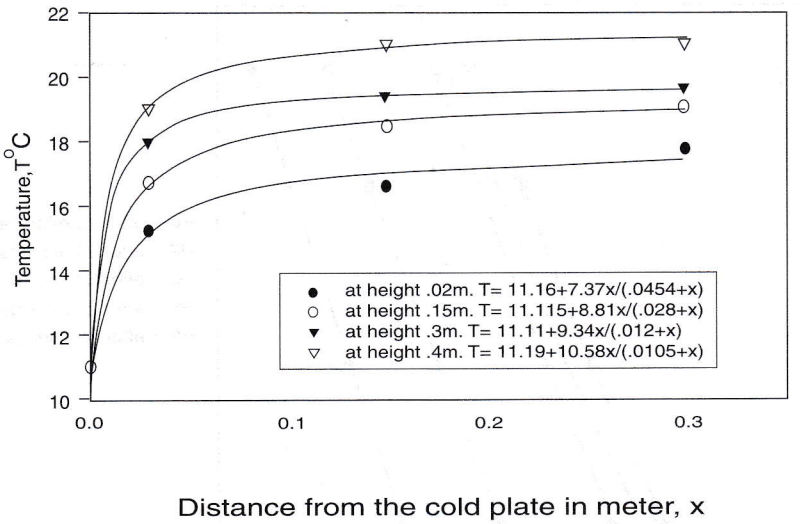

Fig-3. Temperature at different height 'γ' in the enclosure at different distance 'x' from cold plateafter 15 minutes

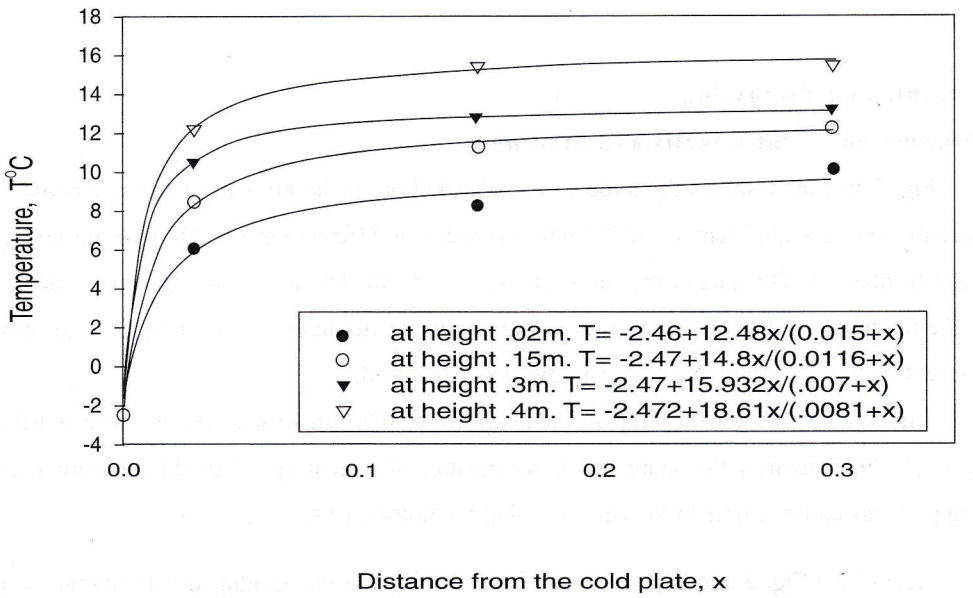

Fig-4. Temperature at different height 'y' in the enclosure at different distance 'x' from the cold plate after 80 minutes

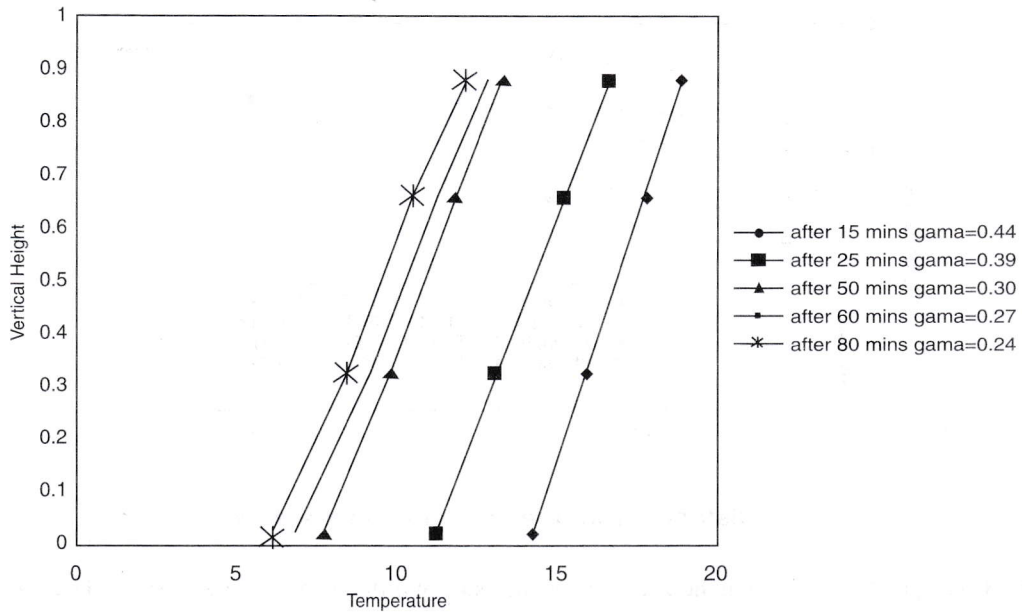

Fig-5. Effect of the enclosure stratification on heat transfer from air to the cold vertical wall (x=0.03 m)

4.0. Result and discussion

4.1. Discussion on the Results and Findings:

Fig. 3 to **Fig. 4** shows the temperature distribution of the air within the enclosure. The data are presented at different height 'Y' in the enclosure at different distance `X' from the cold plate at different intervals. The data at the intervals of 15, 25, 50, 60' and 80 minutes are - analyzed. From the temperature distribution profile in the enclosure the heat transfer rate Q, heat transfer coefficient "h" and average Nusselt number was calculated.

Fig. 3 to **Fig. 4** show the temperature distribution of the air within the enclosure at different intervals. It was found from the figure that the temperature of air at any point gradually decreases with time and air was colder closer to the cold wall and the bottom of the enclosure.

Again from **Fig. 3** and **Fig. 4.** it was found that fluid layers developed with interval of time which were floating on top of increasingly colder layers. It was due to the finite height of the enclosure and eventually cold boundary layer hits the bottom of the enclosure. At that point the colder stream had no choice but discharge horizontally from air of the enclosure. So, the direction of discharge was

horizontal because the cold boundary layer contains fluid colder than the rest of the -enclosure. In this way thermal stratification was developed in the enclosure. From **Fig.5** it was found that the value of γ is decreasing with time. Its shows that at any distance from the cold plate temperature of the stratified layers is approaching a steady state value.

5.0 Conclusions and recommendations

5.1 Conclusions

From this study the following conclusions may be drawn:

(1) The temperature of air at the different parts of the enclosure decreases asymptotically to the steady state value.

(2) Temperature difference between top most and bottom most layer of air at different X value increases initially and then remains constant.

(3) The result shows that the air in a part of the enclosure is substantially stratified.

(4) Stratification indicator γ decreases with the increase of time.

(5) The natural convection of heat transfer coefficient, Nusselt number and Rayleigh number increase with the increase of time.

(6) The experimental data are well correlated with the following correlation

$Nu_H = (0.394\ Ra_H^{0.25})$

5.2 Recommendations

The following recommendations are put forward as future extension of the present investigations:

(1) Further investigation may be carried out with fluid filled rectangular enclosure driven by a single vertical wall with warm and cold regions:

(2) The entire investigation may also be repeated with a square enclosure.

(3) The entire investigation may be carried out employing interferometric. technique. The flow field may also be studied with the help of a Laser Doppler Anemometer.

(4) For comprehensive investigation of natural convection heat transfer of similar type, a test rig consisting of a pressure as well as a vacuum vessel will be helpful. For finding out the effect of Prandtl number test may be carried out with different fluids.

References

[1] S. Ostrach, "Natural Convection in Enclosures," J. Heat Transfer, Vol. 110, pp. 1175-1190, (1998).

[2] Anderson and G. Lauriant "The horizontal natural convection boundary layer regime in a closed cavity.

[3] November, M., and Nansteel, M.W., "Natural Convection in Rectangular Enclosures Heated from below and Cooled Along One Side", Int. Journal of Heat Mass Transfer, vol. 30, no. 11, pp. 2433-2440, 1987

[4] Marcelo M. Ganzarolly and Luiz F. Milanez, "Natural convection in rectangular enclosures heated from below and symmetrically cooled from the sides, " Int. J. Heat Mass Transfer, Vol.38, No.6, pp. 1063-1073, (1995).

[5] Orthan Aydin, Teoman Ayhan, "natural convection in rectangular enclosures heated from one side and cooled from the ceiling ".

[6] N.C. Markatos and K. A. Pericleous, " Laminar and turbulent natural convection in an enclosed cavity," Int. J. Heat Mass Transfer, Vol, 27, No. 5, pp. 755-772 (1984).

[7] Qi-Hong, Deng, Guang -Fa Tang, Yuguo Li, Man Yeong Ha, " Interaction between discrete heat sources in horizontal natural convection enclosures," Int. J. Heat Mass Transfer, Vol.45, pp. 5117-5132 (2002).

[8] I. Sezai, A.A. Mohamad, " Natural convection from a discrete heat source on the bottom from of a horizontal enclosure," Int. J. Heat Mass Transfer, Vol.43, pp. 2257-2266, (2002).

COMPARISON OF PHYSICAL AND MICRO-STRUCTURAL CHARACTERISTICS OF VARIOUS FINE AGGREGATES IN BANGLADESH

Tafsirojjaman[1*], Md. Sabbrojjaman[2], Md. N Islam[3], Md. R Alam[4], Md. K Hasan[5], Md. N Islam[6], Md. M R Majumder[7], Sheikh Mohammed[8], Enamul Haque[9]

***Corresponding author:** [1*] Lecturer, Sonargaon University, Dhaka, Bangladesh,
[2] Dhaka International University, Dhaka, Bangladesh
[3,4,5,6,7,8,9] Sonargaon University, Dhaka, Bangladesh

Email: tafsirojjaman@gmail.com

Abstract

Concrete is a versatile material, which is a mixture of cementious material, coarse and fine aggregate and water. The properties of concrete may vary widely because of seasonal and spatial variations in properties of locally available fine aggregates. As the geological and geo-morphological processes of rock are different, the aggregates formed at various places are also different. The specific objectives of this study has been to observe spatial variations on physical and micro-structural characteristics of fine aggregates collected from different sources in Bangladesh. Fine aggregates have been collected from different sources of Sylhet, Kustia, Pabna, Dinajpur and Dhaka. According to ASTM, sieve analysis, specific gravity (OD and SSD), absorption capacity, moisture content and unit weight have been performed in the laboratory. Non-destructive tests are performed for micro-structural characteristics of fine aggregate. In this study, X-Ray Diffraction (XRD) technique has been used to predict quantitative phase analysis and percent of each compound present in the sample of different fine aggregate. XRD results show the presence of Calcite ($CaCO_3$), Gismondine ($CaAl_2Si_2O_8.4H_2O$), Mullite ($Al_6Si_2O_{13}$) and variation of Quartz (SiO_2) for different samples. The spatial variations in the mechanical and micro-structural properties of fine aggregates have been observed during this study for all the tests. All the test result values of fine aggregates have been compared with standard values of ACI, BS, AASHTO, IS and PWD.

Keywords: *Title, abstract, objective, results, conclusions*

1.0.Introduction

Bangladesh is a developing country. Development program of a country like Bangladesh has a great emphasis on infrastructure. Construction sector is one of the prominent sectors to contribute in gross domestic product (GDP) in Bangladesh. Aggregate is mostly used as construction material in almost every construction work in Bangladesh. Aggregates are collected from different sources. In those places the rocks from which the aggregate is processed are not the same. Moreover the geological and geo-morphological processes, under which the aggregate forming rocks pass, may vary in different locations. For this reason, remarkable variations on the properties of aggregate are observed according

to various sources. Weather condition of the source area is one of them. Temperature, humidity and rainfall etc. varies in different seasons. These variations are very significant with the change of seasons in Bangladesh [1]. Generally in the construction works of Bangladesh, spatial variation of aggregate is not taken into consideration. To achieve required dimensional stability, durability and strength of structures, aggregate characteristics and related engineering properties is one of the main issues needed to be addressed.

For fine aggregate, aggregate become coarser with the increase of FM value. Fine aggregate affects many concrete properties, including workability and finish ability. Usually, a lower FM results in more paste, making concrete easier to finish. For the high cement contents used in the production of high-strength concrete, coarse sand with an FM around 3.0 produces concrete with the best workability and highest compressive strength [2]. The fines content (particles finer than 75 μm) in aggregate has substantial effects on the performance of concrete. Since the fines content has large surface area that would increase the water demand, maximum limits are often imposed.

However, the fines content would also fill into the voids between larger particles to increase the packing density and thus reduce the volume of voids to be filled with cement paste. Hence, the fines content is not entirely undesirable and it has been suggested to raise the limits on the fines content [3]. The water requirement for constant workability fell sharply with increasing amount and fineness of the very fine aggregate due to improved particle packing. At constant, relatively small binder contents of 80–250 kg m^{-3}, modifying the aggregate distribution increased the 91-day strength of 6 mm concrete as much as threefold, e.g. from 20 to 65 MPa at 200 kg m^{-3}. This effect was less significant the greater the binder content. The correlation between strength and porosity was similar regardless of concrete composition. The stress-strain behaviour was more dependent on strength than on composition [4].

Aggregate is a common and widely used construction material and it undergoes chemical changes with time when exposed to various environments. The extent of the damage depends on concrete quality and is rarely damaged in the life time of a structure but chemical changes in aggressive environmental conditions may cause a considerable damage to it. X-ray powder diffraction (XRD), is an instrumental technique that is used to identify minerals, as well as other crystalline materials. X-Ray Diffraction (XRD) technique has been used for quantitative phase analysis and percent of each compound present in the sample [5].

2.0. Materials and methodology

The main source of fine aggregate is river. There are a lot of rivers in Bangladesh. As a result, in whole Bangladesh the source of fine aggregate is also available. Fine aggregates also have been collected from different places in Bangladesh like Sylhet, Pabna, Dinajpur, Kustia and Dhaka. The aggregates were tested for absorption capacity, specific gravity, unit weight, and abrasion. The specific gravity and absorption capacity are determined as per ASTM C128, unit weight as per ASTM C29, and abrasion value as per ASTM C131.

Five types of fine aggregate were used for comparison of compressive strength. Coarse aggregate was collected from Sylhet (Jaflong). Coarse aggregates were mixed as 5% from 25 mm to 20 mm, 57.5% from 20 mm to 10 mm, and 37.5% from 10 mm to 5 mm as per ASTM C33-93. The aggregates were tested for absorption capacity, specific gravity, unit weight, and abrasion. Cylinders of diameter 150 mm and 300 mm height were prepared using the standard moulds. The concrete adopted with mix ratio 1:2:4 and water cement ratio of 0.68. The samples are casted using the five different fine aggregate. Total mixing time of concrete was controlled at 5.5 minutes. After mixing concrete, the workability of concrete was measured by slump cone test. Cylinders are demoulded after 24 hours from casting and kept in a water tank continuously. The compressive strength of concrete was measured at 28 days by using Universal Testing Machine (UTM). The strain of concrete specimens was measured by a strain measurement setup with two dial gauges. The gauge length was 100 mm.

X-ray diffraction (XRD) is one of the most important non-destructive tools to analyze all kinds of matter ranging from fluids, to powders and crystals. This technique uses X-ray diffraction on powder or microcrystalline samples, where ideally every possible crystalline orientation is represented equally. When X-ray radiation is directed on a sample, the X-rays are scattered ("diffracted") by electrons present in the material. If the atoms in the material are arranged in a regular structure, i.e. if the material is crystalline, this scattering results in maxima and minima in the diffracted intensity. The signal maxima follow Bragg's law $n\lambda = 2d\sin\theta$. Here n is an integer, λ is the X-ray wavelength, d is the distance between crystal lattice planes and θ is the diffraction angle (Ref. **Fig.1.**). During an X-ray diffraction (XRD) measurement the angles of incidence and detection are scanned. Bragg's law is satisfied when the path length difference of the X-rays (indicated in green) is equal to $n\lambda$. The diffraction angle θ is half the angle between the incident and diffracted X-rays [6].

Powdered sample were used for XRD analysis. In powder or polycrystalline diffraction, it is important to have a sample with a smooth plane surface. Fine aggregate samples were collected from existing source and grounded the sample down to particles of about 0.002 mm to 0.005 mm cross section. The ideal sample is homogeneous and the crystallites are randomly distributed.

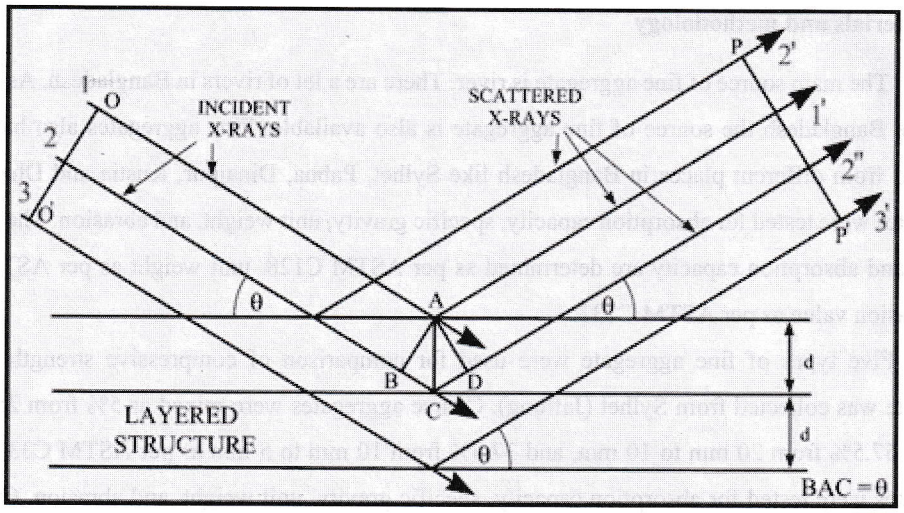

Fig.1. Schematic representation of diffraction of X-rays in a crystalline material

3.0. Results and discussions

The test results of fine aggregates are shown in **Fig.2.** and **Fig.3**. The grading curves (**Fig. 2.(i).**) represent that the samples of Sylhet have larger particle size in comparison with other sources, and the samples from Dhaka have the finest particle size. The other samples show nearly similar distribution in their sizes. The sieve analysis of fine aggregate shows that Sylhet has the maximum FM value of 2.70, and Dhaka has the minimum FM value of 1.40. Moreover, Kustia samples have the minimum (0.54%) absorption capacity, and Sylhet samples have the maximum (1.1%) absorption capacity.

By investigating specific gravity of fine aggregate, it was found that samples of Dinajpur have the maximum values of Specific gravity (OD and SSD) of 2.67 and 2.60 respectively in comparison with other sources; these samples have comparatively high coarse particles. On the other hand, Samples of Sylhet also have higher values of unit weight (loose and compacted) of 1420 and 1610 kg/m3 respectively, and Dinajpur samples have the lower values of unit weight of 1400 and 1595 kg/m3 respectively. Finally, the concrete made with Sylhet sand (3193 Psi) show the maximum compressive strength for same mix ratio and water-cement ratio than others.

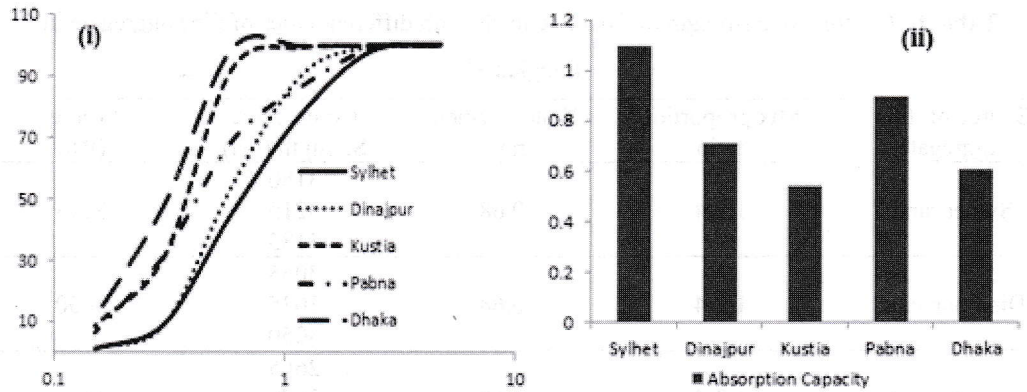

Fig.2. (i) Grading curves and (ii) absorption capacity of fine aggregates

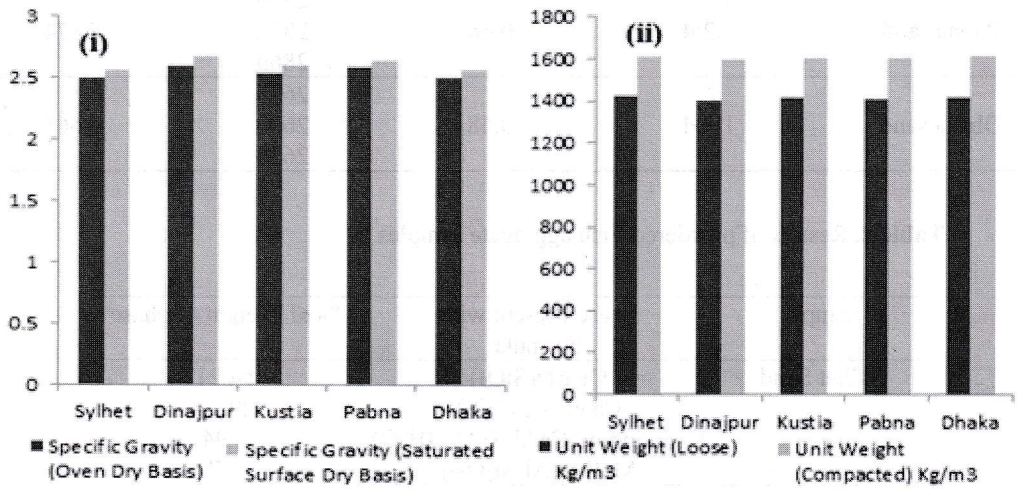

Fig.3. (i) Specific gravity and (ii) Unit weight of fine aggregates

Samples of fine aggregates from Sylhet are satisfied most with the values of standard specifications like FM values of ACI and PWD (for RC.C. work FM value is 2.0 to 3.0); absorption capacity values of ACI (0.5 to 4%) and PWD (1 to 6%) and unit weight (loose and compacted) values of ACI (1280 to 2250 kg/m3) and PWD (1400 to 2250 kg/m3) in comparison with other sources. Samples from Fulbari in Dinajpur have maximum specific gravity [standard values of ACI (2.3 to 2.9) and PWD (2.2 to 2.6)].

Table.1. Compressive strength of Concrete made with different types of Fine aggregate in Bangladesh

Source of fine Aggregate	Mix proportion ratio	Water/Cement ratio	Compresive Strength (Psi)	Average (Psi)
Sylhet sand	1:2:4	0.68	3180 3215 3185	3193
Dinajpur sand	1:2:4	0.68	3065 3035 3050	3050
Kustia Sand	1:2:4	0.68	2665 2670 2645	2660
Pabna sand	1:2:4	0.68	2890 2872 2860	2874
Dhaka sand	1:2:4	0.68	2675 2680 2650	2668

Table.2. Results of powdered Fine aggregate samples

Sample	Phase Present with Formula	% of Weight of phase
Sylhet Sand	Quartz(SiO_2)	54.21
	Calcite($CaCO_3$)	20.15
	Gismondine($CaAl_2Si_2O_8.4H_2O$)	6.94
	Mullite($Al_6Si_2O_{13}$)	18.71
Dinajpur Sand	Quartz(SiO_2)	64.56
	Calcite($CaCO_3$)	16.77
	Gismondine($CaAl_2Si_2O_8.4H_2O$)	11.18
	Mullite($Al_6Si_2O_{13}$)	7.49
Kustia Sand	Quartz(SiO_2)	57.88
	Calcite($CaCO_3$)	21.72
	Gismondine($CaAl_2Si_2O_8.4H_2O$)	8.18
	Mullite($Al_6Si_2O_{13}$)	12.72
Pabna Sand	Quartz(SiO_2)	50.42
	Calcite($CaCO_3$)	21.93
	Gismondine($CaAl_2Si_2O_8.4H_2O$)	13.66
	Mullite($Al_6Si_2O_{13}$)	13.99
Dhaka Sand	Quartz(SiO_2)	77.49
	Calcite($CaCO_3$)	11.73
	Gismondine($CaAl_2Si_2O_8.4H_2O$)	10.78

XRD is normally used for identifying single-phase materials – minerals, chemical compounds, ceramics or other engineered materials, measuring the average spacing between layers or rows of

atoms, determining the orientation of a single crystal or grain, finding the crystal structure of an unknown material, measuring the size, shape and internal stress of small crystalline regions. Table 2 represents the weight (%) of phase of concrete samples under X-Ray Diffraction analysis. Figure 4 to Figure 8 shows XRD diffractogrames for different fine aggregates.

From **Table.2.**, it was observed that the samples indicate higher percentage of quartz (SiO_2) and calcite ($CaCO_3$). Quartz is nearly always inert when used as aggregate (not fine powder as cement replacement material) in concrete. It means that it will not react at normal conditions, possesses less reactivity, more controllable situation in concrete. But under adverse environmental condition alkali-silica reaction can occur in concrete. In concrete, there would be reaction between quartz and the alkaline compounds of the concrete, typically $Ca(OH)_2$, if the proportion of amorphous or cryptocrystalline (very fine crystalline) quartz increases. And quartz (SiO_2) is a glassy or crystalline form of silicon dioxide.

Thus alkali-silica reaction occurs and causing serious expansion and cracking in concrete. Carbonation occurs in concrete because the calcium bearing phases present are attacked by carbon dioxide of the air an converted to calcium carbonate. It is a disadvantage in reinforced concrete, as pH of carbonated concrete drops to about 7. When the pH level is less than 11, and the rods are exposed to aggression by the oxygen and humidity which are present in the atmosphere. Under these conditions, corrosion process of the reinforcement rods initiates, which increases their volume and thus concrete cracks.

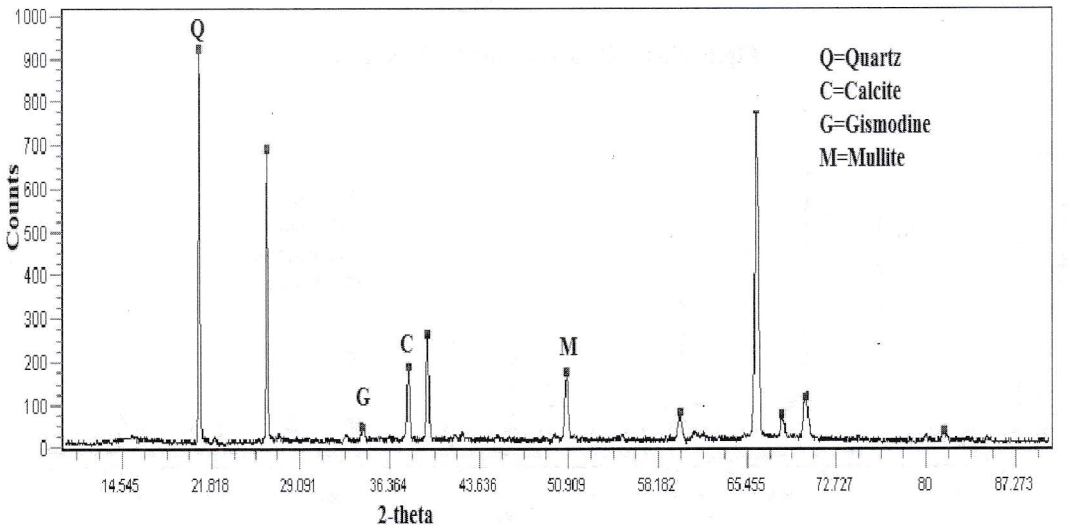

Fig.4. XRD diffractograms for Sylhet Sand

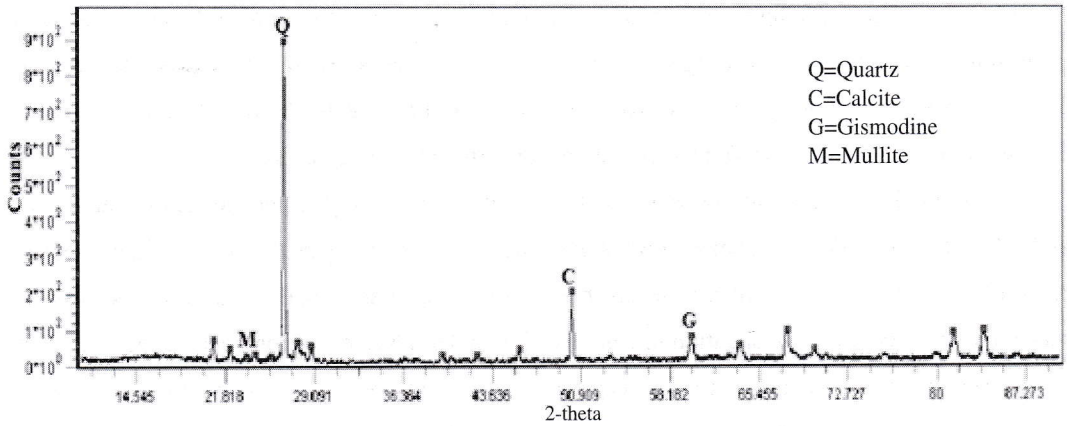

Fig.5. XRD diffractograms for Dinajpur Sand

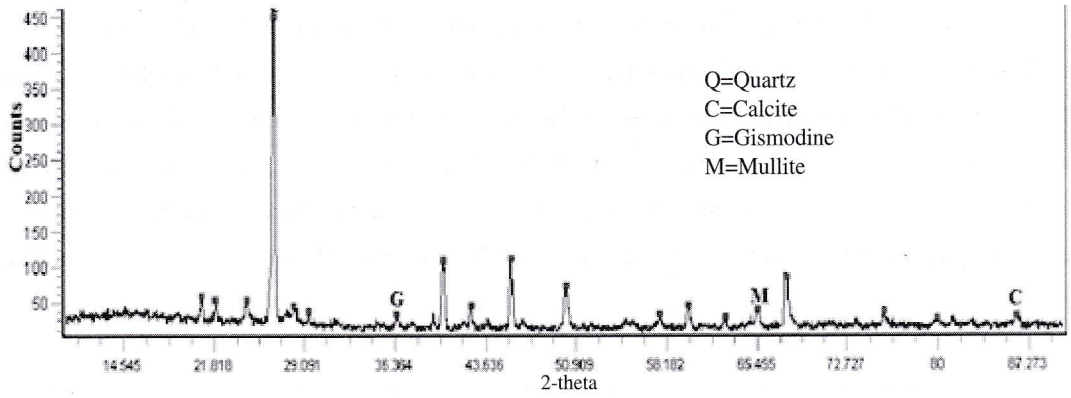

Fig.6. XRD diffractograms for Kustia Sand

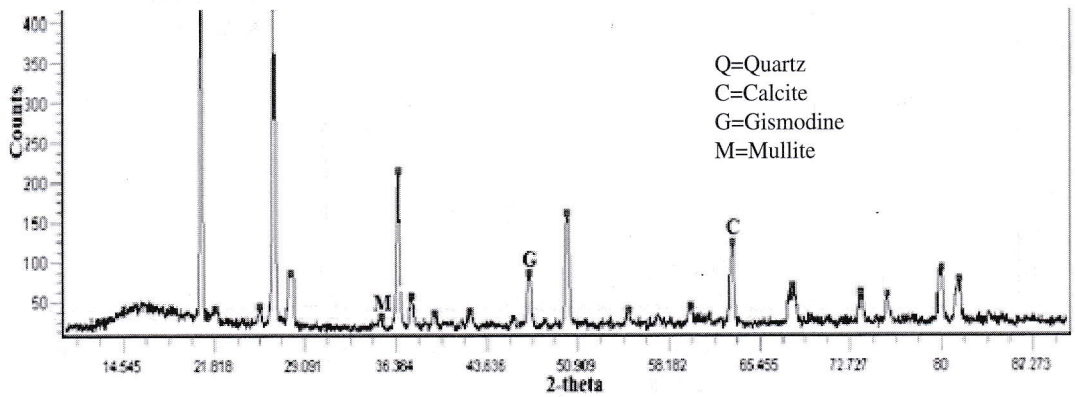

Fig.7. XRD diffractograms for Pabna Sand

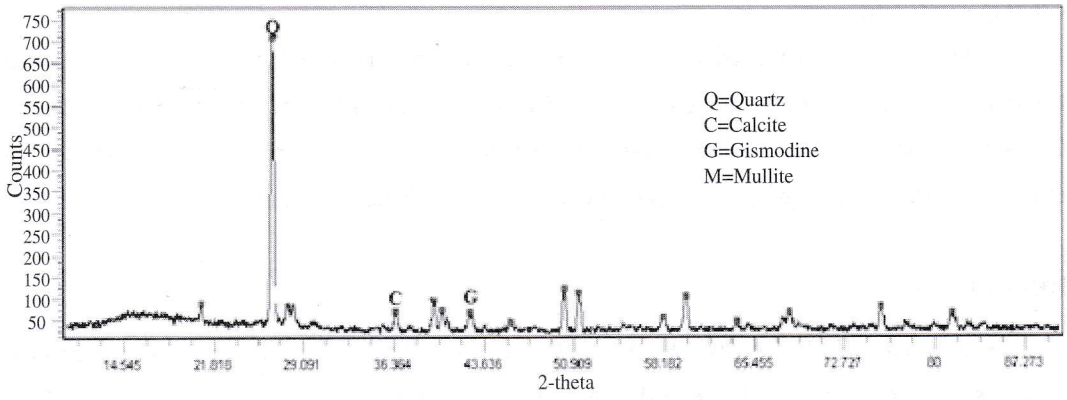

Fig.8. XRD diffractograms for Dhaka Sand

Fig.4. to Fig.8. shows XRD diffractograms of the samples from 1 to 4 for peak list of the samples. X-Ray diffraction analysis indicates predominance of quartz (SiO2) and calcite (CaCO3) peaks.

4.0. Conclusions

This research work represents in depth analysis of fine aggregate properties from different sources in Bangladesh. The spatial variations in the properties of fine aggregates have been observed during this study for all the tests. Physical observations on the collected samples reveal that fine aggregates of Sylhet, Dinajpur and Pabna have comparatively high coarse particle and free from clay and organic matters. All test results of fine aggregates also have been compared with standard values of ACI, BS, AASHTO, IS and PWD. Samples of fine aggregates from Sylhet are satisfied with maximum values of FM, absorption capacity and unit weight (loose and compacted) in comparison with other sources.

In addition, the concrete made with Sylhet sand show the maximum compressive strength of 3193 Psi for same mix ratio and water-cement ratio than others. On the basis of this study, the government and construction companies in Bangladesh can get a clear idea of aggregates from different sources to ensure the quality and strength of concrete. Aggregate can be subjected to different degradation mechanisms. Quartz (SiO2) is identified as a major constituent of the powdered and it is subjected to alkali-silica reaction causing serious expansion and cracking in concrete. The presence of more amount of calcite means that concrete of same component shows more deterioration with sever environment.

4.0. Acknowledgements

The authors acknowledge the experimental facilities provided by strength of materials laboratory, Department of civil engineering of Sonargaon University (SU), Dhaka and Bangladesh Council of Scientific and Industrial Research (BCSIR), Dhaka. The authors also acknowledge the efforts of all staff of strength of materials laboratory who conducted this study.

REFERENCES

[1] Alam, J., Islam, M.S., and Hyder, A.H.M.G. (2014). Comparison of engineering properties of coarse aggregates collected from different sources in Bangladesh, Conference Proceedings of 2nd International Conference on Advances in Civil Engineering 26 –28 Dec, CUET, Chittagong, Bangladesh, pp. 568-572.

[2] Suprenant, B. (1994). The importance of fitness modulus, Publication #J940107, Copyright © 1994, The Aberdeen Group, All rights reserved.

[3] Kwan, A.K.H., Ng, P.L., Huen, K.Y. (2014). Effects of fines content on packing density of fine aggregate in concrete, ELSVIER, Construction and Building Materials, Vol.: 61, pp. 270-277.

[4] Kronlof, A. (1994). Effect of very fine aggregate on concrete strength, Materials and Structures, January 1994, Volume 27, Issue 1, pp 15-25.

[5] Jenkins, R., 1974. An Introduction to X-ray Spectrometry, Wiley/Heyden, London, Chapter 4, 1974.

[6] Bragg, W.H., Bragg, W.L. (1913). The Reflexion of X-rays by Crystals, Proc R. Soc. Lond. A 88 (605): 428–38. Bibcode:1913 RSPSA..88..428B.

Mechanical Properties of Jute hybrid Epoxy Composites and Its Applications in Car Panels

Shekh Md. Mamun Kabir[1*], Rezaul Karim[2] and Md. Khayrul Islam[3]

[*]**Corresponding Author:** [1]Department of Wet Process Engineering, Bangladesh University of Textiles, Tejgaon, Dhaka
[2,3]Department of Textile Engineering, Sonargaon University (SU), Dhaka

Email: s.mamunkabir@yahoo.com

Abstract

The purpose of this paper is to ascertain jute composites to be a substitute to steel and other materials used in making car panels. It is highly important to find lightweight substitutes to steel so as to allow better fuel efficiency, better handling, higher speed limits and good maneuvering capabilities. Composites have been made by jute, glass fibre, resin and hardener hve been mixed at specific ratios and cured at 80°C and 120° C. Tensile tests and flexural tests have been carried out to understand the mechanical capabilities of the composite and are compared to the materials used nowadays for making car panels.

Keywords: Jute, Epoxy Resin, Composites, Tensile Strength, Flexural Strength, Car Panels.

1.0. Introduction

A car is wheeled, self-powered motor vehicle used for transporting passengers. The core element of a car is the body panel it carries and the ways in which it determines the characteristics of the car. The body structure must resist and soften the impact when applied on it, thus protecting the occupants. Also the car panel helps in improving the fuel efficiency and performance of the car. In recent times, the main concerns, due to high levels of global warming, has been to prevent excessive pollution from occurring. Cars have been made one of the highest contributions to pollution and global warming. Biodegradable and recyclable panels, the cars would not harm the environment as they would either mix with the soil or be broken into smaller bits and added to the new set of panel manufacturing [1-2]. Jute fibres are one of the fibres that exhibit environmentally friendly characteristics. Jute is completely biodegradable and compostable. Instead, extensive use of this fibre is advantageous as a hectare of jute plants, consumes about 15 tons of carbon dioxide while releasing 11 tons of oxygen [3]. A composite is a material made by the combination of a polymer matrix

combined with a textile reinforcement. Composites are highly useful as it leads to an improvement in the properties of both the phases that intermingle with each other [4-7].Resins used in fiber reinforced composites are called polymers. Polymers exhibit long molecular chains, containing multiple repeating units. These resins are made by addition reaction. Once cured, these thermosets will not change state in to a liquid form when heated, though after a certain temperature there will be a significant change in the mechanical property of the resin. This change can be reversed on cooling below T_g again. Above the glass transition temperature, stiffness drops sharply, thus decreasing the compressive and shear strength of the composite too [8].

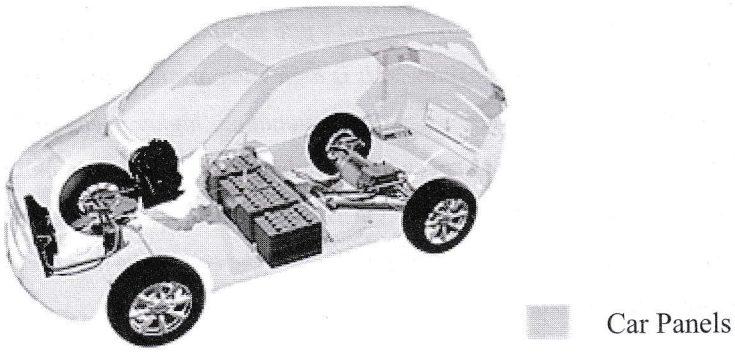

Fig.1. Car Panels

Firstly, steel is far heavier than jute composites. While 118.24 mm^2 of jute composite weighs is 0.4414 N, 102.37 mm^2 of mild steel weighs 2.922 N. This means cars are bulkier, slowe and less fuel efficient while using steel. Jute composites could help improve movement, handling, fuel efficiency, carbon dioxide emission, biodegradability factor and also speed of the car. Secondly, though steel production is very cheap, the initial capital required is very high, especially since steel has to be stamped out. The cost of the machine, including its set up is extremely high. While in the case of making jute composite industrially, the initial capital and production cost would be very low, hence cheaper for the manufacturing company. Thirdly, jute has a higher strength to weight ratio than steel.

In this study, we compared the performance of Jute hybrid epoxy composites are used in car panels like side wall, Roof rail, Roof cross member, Pillar, Pillar, Cross member, Tunnel, Cowl, Rear wall, Floor Cross member etc.

2.0. Experimental

2.1. Materials

Jute yarns are used which have a twist of 136.74 twist/m. Firstly an aluminum tool plate of 50cm x 50cm was used, Peel ply, Blue mesh fabric,A 35x35 cm steel top plate, Sealant tape, Nylon fabric 1.5m wide, Spiral tubes, PVC tubes, Cotton cloth, Nylon bagging film 100mm wide, A vacuum pump and connected nozzle, Epoxy Resin LY113, Hardener XB3043, Degassing chamber, A bench to place the setup and infuse, Clamps, An oven was used for curing the material were used.

2.2. Composite making

Steps to composite prepared in accordance to ASTM D3039 and testing are as follows:-

2.2.1. Laying up

First, a tool plate made of either steel or aluminum is taken and cleaned using a mould cleaner or acetone. This is done to remove any impurities and particles present on the surface of the tool plate, so as to prevent contamination of the composite while infusion and curing occurs. The directions shown below is used to coat the whole plate with the release agent. After this is done, the jute yarns are taken from the prepared cones and laid onto the tool plate using hand-laying technique (**Fig.2.**). The dimensions set for making the composite panel was 28 x 18 cm. The length was kept at 28 cm in accordance to ASTM D3039 standards, which state that the test samples should be of the size 25cm in length and 15mm (1.5 cm) in width.

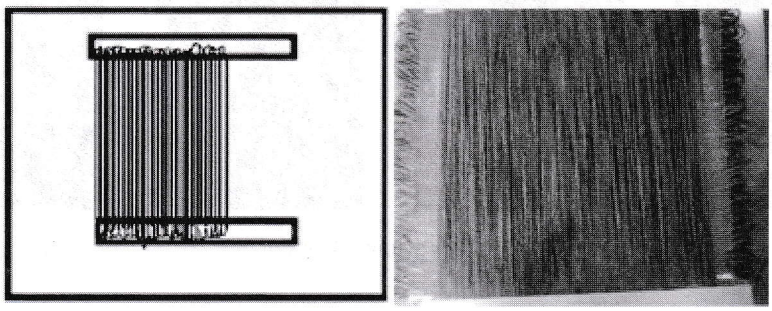

Fig.2. Jute fiber laying up

2.2.2. Vacuum bagging

After the yarns are laid up onto the tool plate, a 5x5 cm yellow sealant tape is cut out and is pressed against all the sides of the plate. This is done to remove any loose fibre present at the edges,

which could prevent vacuum bagging (Figure 3). These loose fibres stick to the tape and after pressing the edges, the sealant tape is disposed of. Also a layer of mould cleaner is applied to remove any other impurity and hand marks present on the edge of the plate.A piece of blue mesh fabric is cut, which cures at a maximum temperature of 120ºC. The blue mesh fabric, helps in smoother and quicker resin transmission, thus improving resin impregnation. The fabric has a mesh like structure which smoothly transmits the resin from one end to the other. Also two pieces of white breathable fabric are cut to size 20cm x 20cm along with two pink plastic tubes of width 10cmof size 25cm. The white breathable fabric and pink plastic tube is used to make a resin trap. Finally a large piece of plastic film is cut out of dimensions 70cmx 70cm.Finally two spiral tubes, each a little shorter than the width of the layup, is cut. Hence a 15cm tube is cut for the tensile specimen and 32cm tube is cut for the flexural test specimen. If the tubes are of the same size as the width of the panel then the gaps would be very minute, which would thus prevent easy flow of resin.

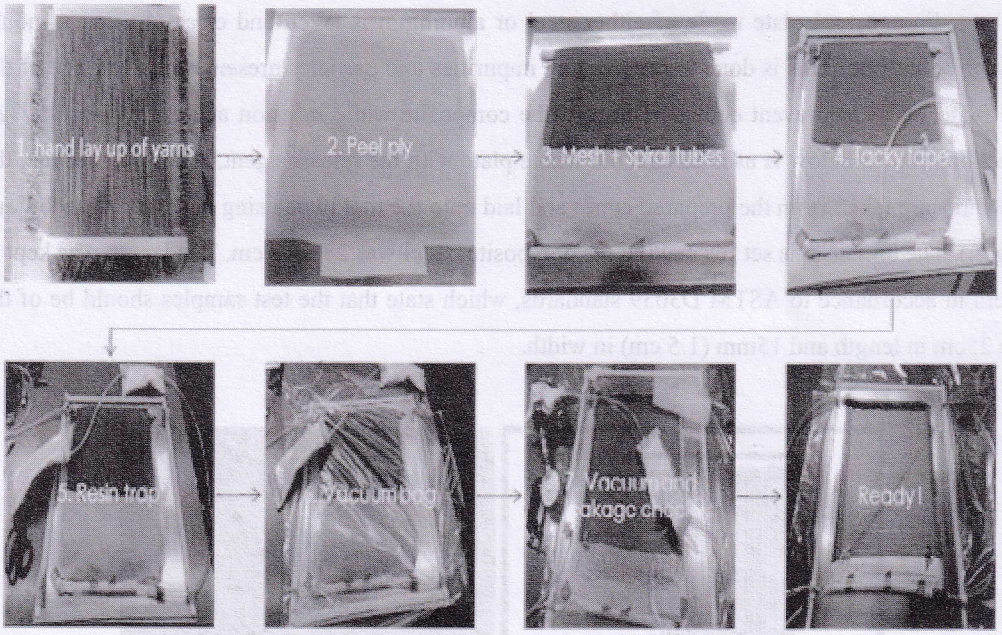

Fig.3. Vacuum Bagging

2.2.3. Resin infusion

First the epoxy resin is mixed with a hardener at a ratio of 100:35. It is noticed that the epoxy resin has a much higher viscosity than the hardener. These liquids are then mixed with the help of a wooden stirrer for a long time so as to get an even mix. This continuous mixing captures

more air bubbles in the mix which is detrimental to the properties of a composite. Thus the mixture is then put into the degassing chamber. The cup holding the mixture is kept in the chamber for about 40 minutes and a constant watch is kept so as to prevent the bubbles from overflowing as it would lead to loss of the mixture and thus may cause shortage of the mixture while infusing. The infusion process (Figure 4), after this, the cup is brought to the tool plate and the sealant tape from the end of the inlet tube is removed, followed by which the tube is dipped into the mixture prepared in the resin cup. Then the valve is attached to the nozzle of a vacuum pump where vacuum is pulled at lower pressure. The vacuum pump is not used to vacuum in this case. The pump is used at lower pressure only to provide better control over the direction of the resin flow.

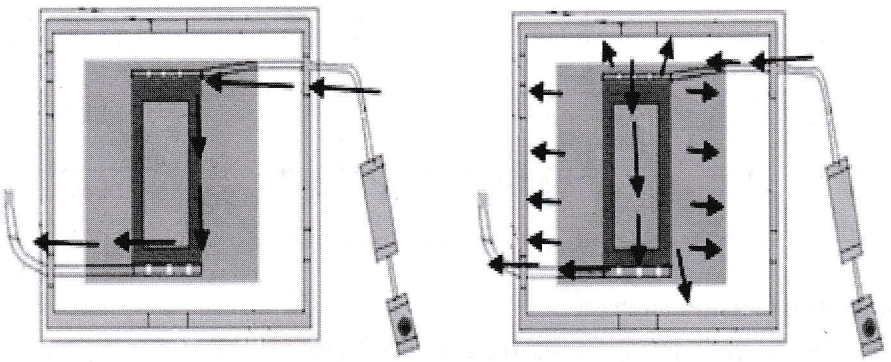

(a) (b)

Fig. 4. Resin Infusion (a) with vacuum pump attached (b) without vacuum pump attached

2.2.4. Curing

The resin infused setup is taking into the curing chamber to allow the sample to be cured. The two resin traps are used specifically for this function. When heat is applied onto the resin, the viscosity of the resin decreases thus making it flow further down the tube. The resin trap helps absorb this excess amount of resin preventing it from reaching the valve and thus preventing any damage to it. In the first hour, the temperature goes up from room temperature to 80°C. After this the temperature stays constant for 2 hours, where curing starts to take place. Then post curing is done where the temperature rises to 120°C in 1 hour 15 minutes followed by 6 hours period of stay at this temperature. This is done so as to set better mechanical property for the composite.

2.2.5. Cutting

Keeping the standards for the D3039 tensile test in check, the 28cm x 18 cm panel was cut in to 5 samples of 25cm x 1.5cm each, with the help of a diamond cutter. While in the case of the flexural test D790, 6 samples of dimensions 10cm x 1.3cm was cut (**Table. 1**).

Table-1: Specimens for Jute composite panels

Specimen	Width (mm)	Thickness (mm)	Length (mm)	Weight (g)
1	14.29	3.005	24.9	13.11
2	15.62	3.239	24.9	14.82
3	14.75	3.077	24.9	13.61
4	15.41	3.101	24.9	14.85
5	15.45	3.197	24.9	14.86

2.3. Measurement of tensile strength

The tensile strength was measured by ASTM D3039-76 at room temperature. First the machine is set to perform the tensile test on the 5 different samples. a hydraulic testing machine Instron H10KSwas used. A 50 kN load cell is applied for the test. The load cell provides an electricalcircuit which helps to measure the instantaneous load applied along the axis of load. (Gurbuz&Cevik et al.). A contact extensometer was used to measure the stress- strain curve and record other data required during the test. The jogs which hold the grips are adjusted to size so as to only allow the tabs to be held by the grips of the machine thereby exposing a 15cm gauge length in between the grips. After this, the specimen protect is turned on and the extensometer is applied to the center of the specimen.

2.4. Measurement of flexural test

The flexural test was measured by ASTM D790-03 at room temperature. In this test, a round cross sectional head with a diameter of 10mm as per the D790 standard. The specimen was of length 150mm length and 15 mm width and were loaded with a span to depth ratio of 16:1. The distance between the two supporting pin from the loading pin should be equidistant. As per the standards, a 16:1 distance is maintained between the gauge length and the thickness.

1.0. Results and discussions

Fig.5. represents tensile modulus curves for each of the five samples. It is found from this figure that the stiffness is maintained at 135.48 MPa which is equivalent to 0.135 GPa. Considering that the stiffness plays an important role in how the panel would behave when impact will apply on to it, it may be said that the stiffness limit is much lower than those of carbon, glass and steel.

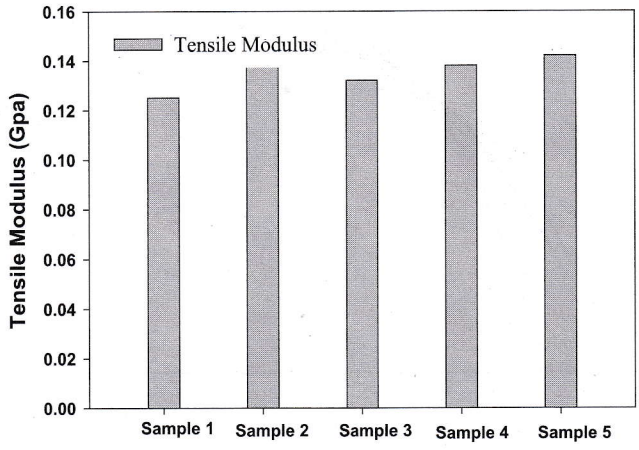

Fig.5. Tensile Modulus comparison of all 5 samples

The yield stress plays a very important role in understanding the basics of cars and the properties required for making a successful car panel.

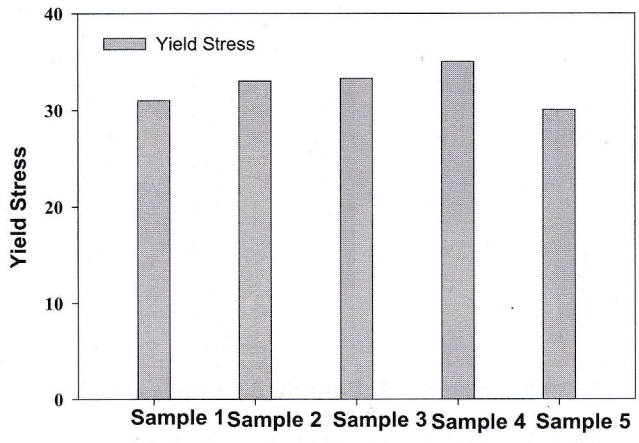

Fig.6. Yield stress in the different yield composites

Yield stress is the point after which the material stops elastic deformation and goes into the zone of plastic deformation. **Fig.6.** shows that the stress applied on a composite is higher than those of composite yield stress, which means that thecomposite is permanently deformed and will not regain its original shape.

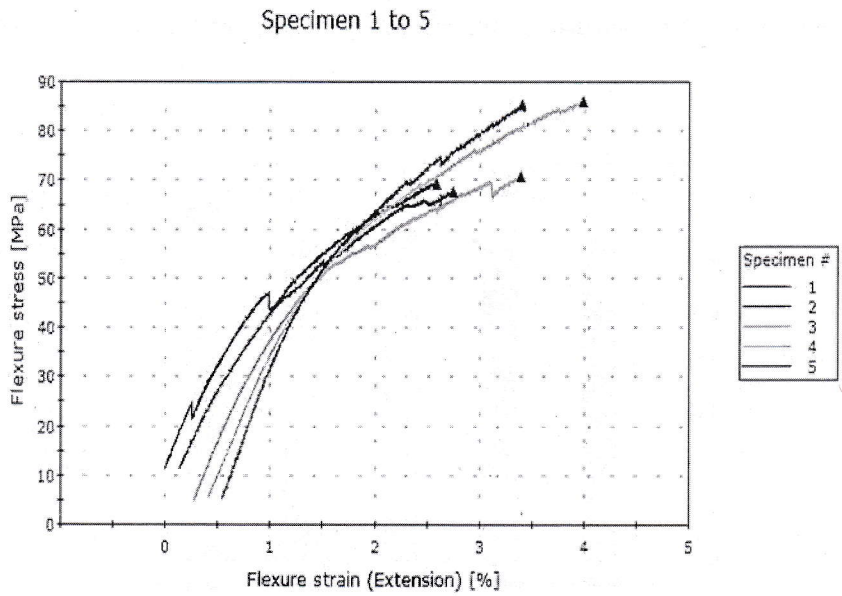

Fig.7. Flexural stress-strain curve on different composites

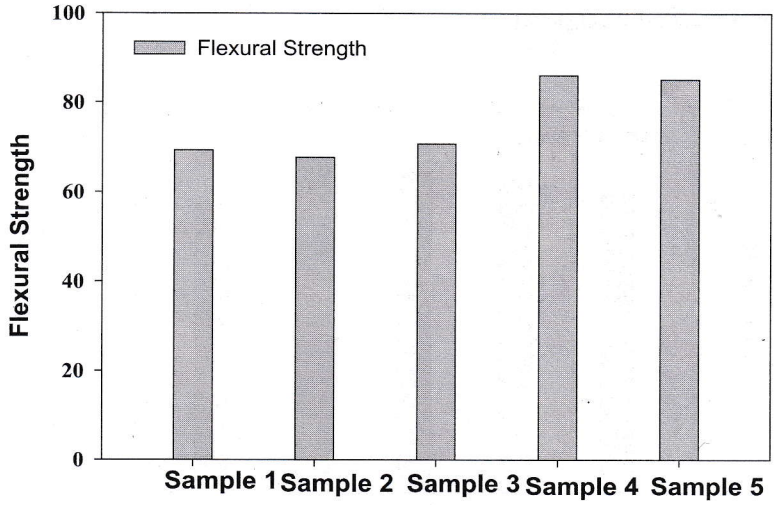

Fig.8. Flexural strength on different composites

As seen in the **Fig.7.** , the final 2 specimen show a little higher flexural strength, meaning that there might have been some minor faults while preparing the composite, though the difference is not very high. The little fluctuations seen in the graph occurs when the force applied on the composite breaks the fibres on the initial layers as the material tends towards failure. It does not imply though that the material has reached failure. Flexural strength is the limit of the composite to withstand flexural stress without failing. When an object is subjected to flexural stress, it goes through both, a tension and compression behavior because of the bending movement. The flexural strength (**Fig.8.**) will depend on the material's tensile or compression strength, whichever is lesser in value. Flexural stress is extremely important as it can predict how a material will react on impact to it and the amount of bend it forms. The flexural modulus is the ratio of the stress to the strain when flexural deformation takes place. Thus it is the materials tendency to bend when force is applied to it. The flexural modulus (**Fig.9.**) plays a very important role for material to be used as a car panel. Even if the material receives high impact but does not fail, it may bend too much harming the users of the car. Therefore, it is very important for the material to have good flexural strength and stiffness.

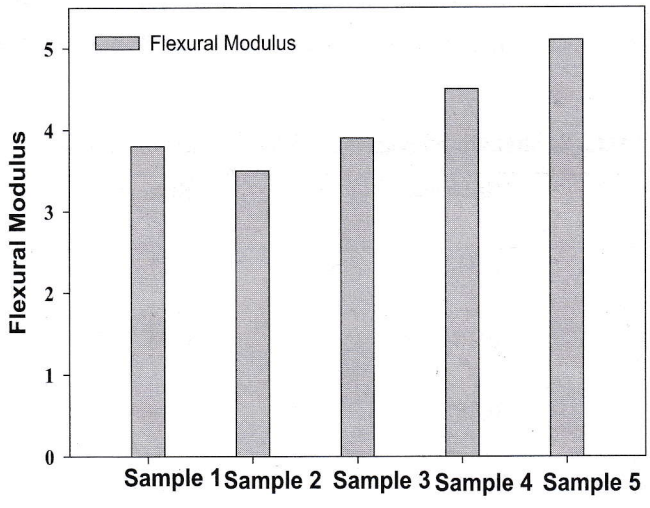

Fig.9. Flexural modulus on different composites

Comparison of the weight to strength ratio shows in **Fig.10.**, it is clearly shows that the weight to strength ratio of composite is a little higher than mild steel. This means that composite materials have less weight and more strength, which could be appropriate for car panels.

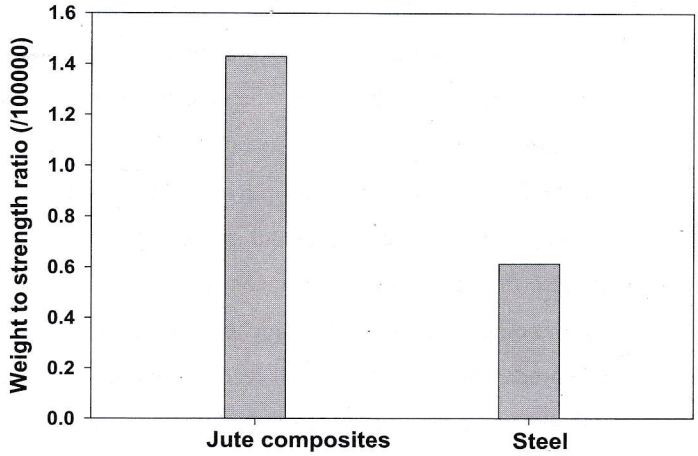

Fig.10. Comparison of the weight to strength ratio

Different parts of the car requires different amounts of yield stress to maintain its safety and security. While some parts of the car play an extremely important role, others are far less affected on the event of a crash. This has been shown in the diagram below, which represents the different yield stresses needed in different parts of the car. On the basis of that the following chart would discuss the stiffness and strength relevance required in every part of the car (Table 2) (European aluminum association, 2010).

Table. 2. Strength relevance of different parts of the car

Car Panel	Stiffness	Strength
Firewall	0.31	0.77
Floor	0.26	0.38
Tunnel	0.38	0.48
Floor Crossover	0.51	0.59
Roofrail	0.31	0.08

Lightweight design play a very important part in the manufacturing process of a car. The reduction of fuel consumption was identified as one of the main purposes, because only one third of

the CO_2 emission occur from engine factors. The next reason for lightweight design was to reduce aerodynamic drag. It helps in better handling and movement of the car. Thirdly, the reduction in rolling resistance plays an important role, even though in the short term. This helps improve the maximum speed acquired by the car. The other additional advantages such as optimization of auxiliary aggregates will help to cause less emission from vehicles and improve vehicle efficiency.

1.0. Conclusions

From this study the following conclusions may be drawn:

(1) This study gives an emphasis on the fabrication of jute composites as the panel of the future as it shows great potential as a future substitute to heavier materials being used for making car panels now a day.

(2) This study has demonstrated all the objectives and come out with some favorable outcomes and has some drawbacks that will have to be looked into in the future as the technology grows.

References

[1] Bastioli, C., 2005. In: handbook of biodegradable polymers. Rapra Technology.

[2] H.K.Mishra, B.N.Dash, S.S.Tripathi & B.N.Padhi, (2000). Study on Mechanical Performance of Jute-Epoxy Composites. India.

[3] S.Shaktivel, O.P. Lakshmanan, A.Zaid Hamsa, S.D. Kiruthika, E. Rajadurai, 2012. Application of Jute and Its overviews. http://www.fibre2fashion.com/industry-article/41/4047/applications-of-jute1.asp

[4] Solemanifar, a., 2014. Damage Tolerance of Composites Containing Hybrid (Carbon - Innegra™) Fibre Reinforcements, Manchester.

[5] Warren, D., 2010. Low Cost Carbon Fiber Overview

[6] Gassan, J., 2002. A study of fibre and interface parameters affecting the fatigue behavior of natural fibre composites.

[7] A.N.Viduran, M., 2014. jute and steel - their problems and prices.

[8] Hossain, M. R., Islam, M. A., Vuurea, A. V. & Verpoest, I., 2013. Tensile behavior of environmental friendly jute epoxy laminated composite, Dhaka.

[9] Hua-Hu, R. et al., 2010. Fully degradable jute fibre reinforced Polylactide Composites, Switzerland.

[10] Koronis, G., Silva, A. & Fontul, M., 2012. Green Composites: A review for adequate materials for automotive applications, Lisbon.

Numerical Simulation Of Non-Newtonian Spiral Flow Through Stenosed Artery With 75% And 96% Area Reductions

Md Ferdous Alam[1*]; Muhammad Rubayat Bin Shahadat[2]; Md. Alamgir Kabir[3]; Md. Mostofa Hossain[4]

***Corresponding author:** [1]Department of Mechanical Engineering, Shahjalal University of Science and Technology, Sylhet, Bangladesh
[2]Department of Mechancial Engineering, Hajee Mohammad Danesh Science and Technology University (HSTU), Dinajpur, Bangladesh
[3]Department of Mathematics, Shahjalal University of Science and Technology, Sylhet, Bangladesh
[4]Head, Department of Mechanical Engineering, Sonargaon University (SU)

Email: mfalam-mee@sust.edu

Abstract

Blood flow through arterial stenosis can play important role in blood vessels and it is a very complex flow as blood is a non-newtonian fluid. In the present study, the Carreau model has been used to find out the characteristics of blood flow through a regular stenosis. The effects of Reynolds number (Re) on Non-Newtonian flow through a 3D model of a biological type arterial stenosis is studied. The shape of the stenosis has been varied. Here, stenosis with 96% and 75% area reduction have been used. The standard k-ω model is used for simulation of blood flow for four Reynolds numbers (Re = 500, 1000, 1500, 2000). Some numerical results such as velocity profile, pressure field, streamline, wall shear stress (WSS), turbulent kinetic energy (TKE) etc. are examined for different spiral velocities at different Reynolds numbers. Details investigation and significant pathological issues are described throughout the investigation.

Keywords: Stenosis, Reynolds number, Blood flow, Wall shear, artery

NOMENCLATURE

Symbol	Meaning	Unit
D	Artery diameter	m
ρ	Density	kgm
r	Radial location from axis of artery	m
μ	Dynamic viscosity	Nsm
V	Stream wise bulk velocity	$m\ s$
v	Instantaneous velocity	$m\ s$
Ω	Spiral velocity	$radsec$
Re	Reynolds number	Dimensionless
R	Radius of blood vessel	m
k	Turbulent kinetic energy	Jkg
μ	Turbulent eddy-viscosity	m/sec
ω	Specific dissipation rate	$1/s$

u	Mean velocity components	$m\ s$
u'	Fluctuating velocity components	$m\ s$
	Constant	Dimensionless

1.0. Introduction

Blood circulation is one of the most important functions of human body and blood vessels are called the high ways of human body. Blood vessels that carry oxygen-rich blood to the heart and other parts of the body are called arteries which have smooth inner walls and blood flows through them easily without any obstacles. Arterial stenosis is an unusual narrowing of an artery where cholesterol and other lipids are deposited in the inner lining of the arterial wall and the cross-sectional area of a blood vessel shrinks. When the depositions of fat and other lipids build up in the beneath artery walls it causes repeated injury to the inner lining of the arteries which results in physical stress in the form of high blood pressure or inflammatory stress, infections, high cholesterol or high blood glucose. When arteries have blockage caused by these types of diseases, it is called atherosclerosis or arteriosclerosis vascular disease (ASVD) Ross et.al. [1]. Such kind of disease is promoted by Low-Density Lipoproteins (LDL) without adequate removal of fats and cholesterol from the macrophages by functional High-Density Lipoproteins (HDL).

When the increasing of fatty material which becomes almost settled in the artery forms a thickened area in the vessel wall called plaque, it reduces the effective cross-section of the vessel and slows down the blood flow. The rupturing of this plaque exposes the fatty core and can lead to the formation of a thrombus, where the blood platelets form a clot about the exposed area which can block off the entire artery and it becomes very dangerous when it obstructs or stop the flow of blood to some major organs, such as the heart or brain that may be the cause of sudden death.

As hemodynamic behavior of the blood flow in arterial stenosis bears some important aspects for medical applications It is therefore no doubt that this topic is now of major concern to the community and the focus of numerous research efforts and more recently, computational techniques have demonstrated the ability to model flow behavior in stenosed arteries with different geometries and conditions that can be specified according to the actual conditions. A thorough understanding of blood dynamics in human vessels has a great interest among the researcher and nowadays the computational simulation is playing a significant role in this field. Therefore a large number of computational and experimental studies have been conducted to simulate and investigate blood flow in arterial stenosis. The hemodynamic factors such as wall pressure and shear stress have major effects in damaging and weakening the internal wall of the artery at the post-stenotic turbulent region. For example, high-wall shear stress associated with turbulence has a significant effect on vascular endothelial injury Fry DL [2].

In some cases, they over-stimulate platelet thrombosis, and then accelerate atherosclerosis, as eported by Stein et al. [3]. On the other hand, the thickening of the intima caused by remodeling of the essel wall is related to the presence of low shear stress at the throat of the stenosis, Ku et al. [4]. Using aser Doppler anemometry and flow visualization techniques, Ahmed and Giddens [5] studied the effect of axisymmetric stenosis on the velocity field in the post-stenosis zone in various percentages. In the experiment, the upstream flow remained stable, the study considered the Reynolds number in the range of 500-2000. Ghalichi et al. [6] used the k-ω of Wilcox turbulence model to study the blood flow in the ame stenotic arterial model as in [5]. Their results show that the k-ω model have a good agreement with experimental data and is superior to the standard k-ε model in predicting blood pressure and turbulence ntensity.

Lee et al. [7] studied the turbulence flow through a series of axisymmetric stenosis by applying stable parabolic profile at the upstream, indicating that the k-ω model has good accuracy for predicting laminar as well as turbulence flow through stenosed artery and more stenoses can result in a lower ritical Reynolds number that means an earlier occurrence of turbulence for the stenotic flows. Paul et l. [8] used Large–Eddy simulation (LES) techniques to study pulsatile blood flow through a 3D model of a biological type stenosis formed on the top wall. The smooth constriction, which was generated using the cosine relation of [5], gives a fairly accurate representation of an arterial stenosis and their esults shows that the high level of flow recirculation associated with complex patterns of transient blood flow have a significant contribution to the generation of the turbulent fluctuations found in the post-stenosis region.

The limitation of the k–ω model in the modelling of transient blood flow through the stenosis s also highlighted in their study. Sarifuddin et al. [9] used three differently shaped stenoses-cosine form, irregular shape and smooth constriction and investigated the blood flow through them numerically prescribing a parabolic velocity profile at the inlet and shows that the post-stenotic results has a good agreement with existing investigations in the steady state but mainly influenced by the choice of the stenosis used in the model. The circular motion of the heart pump causes the blood to pulsate naturally hrough the arteries. The blood flow in the circulatory system is mainly pulsatile laminar flow.

However, due to the combined action of flow pulsation and strong shear, flow separation, ecirculation, and stenotic recanalization, the passage of blood vessels through severe stenos is can lead o periodic transitions in the posterior stenos is to turbulence. As the heart is twisting on its own axis the blood flow through artery is spiral that is obvious from the vivo research of Stonebridge and Brophy [10] and Stonebridge et al. [11] which has a theoretical advantage- forward, rotation-induced stability and lateral force reduction can reduce turbulence and stenosis in the conical branch arterial tree and have a beneficial effect on the mechanism of endothelial damage and repair.

In this study, the Carreau model has been used to model the non-newtonian flow. Four different Reynolds numbers (Re = 500, 1000, 1500, 2000) and corresponding spiral velocities have been used in this study of investigate the effect of Re. Two distinct stenosis model with 75% and 96% area reduction has been used here.

2.0. Problem specification

It is obvious that one of the crucial parts of blood flow simulation is the problem specification and formation for proper investigation. An artificial geometrical model of the stenosis considered as the conventionally used cosine curve in the blood vessel shown in **Fig.1(a)** is created using the following formula [5].

$$\frac{r(Z)}{R} = 1 - \delta_c\left[1 + \cos\left(\frac{Z\pi}{D}\right)\right], \quad -D \leq Z \leq D \quad \text{.....(1)}$$

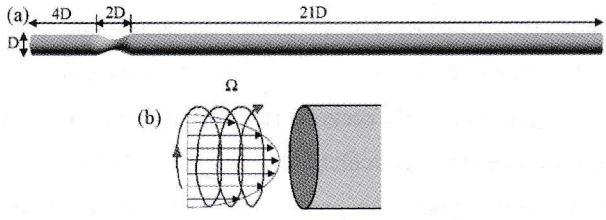

Fig.1. (a) Schematic of the model of a stenosed blood vessel and (b) an interpretation of the spiral boundary condition with the parabolic flow at the inlet of the model. [12]

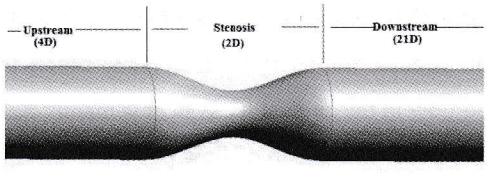

Fig.1. (b) an interpretation of the spiral boundary condition with the parabolic flow at the inlet of the model.

Fig.1. (c) Schematic of 75% and 96% stenosis

Where, r and Z are the radial and axial co-ordinates and R and D are the radius and diameter of the unstenosed vessel respectively and the percentage of the stenosis is control by the parameter δ .The constrictions followed the cosine curve with 75% area reductions. The smooth reduction of the cross-sectional area produced inside the vessel using Eq.(1) provides a fairly accurate representation of the biological form of arterial stenosis as it has been employed previously in theoretical calculations by [5],Deshpande et al. [13] and Smith et al. [14]. The entire span of the biological form model is taken as 540(27D) mm [5], where diameter D=20 mm and the length of the upstream, downstream and stenosed zone are taken as 4D, 21D *and* 2D respectively. Blood flow through the model is considered as incompressible and Newtonian and homogeneous fluid [15] with a density of ρ $1060\ kg/m$ and a constant dynamic viscosity of μ 3.71×10^{-3} Pa s. At the inlet of the model a spiral boundary condition along with a parabolic velocity profile is used which is shown in **Fig.1(b).**

The Navier–Stokes equations are used as the governing equations of motion of the blood flow and after applying the Reynolds time-averaging techniques, the Reynolds averaged Navier–Stokes (RANS) are obtained and written in the tensor form as [16],

$$\frac{\partial u_i}{\partial x_i} = 0 \quad \ldots\ldots\ldots\ldots\ldots\ldots\ldots\ldots\ldots\ldots\ldots\ldots (2)$$

$$\frac{\partial}{\partial t}(\rho u_i) + \frac{\partial}{\partial x_j}(\rho u_i u_j) = -\frac{\partial p}{\partial x_i} + \frac{\partial}{\partial x_j}\left[\mu\left(\frac{\partial u_i}{\partial x_j} + \frac{\partial u_j}{\partial x_i}\right)\right] + \frac{\partial \tau_{ij}}{\partial x_j} \quad \ldots\ldots\ldots\ldots\ldots\ldots\ldots\ldots\ldots\ldots\ldots\ldots (3)$$

where u are the mean velocity components along the Cartesian co-ordinate systems, $x = (x\ y\ z$, p is the pressure and τ are the Reynolds stresses which are modeled employing the Boussinesq hypothesis as,

$$\tau_{ij} = -\rho\langle u_i' u_j'\rangle = \mu_t\left(\frac{\partial u_i}{\partial x_j} + \frac{\partial u_j}{\partial x_i}\right) - \frac{2}{3}\rho k \delta_{ij} \quad \text{.....(4)}$$

Where u_i' are the fluctuating velocity components; $k = \frac{1}{2}\langle u_i' u_j'\rangle$ is the turbulent kinetic energy and μ_t is the turbulent eddy-viscosity obtained by employing the standard $k-\omega$ model of Wilcox [17]. The eddy-viscosity is modeled as

$$\mu_T = \frac{\rho k}{\omega} \quad \text{.....(5)}$$

where ω is the specific dissipation rate. The following modelled transport equations (Wilcox [17]) are solved to obtain k and ω:

$$\frac{\partial k}{\partial t} + \frac{\partial k(u_j)}{\partial x_j} = -\frac{1}{\rho}\left(\rho u_i' u_j'\right)\frac{\partial(u_i)}{\partial x_j} - \beta^* k\omega + \frac{\partial}{\partial x_j}\left[\frac{1}{\rho}(\mu + \sigma^* \mu T)\frac{\partial k}{\partial x_j}\right] \quad \text{.....(6)}$$

$$\frac{\partial \omega}{\partial t} + \frac{\partial \omega(u_j)}{\partial x_j} = -\alpha_1 \frac{\omega}{\partial k}\left(\rho u_i' u_j'\right)\frac{\partial(u_i)}{\partial x_j} - \beta\omega^2 + \frac{\partial}{\partial x_j}\left[\frac{1}{\rho}(\mu + \sigma\mu T)\frac{\partial \omega}{\partial x_j}\right] \quad \text{.....(7)}$$

Where $\sigma * = 0.5$, $\beta * = 0.072$, $\sigma = 0.5$, $\alpha 1 = 1.0$ and $\beta = 0.072$. The details of this turbulent model can be found in [15,16].

3.1. Boundary condition and computational procedure

The artery that has been used in the existing model is considering as an inflexible and impervious circular tube with a no-slip boundary condition for fluid having zero velocity ($u_i = 0$) relative to the boundary along with a parabolic velocity profile

$$v(x,y) = 2V\left[1 - \left(\frac{r}{R}\right)^2\right] \quad \text{.....(8)}$$

which has been imposed at the inlet of the model, where V is the bulk streamwise velocity related to the Reynolds number, $Re = \rho VD/\mu$, of the blood flow. The spiral velocity (Ω) is characterized as a proportion of the forward velocity inside the blood-vessel that has been calculated with the following equation

$$\Omega = \frac{V}{R}C \quad \text{.....(9)}$$

In which C=1/6 as mentioned in [17, 18] is a constant that governs the magnitude of the spiral speed. Additionally, the outlet of the model has been treated as a pressure outlet using the default setting for the gauge pressure to become zero at the outlet. Commercially available CFD software, Fluent [16], has been used in this study. This software uses finite volume method for discretization.

The finite volume method represents and evaluates partial differential equations in the form of algebraic equations. Pressure based solver has been used to solve the flow eqations with implicit formulation method. Additionally, the SIMPLE scheme for pressure-velocity coupling has been used. In the discretisation process, the second order upwind scheme is used for the equations of momentum, turbulent kinetic energy (k) and specific dissipation rate (ω); while the second order accurate scheme is used for the Poisson-like pressure equation. The inlet boundary conditions for the stream wise velocity has been written in C-language using the interface of User Defined Function (UDF) of Fluent and linked with the solver.

The solution process is initiated using arbitrary values of the velocity components and k-ω, and their residuals are monitored at every iteration. The magnitude of the residuals dropped gradually, which is a strong indicator for the stable and accurate solutions, and the iteration process is stopped when the residuals are leveled off at 10^{-6} (in fact the residuals became independent to the iteration number at this level) and the final converged solutions are achieved. Finally this study has been carried out for three different mesh numbers and grid independent test was conducted.

Table.1. Values of spiral velocity (Ω) for the different Reynolds numbers.

Re	C	$\Omega(r\ a\ ds$
0		0.0
500		1.46
1000		2.92
1500	1/6	4.38
2000		5.83

4.0. Results and discussion

In the present study, axial velocity is used as comparing variables for grid independence and the results are shown in Fig.2(a), Fig.2(b) and Fig.2(c) for different grid points. Initially, Grid 1 consists of 50630 cells, and then it was increased by about 99% for Grid 2 that consists of 100630 cells. Finally, Grid 3 was increased by a huge amount (more than 323% including 229680 cells) for the entire computational area. Finally grid 3 was used for calculation This grid independence test has been performed to ensure that the numerical solutions are independent on the choice of the grid arrangements

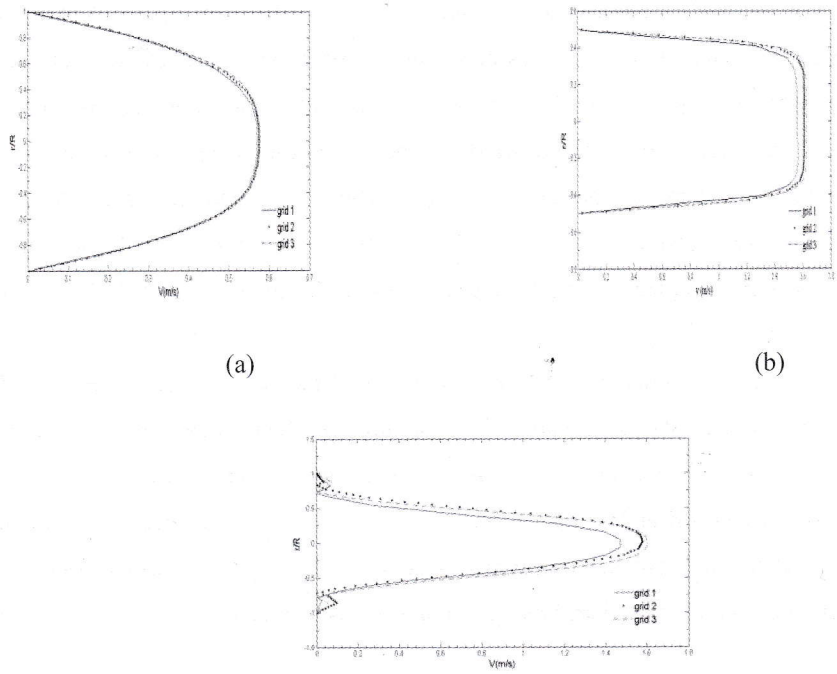

(a) (b)

(c)

Fig.2. Grid independence test shown for axial velocity at different radial positions **(a)** Z=-2D **(b)** Z=0D and **(c)** Z=2D

4.1 Effect on Pressure

The effect of the spiral flow on the total pressure at the centre of the model artery has been stuied (Fig.3). A large pressure drop occurs at 0m axial position, which is the position of the stenosis. However, pressure remains almost constant from 0.1m to the rest of the artery. For larger Re (Re=2000) a slight increase in pressure in the post stenotic region can be observed.

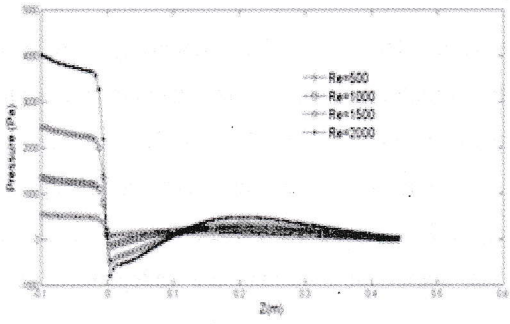

Fig.3. Centerline total pressure at various axial positions for different Reynolds numbers

4.2. Effect on Velocity

Centerline velocities (**Fig. 4.**) have also been studied to investigate the effect of Reynolds. The effect of spiral component can be explained in these figures. From **Table.1** it can be observed that for a higher Re, spiral velocity also increases. With the increase in Re and Ω, magnitude of axial velocity also increases. Due to the stenosis there is a large increase in axial velocity magnitude. The effect of spiral component, however, is quite less on radial and tangential velocity although For lower Re (Re=500,1000) the effect is significant. For comparatively higher Reynolds numbers and gradually higher Ω the effect is not that mentionable.

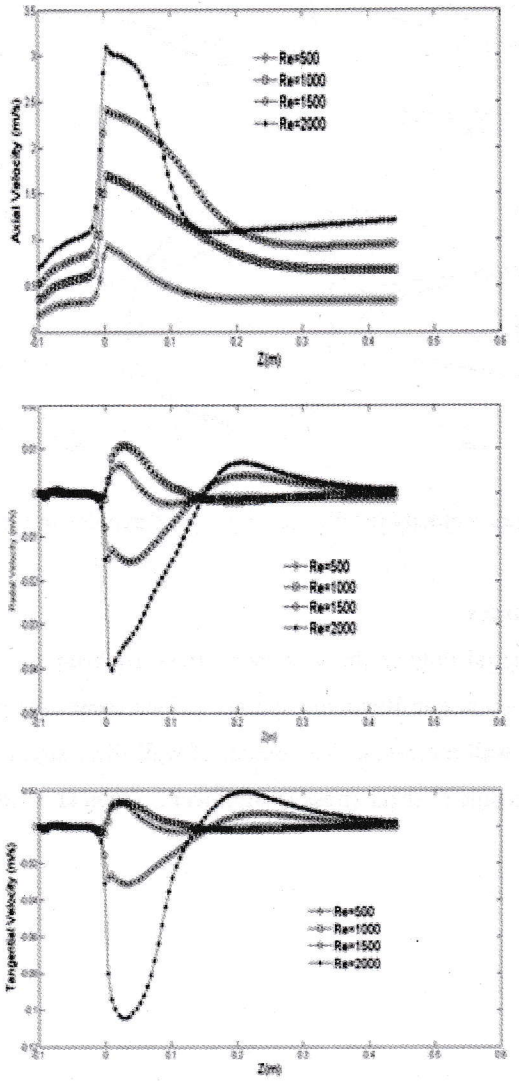

Fig.4. Centerline velocity at different axial positions for different Reynolds numbers

Velocity profiles for different Reynolds number has been shown in Fig.5. A dimensionless parameter (r/R) has been taken on the y-axis. From the figure it is obvious that the magnitude of velocity is maximum at the stenosis and almost 0.9 m/s, 1.6 m/s, 2.3 m/s, 3 m/s for Re= 500, 1000, 1500, 2000 respectively. The parabolic velocity profile before the stenosis also depicts the intial condition, the shape of which changed drastically after the stenosis.

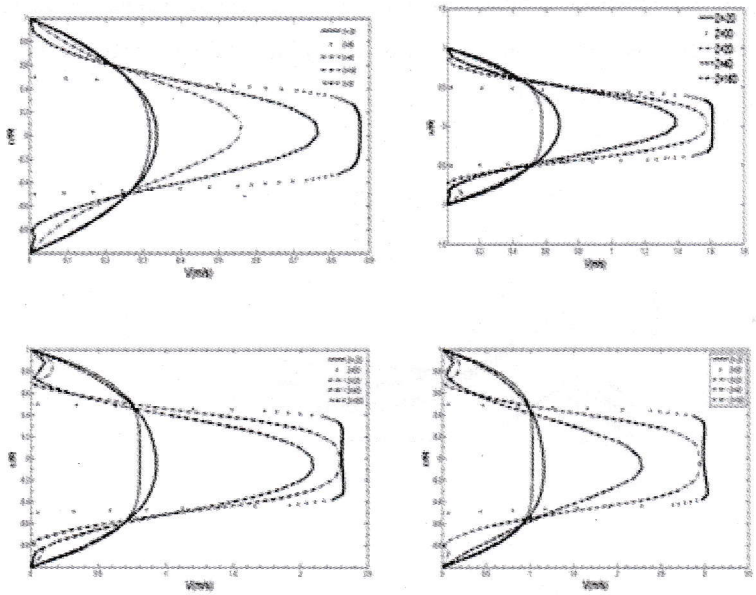

Fig.5. Velocity profiles for different Reynolds number

4.3 Effect on wall shear stress

The influence of spiral flow on the wall shear stress has been elaborat3ed in Fig.6. It can be easily seen that, with the increase in Reynolds number (which means increment in spiral flow) wall shear stress along the pipe wall increases. The contour of wall shear stress is easily observable. Also at the stenotic region the change in shear stress is significant. When $\Omega = 5.83$ rad/sec, maximum wall shear stress is observed.

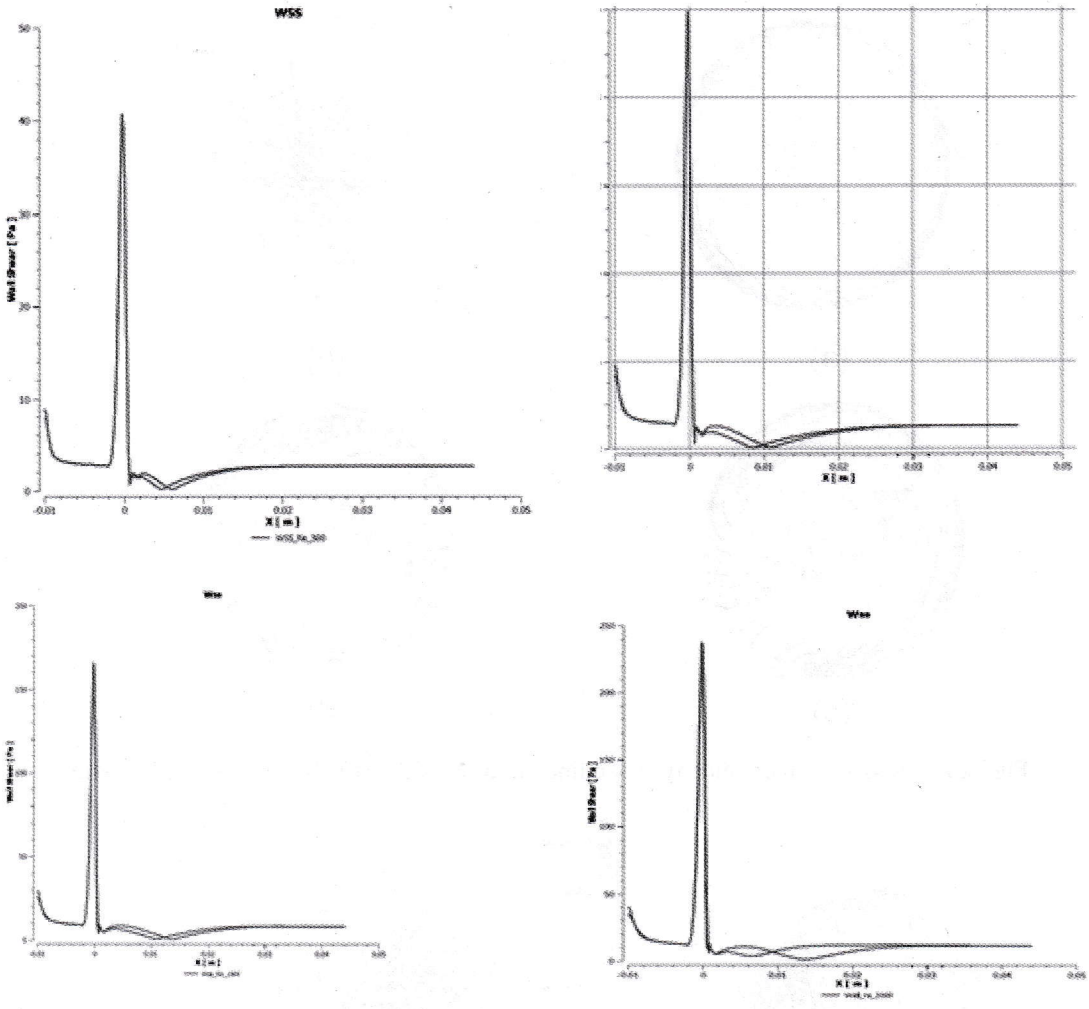

Fig.6. Wall shear stress along the pipe wall

The effect of spiral flow can be described efficiently form the cross sectional views of the velocity streamlines. From Fig.7, the structure of the blood flow at the downstream for different spiral speeds can be investigated. Interestingly, they produce twisted three-dimensional flow. This pattern of flow is similar to that of the MRI measurement of the blood flow in a patient's artery with thrombosis done by Frydrychowicz et al. [19]. The intensity of the twisting flow at 4D distance is quite strong and flow pattern is much chaotic in the downstream region. This chaotic behavior can cause potential damage to blood cells and inner surface of the artery [12].

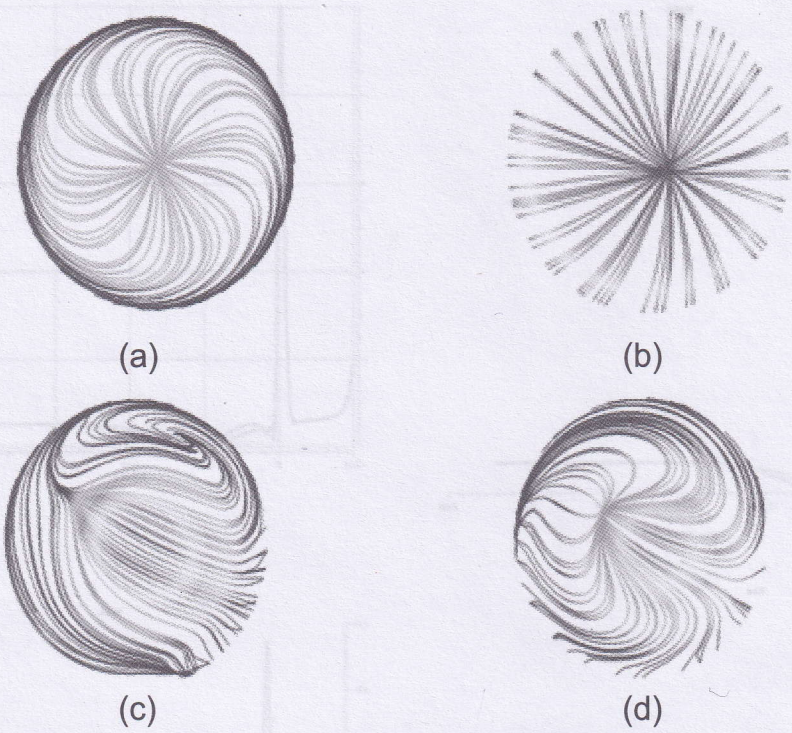

Fig.7.(a). Cross section of velocity streamlines at **(a)** Z=-2D **(b)** Z=0D **(c)** Z=2D **(d)** Z=4D

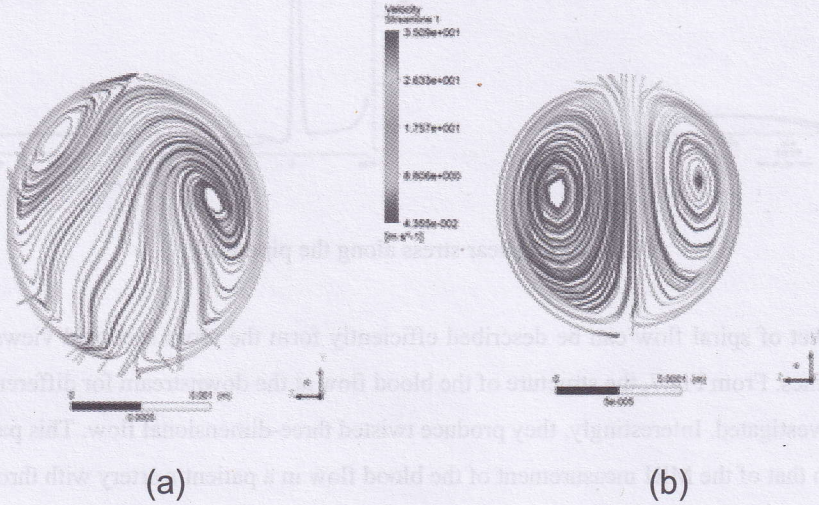

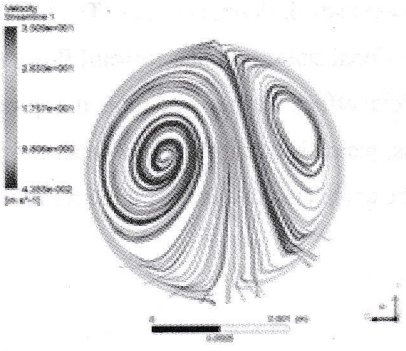

(c)

Fig.7. (b). Cross section of velocity streamlines at 96%stenosis **(a)** Z=-2D **(b)** Z=0D **(c)** Z=2D

4.4 Effect on Turbulence Kinetic Energy

The effect of the Reynolds number on the turbulent kinetic energy (TKE) has been shown in Fig.8. The increase of TKE for Re= 2000 is quite phenomenal compared to other Reynolds numbers, while the effect for Re=500, 1000 can be almost negligible. There is significant increment of TKE in the downstream (in the post stenosis region).

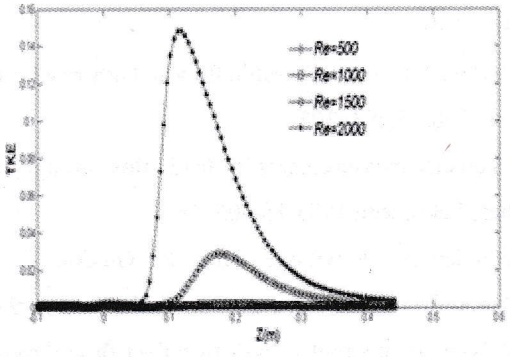

Fig.8. Turbulence kinetic energy at different axial positions for different Reynolds numbers

5. CONCLUSIONS

This paper aims to draw decisive conclusion that spiral component of blood flow has important impact on human artery while the Reynolds number play a crucial role for significant parameters of blood flow. The increase in turbulence kinetic energy in the downstream region is responsible for the destruction of blood cells, and the platelets in the blood are activated, resulting in

many pathologic diseases attack in human body. The turbulent kinetic energy is reduced by the spiral flow as it causes rotational stability in the forward flow as a results it prevents the damage of blood cell which is a beneficial effect. At the same time, the spiral flow in the posterior stenosis in the oscillation wall shear stress, which is harmful. In this paper a simplified model of artery has been used. Further research should be conducted in this regard to investigate the proper biological boundary conditions.

6.0. Acknowledgement

The authors would like to express gratitude to Shahjalal University of Science and Technology for providing the computing facility in Large Scale Computing Laboratory.

REFERENCES

[1] Ross, Russell (29 April 1993). "The pathogenesis of atherosclerosis: a perspective for the 1990s". Nature. 362 (6423): 801–809. PMID 8479518

[2] Fry DL. Acute vascular endothelial changes associated with increased blood velocity gradients. Circ Res 1968;22:165–97.

[3] Stein P, Walburn FJ, Sabbah HN. Turbulent stresses in the region of aortic and pulmonary valves. J Biomech Eng 1982;104:238–44.

[4] Ku DN, Giddens DP, Zarins CK, Glagov S. Pulsatile flow and atherosclerosis in the human carotid bifurcation. Atherosclerosis 1985;5:293–302

[5] Ahmed SA, Giddens DP. Velocity measurements in steady flowthrough axisymmetric stenoses at moderate Reynolds number. J Biomech 1983;16:505–16

[6] Ghalichi F, Deng X, Champlan A, Douville Y, King M, Guidoin R. Low Reynolds number turbulence modelling of blood flow in arterial stenosis. Biorheology 1998;35:281–4.

[7] Lee TS, LiaoW, Low HT. Numerical simulation of turbulent flow through series stenoses. Int J Numer Methods Fluids 2003;42:717–40.

[8] Paul MC, Molla MM, Roditi G. Large–Eddy simulation of pulsatile blood flow. Med Eng Phys 2009;31:153–9.

[9] Sarifuddin, Chakravarty S, Mandal PK, Layek GC. Numerical simulation of unsteady generalized Newtonian blood flow through differently shaped distensible arterial stenoses. J Med Eng Technol 2008;32:385–99.

[10] Stonebridge PA, Brophy CM. Spiral laminar flow in arteries? Lancet 1991;338:1360–1.

[11] Stonebridge PA, Hoskins PR, Allan PL, Belch FF. Spiral laminar flow in vivo. Clin Sci 1996;91:17–21

[12] Paul, Manosh C., and Arkaitz Larman. "Investigation of spiral blood flow in a model of arterial stenosis." Medical engineering & physics 31.9 (2009): 1195-1203.

[13] Deshpande. M. D., Giddens, D. P. and Mabon, R. F. (1976) Steady laminar flow through modelled vascular stenoses. J. Biomechcmics 9. 165-l 74.

[14] Smith, F. T. (1976) On entry-flow effects in bifurcating.blocked or constricted tubes, J. Fluid Mrch. 78. 709736

[15] Ku DN. Blood flows in arteries. Annu Rev Fluid Mech 1997;29:399–434.

[16] FLUENT 6.3. Tutorials Guide. USA: Fluent INC; 2007.

[17] Wilcox DC. Turbulence modelling for CFD. La Canada California: DWC Industries; 1993.

[18] Stonebridge, P. A., et al. "Non spiral and spiral (helical) flow patterns in stenoses: in vitro observations using spin and gradient echo magnetic resonance imaging (MRI) and computational fluid dynamic modeling." *International angiology* 23.3 (2004): 276.

[19] Frydrychowicz, Alex, et al. "Time-resolved, 3-dimensional magnetic resonance flow analysis at 3 T: visualization of normal and pathological aortic vascular hemodynamics." *Journal of computer assisted tomography* 31.1 (2007): 9-15.

Product Diversification and The Enhancement of Export Volume From Bangladesh To EU & Non-Traditional Markets

Md. Ahshan Habib[1]*, Md. Jahangir Karim[2]

***Corresponding Author:** [1]Lecturer & Head Department of Fashion Design & Technology (FDT), Sonargaon University (SU)
[2] Department of Apparel Manufacture & Technology (AMT),Sonargaon University (SU)

Email: habib826620@yahoo.com

Abstract

We have got a very competitive market place, this day. There is a need for business organizations to ensure continual improvement. Garment Manufacturing companies experience growing pressure to improve quality, increase productivity, and reduce cost with limited resources. The paper reviews the literature on this industry, and evaluates future trends in the international and domestic clothing industry. Fashion industry need to reduce response time, eliminate errors, product diversification for search the new market and improve customer satisfaction to increase the volume of export quantity.

Keywords: Increase, export, clothing item, EU, Non-Traditional Markets.

1.0. Introduction

1.1. Background

Readymade Garment industry (RMG) is one of the largest sector in Bangladesh which earning more than 82.01% of total export in the year of 2015-16 [1] of foreign currency, in every year by exporting fashion product (clothing items) from Bangladesh to different region of the world. Bangladesh export garments to more than 40 countries, this export are highly concentrated in two major markets, the USA and EU. In our research we will try to focus the European Union markets. From many years Bangladesh exporting fashion product to the European Union markets and the export volume is larger about 17946.87 Million US dollar in the year 2016 [2] where woven is 8089.91 Million US dollar and 54.18 EU % of world, Knit item is 9856.96 Million US dollar and 71.76 EU% of world [3]. In recent years order stream from EU become steadily rising up. In this paper we will try to find out what is the reason behind this and how the product diversification can help us to increase the export volume to the European Union markets as well as & Non-Traditional

Markets. This paper also addresses some of the important strategic aspect to improve export opportunities, from marketing taking advantage of the trade related assistance offered by the EU to the less developed countries. We believe that this research will be very much helpful for the RMG sector and become an implementable milestone.

1.2. Description

Readymade Garment (RMG) Industry occupies a leading position in the export-manufacturing sector of Bangladesh. The advent of the RMG sector happened during the early 80s in Bangladesh. Since then, due to supportive policies of the Government of Bangladesh, this industry has experienced a significant growth. In 1988, And since then this sector has continued to consolidate it predominant position in the export basket of Bangladesh. According to the export promotion bureau (EPB) data of 2003-2004 financial years, the export earnings from the RMG sector was 5686.09 million US dollars which represent 74.79% of total export and total export of Bangladesh was 7602.99 million US dollars [1] . In 2015-16 financial years export earnings from the RMG sector was 28094.16 million US dollars, which represent 82.01% of total export earnings, and total export of Bangladesh was 34257.18 million US Dollars [1] . The industry, which was started only with a few Factories in 1980s and in the year 1984-85 there was only 384 factories and in 2015-16, it increased into 4328 factories [4]. The RMG sector employed around 0.12 million workers In the fiscal year 1984-85 and in the year 2015-16 the industry employed 4.0 million workers [4].Today's market is very competitive and Bangladesh RMG industry exporting basically classic product which is very easy to produce and sell them to the world market. And so many countries doing the same thing in the same way, and retailers take the chance to bargain with the manufacturers. As a result the garment exporters have no other way to take the enormous volume of order with in very low profit. Another way how we can make more profit and boost up the export volume by doing product diversification as well as market diversification .It means that besides doing the classic we need to develop and create new innovative product and exporting them to the existing and new market.

2.0. Data collection

The purpose of data collection was to understand the present situation of garment industry in Bangladesh and what is the present export quantity in this paper basically contain on line publishing base information like journals, books, others researcher projects and online clothing and garment industry base web portals.

2.1. Data analysis

In this paper collected data were analysis by the requirements of in terms of the input, output, control systems, human resources, and technology, time, decision-making and communication systems. Main analysis and discussions have been made on the basis of the information obtained from the BGMEA web site and also data collected from the Export Promotion Bureau (EPB) and world famous renowned web portals. Some data are taken from interview that was published in the daily newspaper and as well as from the Apparel summit where the guest spoken about the Readymade Garments (RMG) industries. This paper has focused upon the various issues which are regarding with the garment company and the success of these industries. This study based on secondary data that are available in the government web site EPB and BGMEA, which are very authentic and accurate so there is no possibility of fakeness. The limitation of this paper is primary data were not collected like garments factory owner answer the questionnaire/interview.

So we couldn't evaluate and analysis their opinion and suggestions. But in this paper demand the authentic and accurate data that's why we focused and depended on secondary data. Another problem in the primary data collection questionnaire and interview the respondent might provide socially acceptable answer. Most of case the person's private information was not disclosed which could be very helpful.

3.0. Good Practise of research and development (R&D)

Fashion consumers are now very fashion and style conscious, they are always looking for new design and style. As a result international fashion sourcing companies are also searching for new design/ style, innovative creative fashion products. Basically in Bangladesh, most of the garment manufacturers follow the "cut-n-sew" theory that means sewing only the classic product. Most of the factories are base on Basic fashion production like- basic-shirts, trousers, jackets, T-shirt and sweater [5]. Some fashion product like Outerwear, technical sportswear, swimwear, underwear, shape- body and lingerie- a product that Bangladesh used to make in the past [6]. Designs like- Ski wear- tracking- hiking- and biking unfortunately the export volume is very poor in quantity. So we can start develop these item and offer to the buyer. And only 5% market share high price luxury segment, 15% market

aware ab

Appendix-A

Membership And Employment

1458.93	4583.75	2001-2002	3124.82	

				Sub-Total							

A Study on The Perf[illegible] of Hybrid Power Generation

1.3. Solar Photovoltaic System

Photovoltaic cells are widel

Where,

Ins (t) = insolation data at time t (kW/ m^2)

1.5.1. Working of a solar panel

Now a days, few existing software are available for cooling load calculation but its demand is

a) Vapor compression chiller for Supermarket [illegible]

element of blue economy. Through the integrated plan it can have a huge impact in the developmen

e system internally with formal

concern. Many countries in the world developed quality assuran